Ore Geology Reviews 106 (2019) 273–299

Contents lists available at ScienceDirect

Ore Geology Reviews

journal homepage: www.elsevier.com/locate/oregeorev

Invited Review Article

Post-Variscan structurally-controlled hydrothermal Zn-Fe-Pb sulfide and F-Ba mineralization in deep-seated Paleozoic units of the North German Basin: A review

Patrick Nadoll[a], Marta Sośnicka[b], Dennis Kraemer[c,*], Florian Duschl[d]

[a] GeoZentrum Nordbayern, Friedrich-Alexander-Universität Erlangen-Nürnberg, Schlossgarten 5, 91054 Erlangen, Germany
[b] GFZ German Research Centre for Geosciences, Telegrafenberg, 14473 Potsdam, Germany
[c] Jacobs University Bremen, Campus Ring 1, 28759 Bremen, Germany
[d] GZG Geowissenschaftliches Zentrum, Georg-August-Universität Göttingen, Goldschmidtstr. 3, 37077 Göttingen, Germany

ARTICLE INFO

Keywords:
North German Basin
Zn-Fe-Pb sulfides
Fluorite
Hydrothermal
MVT
Permian

ABSTRACT

Hydrothermal Zn-Pb-Fe sulfide and F-Ba mineralization occur as open space fillings, veins, and fracture coatings in various parts of the North German Basin in Paleozoic sedimentary rocks and volcanic units at depths of up to four kilometers. We present a petrographic and geochemical (fluid inclusion, mineral and formation water geochemistry) inventory of the mineralized zones and review the basin architecture, evolution, and stratigraphy in order to decipher the timing, extent, fluid pathways, and fluid-rock interactions associated with the ore formation. A particular focus lies on the sediment-hosted Zn-Fe-Pb sulfides in the western part of the North German Basin, the Lower Saxony Basin. Samples from hydrothermal veins from the Pre-Permian basement are also being investigated and compared to the North German Basin-style mineralization to uncover possible genetic links between them. The sediment-hosted sulfide mineralization in the Lower Saxony Basin in the Permian Stassfurt Carbonate unit (Ca2) shares many characteristics that are typical for carbonate-hosted base metal sulfide deposits such as MVT deposits. Petrographic observations, fluid inclusion and isotope data provide evidence that Zn-Fe-Pb sulfides were deposited by highly saline metal-rich basinal brines at temperatures of ~160 °C. Carbon and oxygen isotope data point toward fluid mixing augmented by structurally-controlled fluid migration during the late Cretaceous basin inversion as the primary ore precipitation mechanism with no magmatic component. In the Altmark-Brandenburg Basin, steeply-dipping F-Ba (calcite, anhydrite, quartz) veinlets in Permo-Carboniferous sandstones and volcanic units are evidence for enhanced post-Variscan structurally-controlled fluid flow. Sulfides are, apart from rare occurrences of chalcopyrite, absent. This is interpreted to reflect the paleogeographic position of the Altmark-Brandenburg Basin (deeper paleogeographic basin position without carbonate aquifers), the lack of reductants, and the predominance of nitrogen-rich fluids as documented by fluid inclusions. Measurements on formation waters from the NGB show geochemical similarities to fluid inclusions in ore and gangue minerals and could represent a potential future exploration tool for hydrothermal ore deposits. This has the potential to aid future research and exploration of deeply covered sediment-hosted deposits and to meet future mineral resources demands.

1. Introduction

Deeply-covered hydrothermal mineralization in Permian units within the North German Basin (NGB, Fig. 1) have first been discovered in exploration and production drill cores more than 50 years ago. Since the 1960s researchers have recognized the occurrence of these mineralized zones in Permian strata of the NGB at depths of up to four kilometers and historic mining for sphalerite and galena is documented in parts of the Lower Saxony Basin (LSB; i.e., Silberberg and Hüggel) where rare outcrops of the corresponding host rock lithology exist (Mempel, 1962; Mempel et al., 1965). However, little is known about the fluid and metal sources and the processes that led to the formation of the sediment-hosted hydrothermal Zn-Fe-Pb sulfide, fluorite-barite, and vein-type quartz-calcite-(specular) hematite mineralization in Permian host rocks across the NGB. The origin and character of the hydrothermal activity in the LSB and Altmark-Brandenburg Basin (ABB) is still under debate and has been the subject of several recent research efforts, e.g., Will et al. (2016) and Wüstefeld et al. (2017), who focused their investigation on unravelling the thermal history and fluid evolution within the basin. Most recently, Sośnicka and Lüders (2018a) and Knorsch (2017) provided findings that class the sulfide mineralization in the LSB as the deep-seated expression of a potential Mississippi Valley-Type (MVT) deposit. Mempel (1962) was the first to note the different expressions of hydrothermal mineralization in the western and eastern part of the NGB, the LSB and the ABB, respectively. Dolomitic Zechstein (upper Permian) carbonates of the Stassfurt carbonate unit (Ca2) in the LSB host sulfides such as sphalerite, galena and pyrite, whereas sulfide mineralization is absent in Permian strata and volcanic host rocks of the ABB (Mempel, 1962; Mempel et al., 1965)—merely some occurrences of pyrite have been reported but are not thought to be related to hydrothermal activity. In the latter, vein-type quartz-calcite-(specular) hematite and fluorite-barite mineralization are evidence for widespread hydrothermal activity.

* Corresponding author.
E-mail address: d.kraemer@jacobs-university.de (D. Kraemer).

https://doi.org/10.1016/j.oregeorev.2019.01.022
Received 9 October 2018; Received in revised form 15 January 2019; Accepted 25 January 2019
Available online 29 January 2019
0169-1368/ © 2019 The Authors. Published by Elsevier B.V. This is an open access article under the CC BY license (http://creativecommons.org/licenses/BY/4.0/).

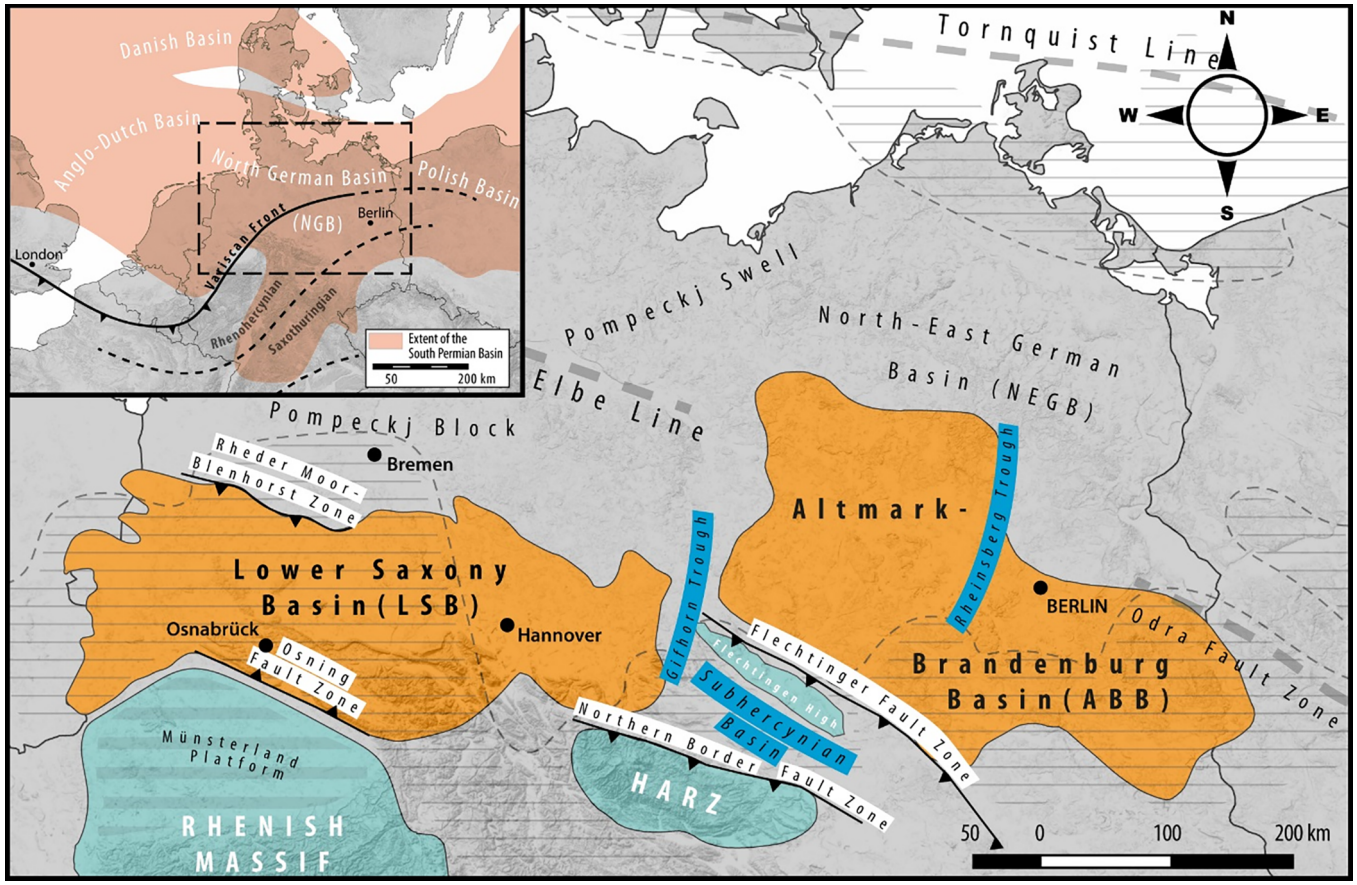

Fig. 1. Top left: Overview map showing the extent of the South Permian Basin and its sub-basins. Main map: Location and extent of the Lower Saxony Basin and the Altmark-Brandenburg Basin and relevant structural features. The dashed line represents the approximate extent of the central North German Basin and the hatched area represents the shallow basin margins, i.e., carbonate platform. (after Betz et al., 1987; Kley and Voigt, 2008; Littke et al., 2008a; Scheck et al., 2002; Senglaub et al., 2006; Ziegler, 1990, 1987).

According to Mempel (1962) and Mempel et al. (1965) galena, sphalerite, pyrite, chalcopyrite, barite, celestine, and fluorite occur along fault planes and in open space fillings in Zechstein sedimentary rocks and volcanic units. The extent, petrography and geochemical variability of these mineralized zones are still widely unknown. However, more recent research efforts by Sośnicka and Lüders (2018a) and Knorsch (2017) have provided a more in-depth investigation of the petrography, isotopic composition and fluid inclusion chemistry of the ore minerals, specifically sphalerite. Both studies concluded that mixing of basinal brines precipitated the Zn-Fe-Pb mineralization at temperatures of up to ca. 200 °C and that the mineralization in the Ca2 carbonates of the LSB may be classed as a cluster of deep-seated thermochemical sulfate reduction (TSR)-controlled MVT deposits.

In this context we present petrographic (optical and scanning electron microscopy including cathodoluminescence) and geochemical data (electron probe microanalysis, laser ablation ICP-MS, ICP-OES, fluid inclusions, stable isotopes – $\delta^{13}C$, $\delta^{18}O$, $\delta^{57}Fe$) and review the formation and structural evolution of the NGB to further elucidate the formation conditions and mineral and elemental inventory of the deep-seated sediment-hosted Zn-Fe-Pb and fluorite-barite mineralization in the LSB and ABB. We discuss (a) the petrography and mineral chemistry of host rocks and mineralized zones, (b) the fluid, sulfur and metal sources, and (c) the hydrothermal fluid systems (fluid inclusion and isotope chemistry as well as formation waters) including pre-existing structures and other structural controls. Furthermore, we put the Zn-Fe-Pb and fluorite-barite mineralization in context with known mineralized zones in the Harz Mountains and the Flechtingen Calvörde Block (FCB)—both representing outcrops of the Variscan or pre-Permian basement in northern Germany—as well as the polymetallic Kupferschiefer deposits, to reveal possible genetic links or similarities in their formation.

The NGB's structural evolution and the development of fluid systems through time as well as detailed petrographic and geochemical data can help to constrain the occurrence and distribution of mineral resources within the NGB and its sub-basins and also give new insights into mineral system scale models of deep-seated deposits. Moreover, the potential of the observed ore minerals to host strategic elements such as Ge, Ga, In (sphalerite), and REE (fluorite) makes them a valuable research and possible exploration target.

2. Geologic overview

The northern European continent comprises several large superimposed basins that form the Central European Basin System (e.g., Littke et al., 2008a). During the late Carboniferous to early Permian three sub-basins developed—the Northern Permian Basin (NPB), the Southern Permian Basin (SPB) (Fig. 1), and the Polish Trough (Littke et al., 2008a; Maystrenko et al., 2008; Ziegler, 1977, 1990). The SPB is itself composed of various sub-basins and depressions divided by swells and highs that have experienced different modes of deformation and faulting associated with various (mostly post-Permian) subsidence and uplift events (e.g., Betz et al., 1987; Littke et al., 2008a; Ziegler, 1990). The SPB extends over 1600 km from the east coast of England to Poland and is filled with sediments that can reach a thickness in excess of five kilometers (Bachmann and Grosse, 1989; Brink, 2005; Plein, 1993; Ziegler, 1990). The dominant strike direction of the basin features is WNW–ESE, parallel to the Tornquist-Teisseyre-Zone (TTZ) in the North. The Elbe Line, an inferred contact zone between Baltica and Avalonia, and the Elbe Fault Zone (EFZ) are demarcating the southern margin of the basin (Maystrenko et al., 2008; Wilson et al., 2003; Ziegler, 1990). The difference in strike to the SW–NE-striking late Carboniferous Variscan Foreland Basin (Westphalian Foreland Basin) reflects a fundamental change in the overall stress regime (Scheck et al., 2002; Scheck-Wenderoth and Lamarche, 2005). Structurally similar sub-basins of the SPB include, amongst numerous others, the LSB, the Subhercynian Basin (SHB), and the North East German Basin (NEGB) including the ABB in Northern Germany (Figs. 1–3) (Benox et al., 1997; Brink, 2005; Brink et al., 1992; Stackebrandt, 1986), and the Mid-Polish Trough to the

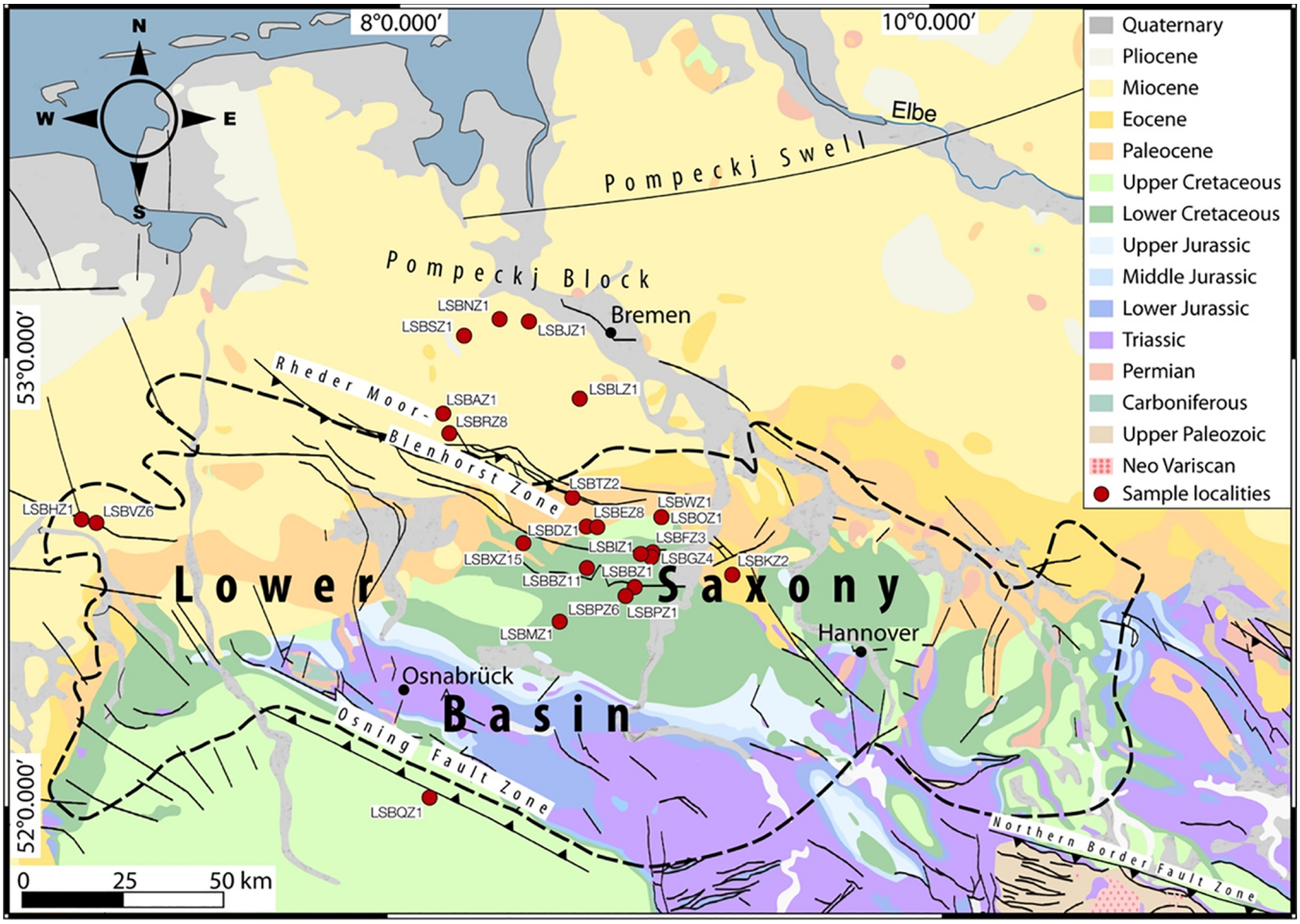

Fig. 2. Sample localities within or near the LSB and exposed geology and structural features. The dashed line represents the outline of the LSB.

east (Dadlez, 2006; Dadlez et al., 1995; Lamarche and Scheck-Wenderoth, 2005). Intensive drilling (more than 1000 wells) in the middle of the last century helped to gain a more comprehensive picture of the basin structure and the stratigraphy of deeply covered Permian units within the NGB (Brink, 2005; Gerling et al., 1999; Littke et al., 2008a; Lokhorst et al., 1998; Maystrenko et al., 2008; Plein, 1995). Information on basin infill and structural differentiation of the NGB into sub-basins mainly during the Mesozoic is compiled in Baldschuhn et al. (2001, 1991), Kockel (2002, 1994), Littke et al. (2008a), and Pharaoh et al. (2010), among others. The structure of the pre-Permian basement, especially in the NEGB, is also well understood thanks to large-scale deep seismic sections such as the European Geotraverse and the DEKORP-line (Blundell et al., 1992b, 1992a; Krawczyk and Stiller, 1999).

2.1. North German Basin

The NGB is located in the central part of the SPB (Fig. 1), extending over 500 km length and 200 km width (Bachmann and Grosse, 1989; Ziegler, 1990). It is framed by the Anglo-Dutch Basin to the West and the Polish Basin to the East. The NGB can be further subdivided into the LSB and the NEGB which are separated by a succession of subtle ridges from the Altmark High to the East Holstein Platform (Gast et al., 1998). The southern basin margin is characterized by numerous steeply dipping fault lines of the NW–SE striking EFZ (Franke et al., 1996; Littke et al., 2008a; Scheck et al., 2002). Major structural elements of the NGB are illustrated in Figs. 1–3.

The NGB has been interpreted to be the result of crustal thinning during a late Carboniferous to early Permian rift process with extensive magmatic and volcanic activity that affected the Variscan basement and generated NE–SW and NW–SE trending fault zones (Bachmann and Grosse, 1989; Brink et al., 1992; Gast, 1988; Littke et al., 2008a; Maystrenko et al., 2008; Stottmeister and Poblozki, 1999; Wilson et al., 2003; Ziegler, 1990). From a geodynamic-metallogenetic point of view the late Variscan and subsequent Upper Carboniferous to Permian period also produced a wealth of mineral deposits that were directly or indirectly related to the emplacement of various types of intrusions and volcanics (Dill, 1996; Dill et al., 2008a, 2008b). Most fault systems of the NGB reflect a major WNW-ESE trend whereas the second N-S trending fault system can be distinguished at the Horn Graben, Glückstadt Graben or Gifhorn Trough (e.g., Lamarche and Scheck-Wenderoth, 2005; Scheck et al., 2002). Ascending mafic magmas caused partial melting of the lower crust which is evident in extensive ignimbrite sequences within the NGB but especially in its eastern part, the NEGB (Breitkreuz and Kennedy, 1999). Basin formation, i.e. subsidence, was further induced by post-Variscan wrench tectonics leading to pull-apart structures that were successively filled with thick clastic and evaporitic sediments (Behr and Gerler, 1987; Betz et al., 1987; Maystrenko et al., 2008; van Wees et al., 2000; Ziegler, 1990). Progressive subsidence and further differentiation of the basin continued well into the Jurassic (Littke et al., 2008b; van Wees et al., 2000; Ziegler, 1990). Upper Cretaceous re-activation of Variscan NW–SE striking fault systems led to basin inversion (Littke et al., 2008a; Ziegler, 1987), triggering halokinesis (salt tectonics) (Glennie, 1995), and locally, also resulted in structurally controlled mineralization (Möller and Lüders, 1993). Modern 3D numerical simulations based on high-resolution seismic lines have given new insights into the timing of basin evolution in different areas of the NGB and helped to understand basin dynamics from subsidence to inversion (Gemmer et al., 2003, 2002; Hansen et al., 2007; Hecht et al., 2003; Lamarche and Scheck-Wenderoth, 2005; Müller et al., 2016; Scheck and Bayer, 1999).

The Harz Mountains (Fig. 1), though not being part of the NGB *sensu stricto,* share the same fate as the basin infill of the Mesozoic sub-basins as they were uplifted during the Upper Cretaceous-early Cenozoic basin inversion (e.g., Franzke et al., 2004; Kley et al., 2008). However, their position along the southern margin of the EFZ, between the two major sub-basins, the LSB in the northwest and the ABB in the northeast (Figs. 2 and 3), as well as their similar tectonic

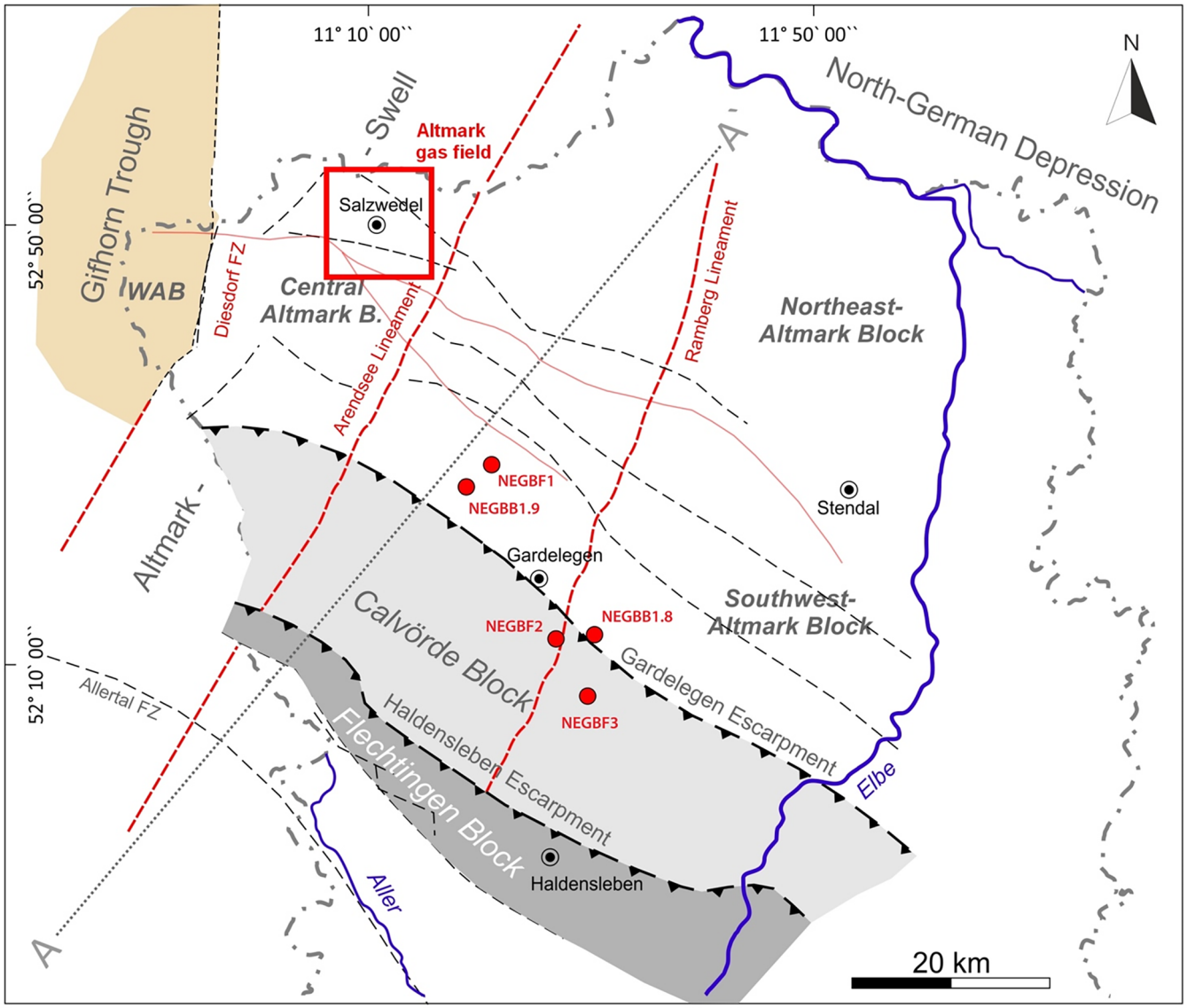

Fig. 3. Sample localities, major structural units, and fault zones of the western Altmark-Brandenburg Basin. Red lines represent faults in the Permian basement as inferred from Schumacher and May (1993), Borsdorf (1976) and Benox et al. (1997), black lines mark Mesozoic faults (Benox et al., 1997). Red dots indicate wells containing fluorite mineralization. WAB = West Altmark Block, FZ = Fault Zone.

history make the Harz Mountains a tectonic key element regarding the geomechanical properties of the Variscan basement during the Upper Cretaceous basin inversion (Gabriel et al., 1997; Tanner and Krawczyk, 2017). Especially the occurrence of major fault-related hydrothermal mineralization in the Harz Mountains and their association with the complex tectonic history may support the understanding of fluid migration in adjacent sedimentary basins.

2.1.1. Lower Saxony Basin

The E–W trending LSB is located in the NW-part of Germany, north of the Rhenish Massif (Betz et al., 1987; Ziegler, 1977) (Figs. 1 and 2). The LSB developed during a tectonically active period in late Jurassic to mid-Cretaceous times along NW–SE trending faults systems, superimposing the late Carboniferous Variscan Foreland Basin and parts of the Variscan Fold Belt (Betz et al., 1987; Boigk, 1981; Doornenbal and Stevenson, 2010). The northern boundary of the LSB is marked by the Pompeckj Block, the southern basin margin is bordered by the Münsterland Platform and the N–S trending Gifhorn Trough marks the Eastern limit of the LSB (Betz et al., 1987; Brink et al., 1992; Glennie, 1990; Ziegler, 1990, 1987). Friesland Platform and Texel-Ijsselmeer-High mark the western border of the LSB (Pharaoh et al., 2010). The Osning Mountains, Osning Thrust Zone (also referred to as Osning Fault Zone), situated at the southern margin of the LSB, represent the most intensely inverted part of the LSB (Baldschuhn and Kockel, 1999; Betz et al., 1987) (Fig. 4A). During the Upper Cretaceous basin inversion, the LSB was in part overthrusted on the southern Münsterland block along the Osning Thrust Zone (Baldschuhn and Kockel, 1999; Josten et al., 1984; Lüders et al., 2012). Faults of Permian age (Ziegler, 1990) limit the Osning Thrust Zone to the south.

Three prominent horst structures, namely Schafberg, Hüggel, and Piesberg, are of significance for mineral exploration in the LSB as they coincide with historical mining areas, where Zn-Pb and metasomatic iron ores were mined. The Perm mine and the Schafberg (Harms, 1984), however, represent Pb-Zn mineralization hosted in Zechstein Ca1 carbonate and not in the stratigraphically younger Ca2 dolostone.

2.1.2. Altmark-Brandenburg Basin (ABB)

The ABB represents the south-western part of the NEGB (Figs. 1 and 3). The structural evolution of the ABB and NEGB are essentially the same. The general structural organization of the ABB is detailed in Benox et al. (1997). The pre-Permian basement of the ABB is subdivided into several tectonic units that are delineated by major NNE–SSW and NW–SE striking lineaments. The Flechtingen Fault Zone and the NNE–SSW trending Gifhorn Trough—a major depression that formed due to the early Permian extensional tectonics— mark the southern and western border of the ABB, respectively (Gast et al., 1998; Hübscher et al., 2010) (Fig. 4B). The predominant lineament in the western parts of the ABB, the Diesdorf Fault Zone, divides the Gifhorn Trough from the adjacent Altmark Swell. The

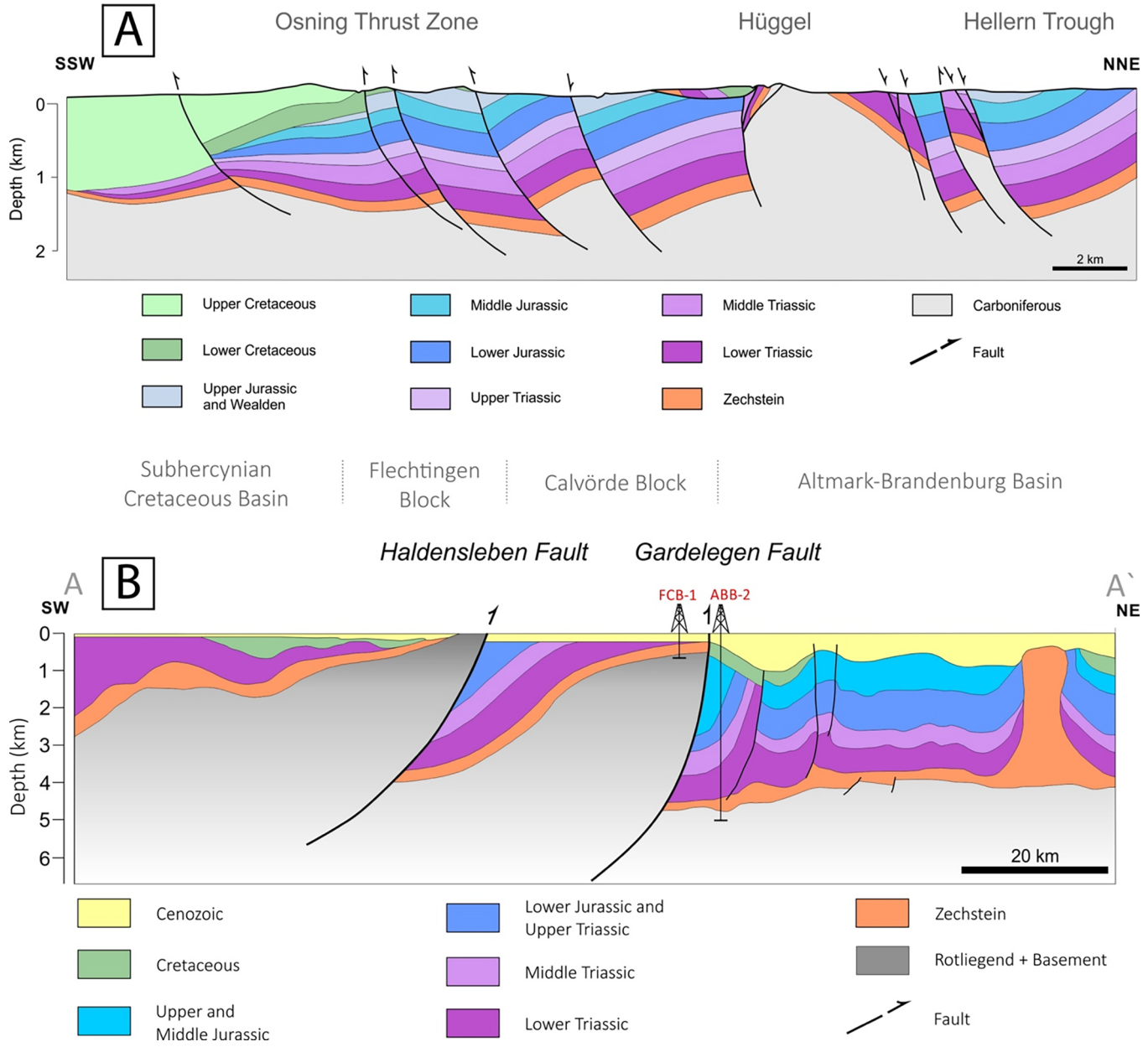

Fig. 4. A: Cross-section across the southern margin of the LSB (Osning Thrust Zone and Hüggel area) (after Baldschuhn and Kockel, 1998; Pharaoh et al., 2010). B: Schematic geological cross section through the Flechtingen-Calvörde Block and the Altmark-Brandenburg Basin showing major SW-dipping reverse faults, which delineate important thrust zones that formed during late Cretaceous-early Cenozoic convergence. The origin of NW-SE striking fault systems in the study area dates back to pre-Mesozoic times, however, their kinematic nature during Triassic and Jurassic times – prior to basin inversion – was most likely transtensional (modified after Pharaoh et al., 2010). Relative well positions are projected into the cross section.

West Altmark Block, the smallest structural unit in the ABB, occupies the easternmost part of the Gifhorn Trough. The Altmark Swell area north of the Gardelegen Escarpment is referred to as Central Altmark Block (Figs. 1 and 3).

In contrast to the LSB and the pre-Permian basement of the NGB, the NEGB, including the ABB, is commonly considered devoid of any known economic mineral and/or metalliferous mineralization. However, abundant hydrothermal vein-type fluorite-barite and quartz-hematite mineralization hosted by lower Permian volcanic rocks and Permian sandstones were first documented in drill cores during gas exploration in the Altmark area by Stedingk et al. (1995). These structurally-controlled veins found at up to 4 km depth generally vary between < 0.1 to < 1 m in thickness and are associated with NW-SE and NE-SW striking and steeply dipping faults and lineaments.

2.1.3. Stratigraphic overview

The Rotliegend represents the lowermost Paleozoic stratigraphic unit of the NGB infill and comprises up to 3000 m thick volcanic units (Altmark Subgroup) and a suite of red bed clastic sedimentary rocks that were deposited under semi-arid conditions on a continental flood plain (playa) (Fig. 5) (Bachmann and Hoffmann, 1995; Gaupp et al., 2000). The Rotliegend is overlain by sedimentary rocks of the Zechstein. At its base, acting as a marker horizon, is a thin (commonly less than 0.3 m thick) marine black shale layer with high organic contents—the Kupferschiefer (*sensu stricto*) (e.g., Alderton et al., 2016; Borg et al., 2012; Dill, 1996; Speczik, 1995). In some parts of the Permian basin, i.e., the Mansfeld and Lausitz area in Germany or southwest Poland, the Kupferschiefer has been mined primarily for its high polymetallic content (Cu, Zn, Ag and Pb) since medieval times. It can also contain elevated concentrations of certain critical metals such as Mo, Pt, Pd, Te, Au and U (Bechtel et al., 2001; Kucha et al., 1993; Piestrzyński, 1990; Piestrzyński and Wodzicki, 2000).

As illustrated in Fig. 5, the NGB transgressional transitions from the clastic sediment-dominated lower Permian to the upper Permian are characterized by cyclic clastic sediments such as silt and claystones during early transgression and carbonates, sulfates, and halite units at later stages when the basin was fully

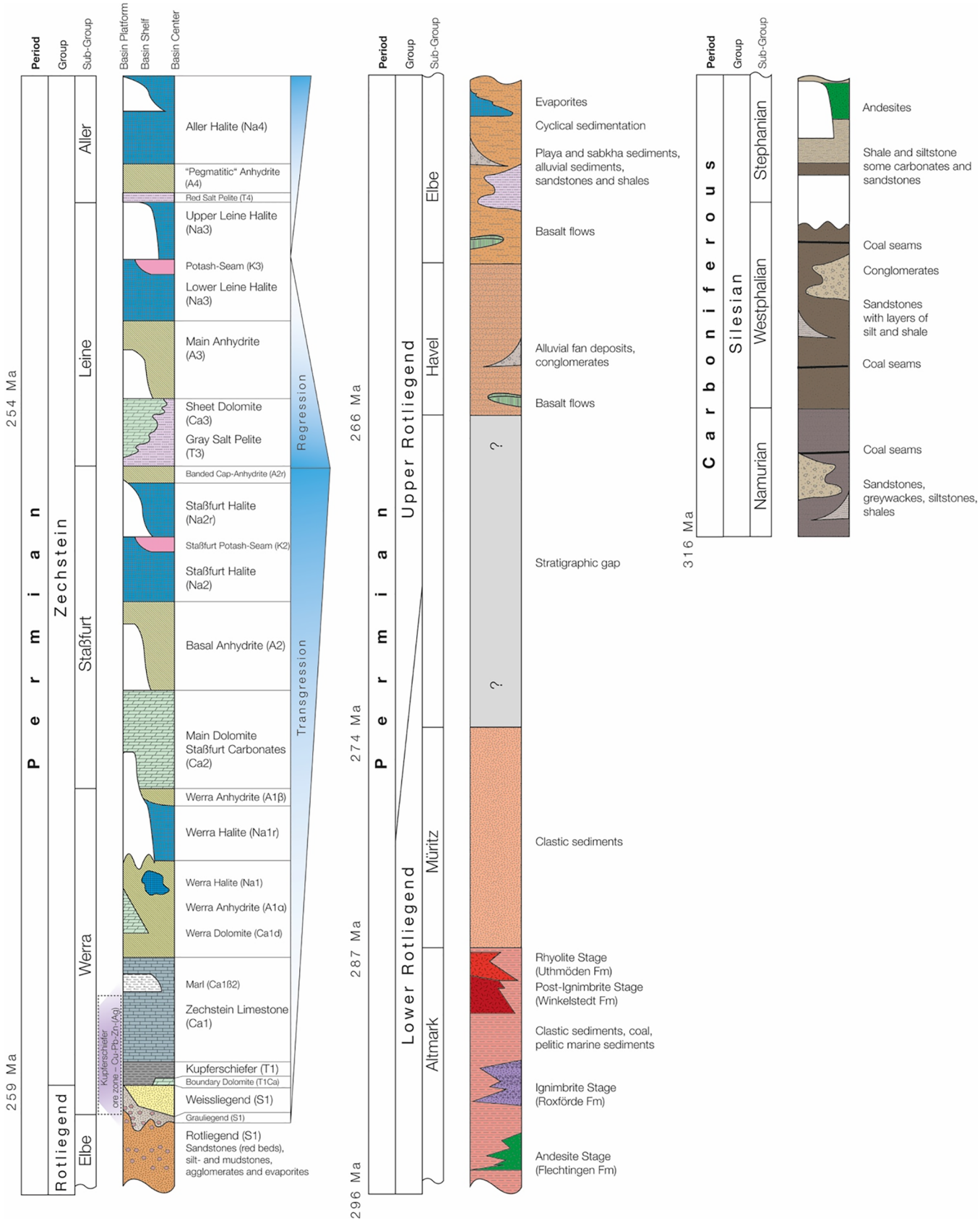

Fig. 5. Permian and Pennsylvanian (upper Carboniferous) stratigraphic units (generalized, arbitrary scale) of the North German Basin (compiled from and edited after Bachmann and Grosse, 1989; Bachmann and Hoffmann, 1995; Borg et al., 2012; Göthel, 2012; Lützner and Kowalczyk, 2013; Plein, 1995; Schröder et al., 1995; Wrede, 2005). Paleogeographic divisions (basin platform, shelf and center) apply to the Zechstein (upper Permian) units. Rotliegend (lower Permian) and upper Carboniferous strata represent the dominant basin-wide units, i.e., are more generalized.

flooded (Bachmann and Hoffmann, 1997; Legler et al., 2005; Stollhofen et al., 2008). Four major evaporitic cycles have been described, although up to eight evaporitic cycles have been documented in the more than 1.5 km-thick Zechstein basin infill (Littke et al., 2008a; Scholle et al., 1995). Zechstein evaporite cycles can exceed 2000 m in thickness in the basin center (Lüders et al., 2010). These evaporitic sediments and their contribution to fluid, sulfur, and salinity budgets play an important role for the formation and evolution of basinal brines within the NGB.

Paleogeographically, most of the LSB is located at the transition between the lagoon and slope of the SPB (Figs. 1 and 5) which is reflected in the observed sedimentary structures and textures. The basin infill comprises thick (up to 2400 m) sequences of Permian to late Cretaceous sediments which are overlain unconformably by Cenozoic sediments (Betz et al., 1987; Boigk, 1968; Glennie, 1995). Permian strata in the region are predominantly represented by Zechstein sediments that often discordantly overlay upper Carboniferous rocks such as shales and sandstones. However, lower Permian sediments are also present in several wells (Doornenbal and Stevenson, 2010; Kockel, 2003).

The ABB has been affected by an extended subsidence during the late Permian to Triassic and was successively filled with sedimentary and volcanic material of up to 5.5 km thickness (Pudlo et al., 2011; Scheck-Wenderoth and Lamarche, 2005; Stottmeister and Poblozki, 1999; van Wees et al., 2000) (Fig. 4B). Widespread volcanism at the early stages of basin formation is documented in the Altmark sub-group (lower Rotliegend) by thick volcanics and volcanoclastics that changed their chemistry from early andesitic compositions to late rhyolitic stages (Bachmann and Hoffmann, 1997, 1995; Littke et al., 2008a; Marx et al., 1995; Plein, 1995; Scheck-Wenderoth and Lamarche, 2005). Lower Permian sediments in the ABB are dominated by clastic sediments with laminated claystones to coarse grained sandstones, which are characteristic for a continental flood-plain environment under semi-arid conditions (Pudlo et al., 2011).

3. Results

3.1. Petrography of host rocks and mineralized zones

3.1.1. Lower Saxony Basin

The upper Permian Stassfurt Carbonate (Ca2) is the predominant host rock for the sediment-hosted Zn-Fe-Pb sulfide mineralization in the LSB (Fig. 6A, B, C, D, E). Sphalerite, pyrite and galena are the major hydrothermal sulfides that occur in varying modal abundances in samples from the investigated wells in the LSB (e.g., Fig. 6F). Cyclical growth bands and sectoral zoning in sphalerite and pyrite can be observed in many samples (Fig. 6A, D, G, H). Bedding is often readily apparent in the Ca2 carbonates, especially where bituminous or clastic material and bedding-parallel deposition of sulfides retraces grading textures, which also reflects pre-existing permeability contrasts (Fig. 6B). Some samples feature ooidal and peloidal packstone, indicating that they were likely deposited on the offshore banks of the SPB under lagoonal conditions (see Fig. 1). Anhydritic dolomites with minor organic components also occur. Slumping textures are present especially in fine-grained dolostones with siliciclastic components (Fig. 6B). Stylolites, most likely comprising clay and organic material, are a common feature and are predominantly oriented parallel to bedding. In some cases, hydrothermal pyrite is closely associated with these stylolites, suggesting a genetic link (Fig. 6B).

A mixture of open space fillings, massive mineralization (i.e., pervasively mineralized zones dominated by sulfide minerals), veins (cm-scale) and veinlets (mm-µm-scale) can be found in the drill core samples from the LSB. Fracturing and small scale brecciation can be observed in many samples in the form of filled fractures crosscutting the host rocks and earlier mineralization stages or sharp-edged host rock fragments floating in a matrix of hydrothermal mineralization, i.e. calcite, anhydrite, quartz and sulfides. These fractured zones can be attributed to hydrothermal brecciation rather than the dissolution and re-crystallization of so-called pseudobreccias.

Carboniferous units were also sampled in a few wells (i.e., LSBHZ1, LSBPZ1, and LSBPZ6) and comprise clastic sedimentary (shales and sandstones) or volcanic rocks such as the amygdaloidal, porphyritic rock (melaphyre) in Fig. 6L. These units are free of sulfide mineralization but do display signs of alteration and are often crosscut by veinlets filled with carbonates (including siderite) or quartz.

3.1.1.1. Pyrite. Authigenic sedimentary to diagenetic pyrite is a common feature in the Ca2 (Fig. 6A) and other neighboring lithologies. These predominantly small, sub- to euhedral pyrites (~1–10 µm) are not linked to fractures, stylolites, open space fillings, or veins and occur as isolated disseminated grains throughout the carbonate. Hydrothermal pyrite appears to have formed in three distinct textural varieties in the LSB: (1) aggregations of uniformly sized pyrite microcrystals (< 10–50 µm) which form spherical to irregular annealed clusters along stylolites or in cavities within the dolostone (Fig. 6B, C and D). These hydrothermal pyrites are also present in narrow bands within veins and veinlets (Fig. 6C). (2) 'dusting'—thin accumulate layers of single crystal pyrites settling on top of other mineral phases such as sphalerite or galena (Fig. 6F). Euhedral, small-scale pyrites form centimeter-scale bands throughout the sulfide assemblage and are sometimes enveloping sphalerite grains. They often show cyclical growth bands (Fig. 6G) or occur as distinctly euhedral growth rims around earlier pyrites. They are bound to fractures, veins or open space fillings. (3) anhedral pyrites with grain sizes of up to a few centimeters are associated with secondary hydrothermal carbonates or occur within the sulfide assemblage. These grains commonly display micro-fractures. This type of pyrite formed co-genetically with other sulfides as displayed by sharp grain boundaries with sphalerite, indicating equilibrium conditions. No major dissolution processes or alteration halos were detected for both sedimentary or hydrothermal pyrites.

3.1.1.2. Sphalerite. Sphalerite is the predominant sulfide in the mineralized zones in the LSB (Fig. 6H). A detailed investigation of the petrography and mineral chemistry of sphalerite from the LSB has been undertaken by Knorsch (2017). Vein-type mineralization (mm-dm scale) and massive aggregates of up to cm-scale sphalerites with distinct color variations (colorless to dark brown) and sectoral zoning can be found in the Ca2 dolostone. Cyclical growth bands are a common feature in sphalerite, indicating compositional variations in the corresponding mineralizing fluid (Fig. 6H). Colloidal (i.e., concentric and colloform) growth, which is a common feature in sphalerites from many MVT deposits, could not be observed. Larger grains often display inclusions of gangue minerals such as quartz, carbonate and anhydrite. Inclusions of other sulfides such as pyrite and galena can also be observed, indicating that the corresponding sphalerite was a later or contemporaneous phase. Galena appears to be a late phase in many samples and often occurs as open space fillings enveloping previous mineral phases such as sphalerite (Fig. 6F). However, inclusions of galena within sphalerite can also be observed in some samples and suggest a contemporaneous crystallization with sphalerite (Fig. 6I). Other sulfides such as chalcopyrite, sulfosalts (tennantite-tetrahedrite series) and covellite are minor constituents in only a few samples. Covellite replaces chalcopyrite as a secondary sulfide, whereby several degrees of progressive replacement can be observed in the polished sections (Fig. 6J). Tennantite-tetrahedrite series minerals are only present in well LSBQZ, near the southern boundary of the LSB.

3.1.1.3. Fluorite-barite. Hydrothermal fluorite commonly occurs as small interstitial grains, on planes of motion, and in veinlet fillings (Fig. 6E, K). Intricate growth textures could be observed under the SEM suggesting complex dissolution-recrystallization processes (Fig. 6K). Barite is only an accessory phase (< 1% modal abundance) but is present in some veinlet fillings or as individual relatively large grains (< 250 µm) in a few samples.

3.1.2. Altmark-Brandenburg Basin and Flechtingen Calvörde Block

Rotliegend sandstones (red beds), finer-grained siliciclastic sediments (i.e., mudstones) and thick volcanics of varying chemistry (andesite to rhyolite stages) are the predominant host rock types in the ABB (Fig. 7A, G). Carbonate cement is common in the clastic sediments. Hydrothermal calcite and anhydrite are the dominant gangue minerals within mm-cm scale veins or thin µm-scale veinlets and also occur as massively mineralized zones, i.e. open space fillings that are dominated by these minerals. Sulfides are much less abundant than in the LSB. Sphalerite and galena are entirely absent; an observation which concurs with Mempel's (1962) early work. Chalcopyrite does occur as up to cm-size aggregates in calcite veins but is merely a rare accessory phase.

3.1.2.1. Fluorite-barite. Fluorite is an abundant mineral phase and occurs as small (< 50 µm) solitary grains, small-scale veins, vuggy open space-fillings, and as coatings on fracture planes. Fluorite veins can reach several mm to cm in thickness. Greenish and pinkish fluorite varieties could be observed; however, clear varieties dominate. Hydrothermal fluorite is in some cases accompanied by later barite veins that also crosscut the gangue calcite (Fig. 7A–F). Barite is often fine grained (< 25 µm) and dispersedly distributed throughout mineralized zones. Barite veins and larger crystals also occur but are less abundant (Fig. 7A–E).

3.1.3. Cathodoluminescence (CL)

CL can reveal structural and textural features on a thin section and mineral scale. Minor differences in REY and trace element composition in hydrothermal fluorite resulting from sectoral zoning or multiple growth events can also be

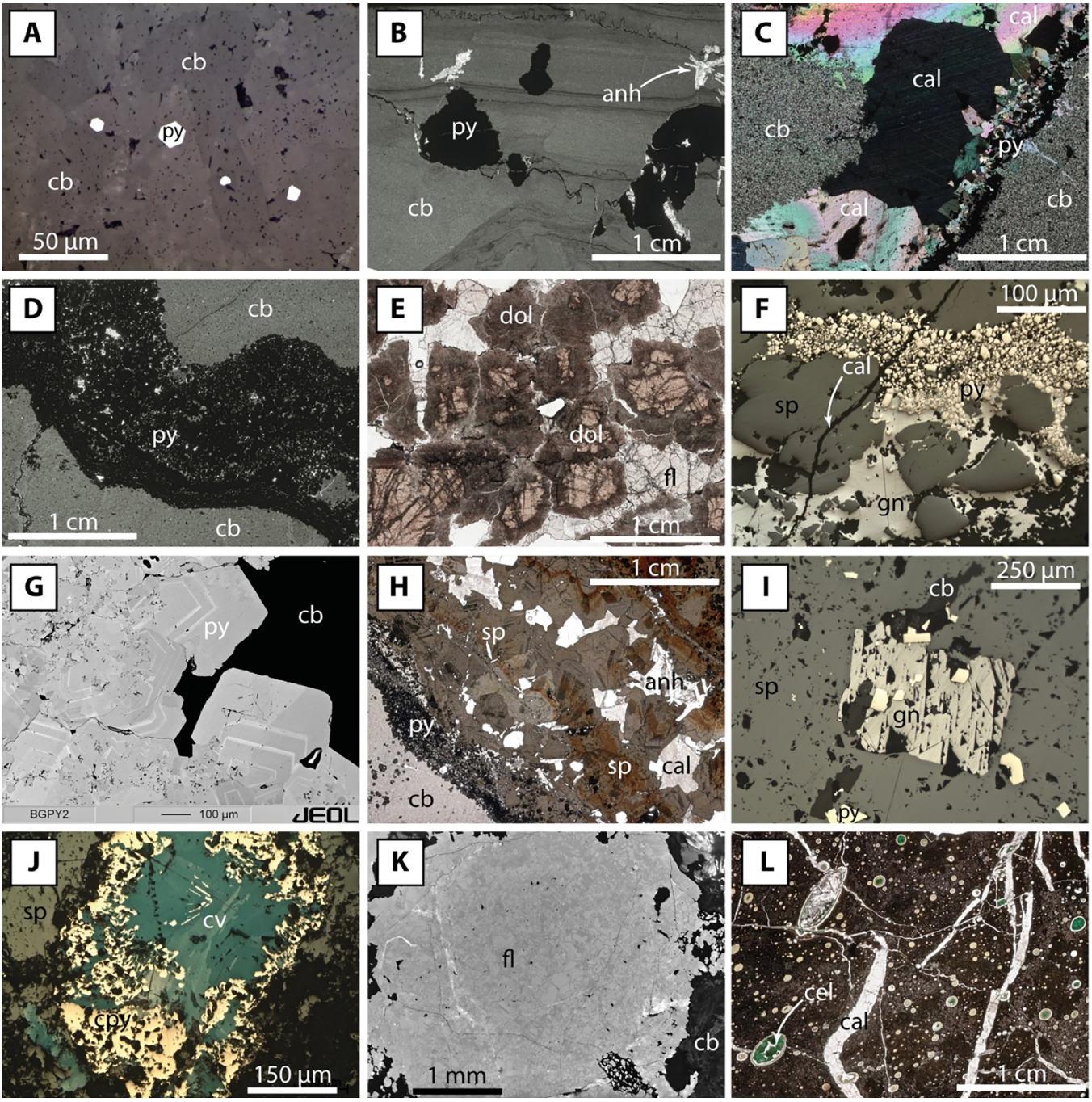

Fig. 6. Photomicrographs and SEM images of petrographic features in samples from the LSB. A: Sedimentary euhedral pyrite grain in Main Dolomite. (reflected light, pp) B: Stylolites (sub)-parallel to bedding in a Ca2 dolomite. Organic material retraces the bedding textures and sedimentary structures (slumping). Pyrite is often associated with the stylolites but also occurs as isolated grain aggregates within the carbonate. Anhydrite occurs in mm-size aggregates commonly associated with the sulfide mineralization. (transmitted light, pp) C: Calcite-pyrite vein in Main Dolomite. Large, cm-size calcite is accompanied by a narrow band of pyrite. Solution textures are visible at the interface between hydrothermal calcite and the carbonate host rock. (transmitted light, cp) D: Pyrite band in Main Dolomite (Ca2) consisting of small (< 200 µm) individual grains. (transmitted light, pp) E: Dolomite (brown shades) and fluorite. (transmitted light, pp) F: Typical sulfide assemblage of sphalerite, galena and pyrite. A late calcite vein is crosscutting the sulfides. (reflected light, pp) G: Backscattered SEM image of hydrothermal pyrite hosted in carbonated illustrating the growth bands which are not visible in plain light. H: Banded and zoned sphalerite (brown shades, dark zones) associated with hydrothermal calcite and anhydrite. A band of fine-grained pyrite marks the boundary to the carbonate host rock. transmitted light, pp). I: Sphalerite with abundant carbonate inclusions and euhedral pyrite and galena. (reflected light, pp) J: Rare occurrence of covellite as a secondary alteration product of chalcopyrite surrounded by sphalerite (reflected light, pp) K: SEM-Cathodoluminescence image of fluorite displaying the otherwise invisible complex mosaic of growth textures (lighter and darker greys). L: Rotliegend volcanic (melaphyr) with abundant vesicle that are filled with calcite and green celadonite. Thin calcite veins crosscut the host rock. (transmitted light, pp).

visualized with CL by applying different electron densities. This may be especially helpful in interpreting REY patterns in fluorite, as shown by Nadoll et al. (2018). Fig. 8 shows two detailed examples of common observed textural and structural features of hydrothermal fluorite-quartz mineralization in sandstone-hosted fractures from two wells in the ABB (NEGBB1.16 and NEGBF1.1). Fig. 8A_{1-3} demonstrates the different luminescence properties of detrital and hydrothermal quartz, and thereby reveals brittle deformation within the wall rock prior to mineralization. Fig. 16B_{1-3} shows partial replacement of hydrothermal wall-lining

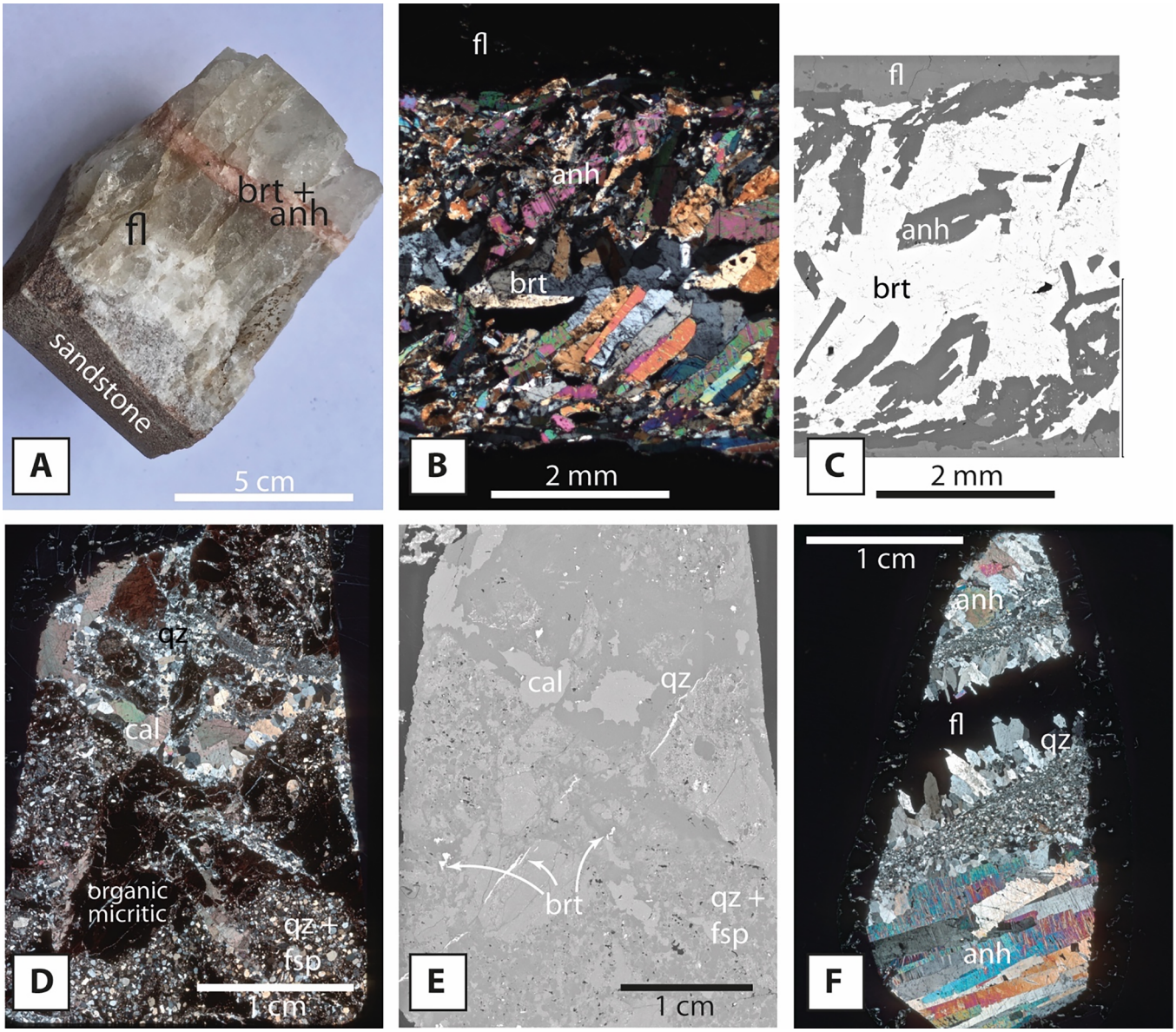

Fig. 7. Photomicrographs and macroscopic photos of samples from the ABB. A: Corresponding hand sample to B and C showing the massive colorless fluorite mineralization with the barite-anhydrite vein in the center. The host rock is a Rotliegend sandstone (bottom left corner). B: Barite vein with abundant elongated mm-size anhydrite crystals in fluorite (dark outer areas). (transmitted light, cp) C: SEM image of the same barite vein shown in B. Barite is more easily distinguishable due to its bright white BSE appearance. Anhydrite crystal within the barite vein show a dark grey whereas the surrounding fluorite has a slightly lighter grey appearance. (BSE-SEM image) D: Crosscutting quartz-calcite veins in micritic organic-rich carbonate rich siliciclastic sediment (dark brown patches which is also crosscut by fine barite-veinlets. (transmitted light, cp) E: BSE image of D displaying the elusive distribution of barite in the quartz, carbonate, feldspar matrix (clastic sedimentary)—Barite (bright white in the BSE image) is finely dispersed in small cavities and in fine veinlets crosscutting host rock matrix. A calcite cement (darkest grey) seems to be the last mineral phase to have crystalized in this sample. F: Quartz (grey)-fluorite (dark) vein. Note the syntaxial, partly feathery growth of the vein quartz (comb quartz) along the edges of the vein toward the center. The bottom third shows elongated anhydrite with typical high interference colors and parallel twinning. The vein is framed by deformation bands that display grain size reduction (transmitted light, cp) G: Specular hematite-calcite vein in rhyolitic Rotliegend volcanic of the FCB. H: Specular hematite (light grey needles) surrounding a fluorite grain (dark grey) in hydrothermal anhydrite (medium grey). (reflected light, pp) I: Chalcopyrite (light yellow) and hematite (light grey) in carbonate. Chalcopyrite is not an abundant mineral phase and usually occurs as disseminated, mostly unaltered grains of up to 1 mm diameter in hydrothermal carbonate from the FCB. (reflected light, pp).

quartz by fluorite. Further description in the figure caption.

3.2. Mineral chemistry

3.2.1. Pyrite

The complete LA-ICP-MS data can be found in the Electronic Appendix (8.1). The overall content of minor and trace elements in all types of pyrite (sedimentary and hydrothermal) is low. Only Pb, Mn and As have median concentrations above 10 ppm. The remainder of measured elements have median concentrations below 10 ppm (Co, Ni, Cu, Se) or below 1 ppm (Ge, Mo, Cd, Sb, Te, Au and Bi). However, particularly Pb, As, Ni, and Co show a wide variability among the different types of pyrite, with upper quartile (95%) values reaching several 1000 ppm in some samples. Compositional variations exist between different generations of pyrite and within growth bands (Fig. 9A, B, Fig. 10).

3.2.1.1. $\delta^{56}Fe$. Preliminary results for the iron isotopic composition of diagenetic and hydrothermal pyrite from the LSB range between $\delta\,^{56}Fe$ −0.34 and +1.11%. There is a large overlap among samples and no clear trend that discriminates these two types of pyrite or core and rim areas within individual pyrite grains (Fig. 11).

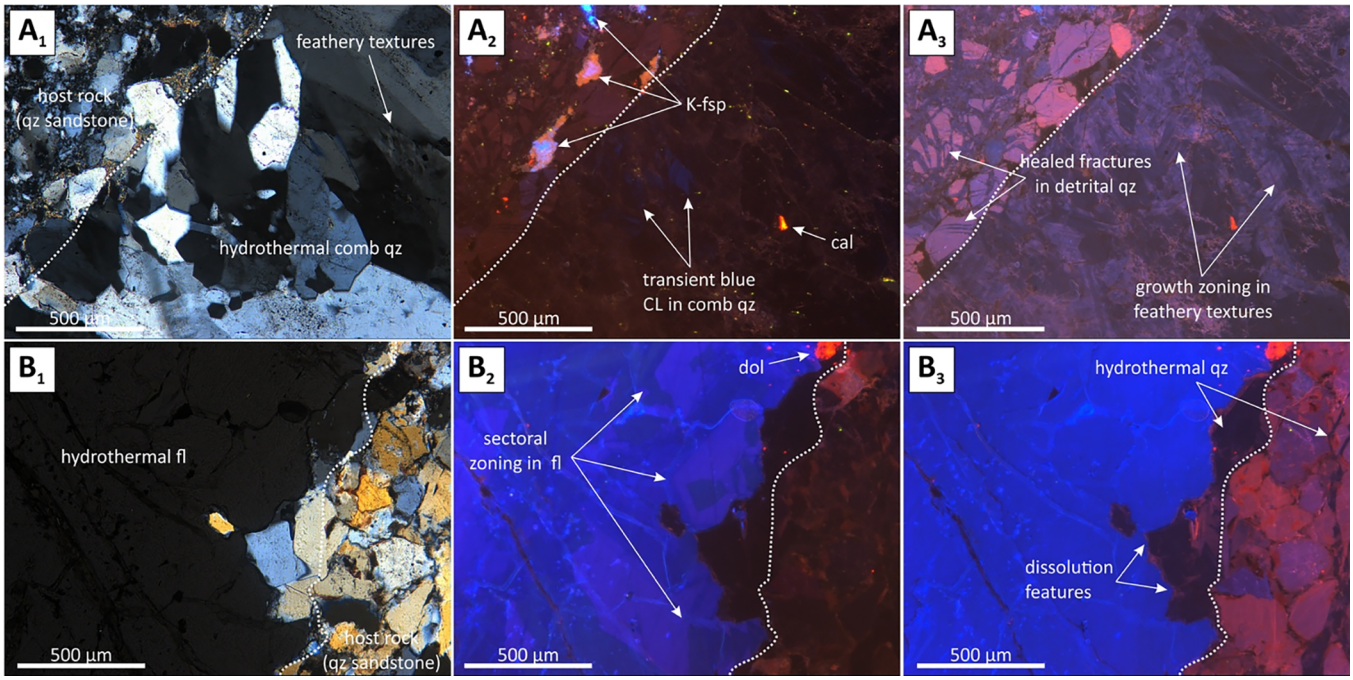

Fig. 8. A_1) Photomicrograph of a hydrothermal fracture mineralization in Rotliegend sandstone from the ABB (compare Fig. 15F) showing detrital quartz grains of the host rock and fracture-filling hydrothermal comb quartz (crossed polarizers). A_2 and A_3): same view as shown in A_1 in CL mode. Cathodoluminescence exhibits healed microfractures in detrital quartz grains in the host rock that prove some shearing during fracture formation. Comb quartz is characterized by transient blue CL (intense green dots: abrasive powder). B_1) Photomicrograph showing fracture-filling fluorite in eolian sandstone (Rotliegend) (crossed polarized light). B_2) and B_3): same view as B_1 in CL mode. Here, CL reveals growth zoning features in fluorite that help to distinguish between different growth events that explain varying trace element concentrations. Moreover, hydrothermal quartz can thereby be distinguished from detrital host rock grains.

3.2.2. Sphalerite

A detailed investigation of the sphalerite geochemistry in samples from the sediment-hosted Zn-Fe-Pb mineralization in the LSB has recently been conducted by Knorsch (2017). While the overall minor and trace element content of the investigated sphalerites from the Ca2-hosted Zn-Fe-Pb mineralization are low, i.e., median values for Ga, In and Tl are 0.99 ppm, 0.064 ppm, and 0.65 ppm, respectively (Knorsch, 2017), there are several compositional trends that seem to reflect changes in the physicochemical attributes of the corresponding mineralizing fluid over time. Fig. 12 shows As, Tl, Cd, Pb and Fe concentrations in a sphalerite from Well LSBHZ1 which illustrates these trends that are linked with the observed sphalerite colors (i.e., dark – high Fe, Cd, Pb and low As and Tl).

3.2.3. Carbonates

Vein carbonates from several drill cores within the LSB were investigated (see Electronic Appendix, Table EA 3, Table EA 4 for details).

The REY concentrations of hydrothermal carbonates hosted in Devonian, Carboniferous and upper Permian units in the NGB can be found in the Electronic Appendix (Table EA 4). Hydrothermal carbonates hosted in Devonian limestones have low overall REY contents (ΣREY = 18.51 mg*kg^{-1}), whereas Carboniferous carbonates have higher total REY concentrations (ΣREY = 5.13–263.72 mg*kg^{-1}) and upper Permian carbonate mineralization is in the range of 3.19 and 93.2 mg*kg^{-1} total REY. REY_{SN} patterns (SN: shale-normalized, Taylor and McLennan (1985); Fig. 13a) of vein carbonates hosted in Ca2 from the investigated drill cores in the LSB show significant variations, but an overall trend towards $LREY_{SN}$ depletion and $MREY_{SN}/HREY_{SN}$ enrichment can be seen in the data. The different shale-normalized REY patterns imply the presence of different fluid and metal sources. Similar patterns are observable for hydrothermal carbonates hosted in Carboniferous and Devonian strata (Fig. 13b). However, in the Carboniferous-hosted carbonate mineralization, the fractionation between LREY and MREY is even more prominent than in Ca2 mineralization. Those hosted in Carboniferous strata show a depletion in LREY over MREY and HREY and overall considerably elevated REY concentrations. Well LSBQZ1 hosts calcite veinlets in Devonian carbonates (Massenkalk) that are associated with traces of Zn-Pb sulfide mineralization at around 5280 m. The REY compositions of vein carbonates hosted in these Devonian units in the LSB (Fig. 13b) differ markedly from those found in Ca2-hosted vein carbonates. A small but distinct negative Ce_{SN} anomaly is present in the patterns in Fig. 13b along with a positive Eu_{SN} anomaly. However, in contrast to mineralization hosted in Carboniferous and upper Permian strata, the REY_{SN} patterns are remarkably flat without significant decoupling of any specific REY or groups of REY. Yttrium-Holmium ratios are sub- to superchondritic in all investigated fracture-filling carbonates, ranging from 22.7 to 36.1.

3.2.3.1. Oxygen and carbon isotopes. Oxygen and carbon isotope values have been measured in host rock and hydrothermal carbonates (i.e., calcite and dolomite) (see also Discussion Fig. 20). The complete dataset can be found in the Electronic Appendix (Table EA 5). Hydrothermal calcite and dolomite from the LSB range between −5.36 and +4.22 $\delta^{13}C$ (%, PDB) and +18.98 and +22.7 $\delta^{18}O$ (%, SMOW), whereas hydrothermal calcite and dolomite range between −9.01 and −2.09 $\delta^{13}C$ (%, PDB) and 16.05 and 24.08 $\delta^{18}O$ (%, SMOW). Two measurements on host rock calcite and dolomite show distinctly different values of +6.33 and +7.1 $\delta^{13}C$ (%, PDB) and +32.05 and 32.32 $\delta^{18}O$ (%, SMOW). Hydrothermal calcite from a reference sample from the Biwender Vein (Harz Mountains) has the lowest overall $\delta^{13}C$ and $\delta^{18}O$ values with −10.8/-10.94% and 13.29/13.43%, respectively.

3.2.4. Fluorite

The shale-normalized patterns from fluorites in the NGB (Fig. 13c) indicate significant variation in the geochemical composition of the REY among vein fluorites from different sub-basins and among vein fluorites hosted in different formations. Rare earth element concentrations in fluorites from the LSB are consistently low with ΣREY = 2.22 and 3.85 mg*kg^{-1}. The REY_{SN} patterns of the fluorites are rather flat with an enrichment of HREY over LREY. One of the Ca2-hosted vein fluorites shown in Fig. 13c is directly associated with the Zn-Fe-Pb mineralization and the REY_{SN} pattern shows a pronounced enrichment of MREY over HREY and LREY and a REY_{SN} pattern that differs considerably from other vein fluorites. This fluorite is significantly enriched in total REY with ΣREY = 221.31 mg*kg^{-1}. However, most of the overall enriched REY content can be attributed to significantly elevated Y concentration of 197 mg*kg^{-1}. The ABB fluorites are also enriched in total REY relative to the low REY LSB fluorites with ΣREY of 35.06 and 65.82 mg*kg^{-1}, respectively. The REY_{SN} patterns are flat with minor positive and negative Eu_{SN} anomalies. The investigated fluorite minerals from both the LSB and the ABB are enriched in Y relative to Ho in shale-normalized patterns, implying Y/Ho fractionation during fluorite formation from

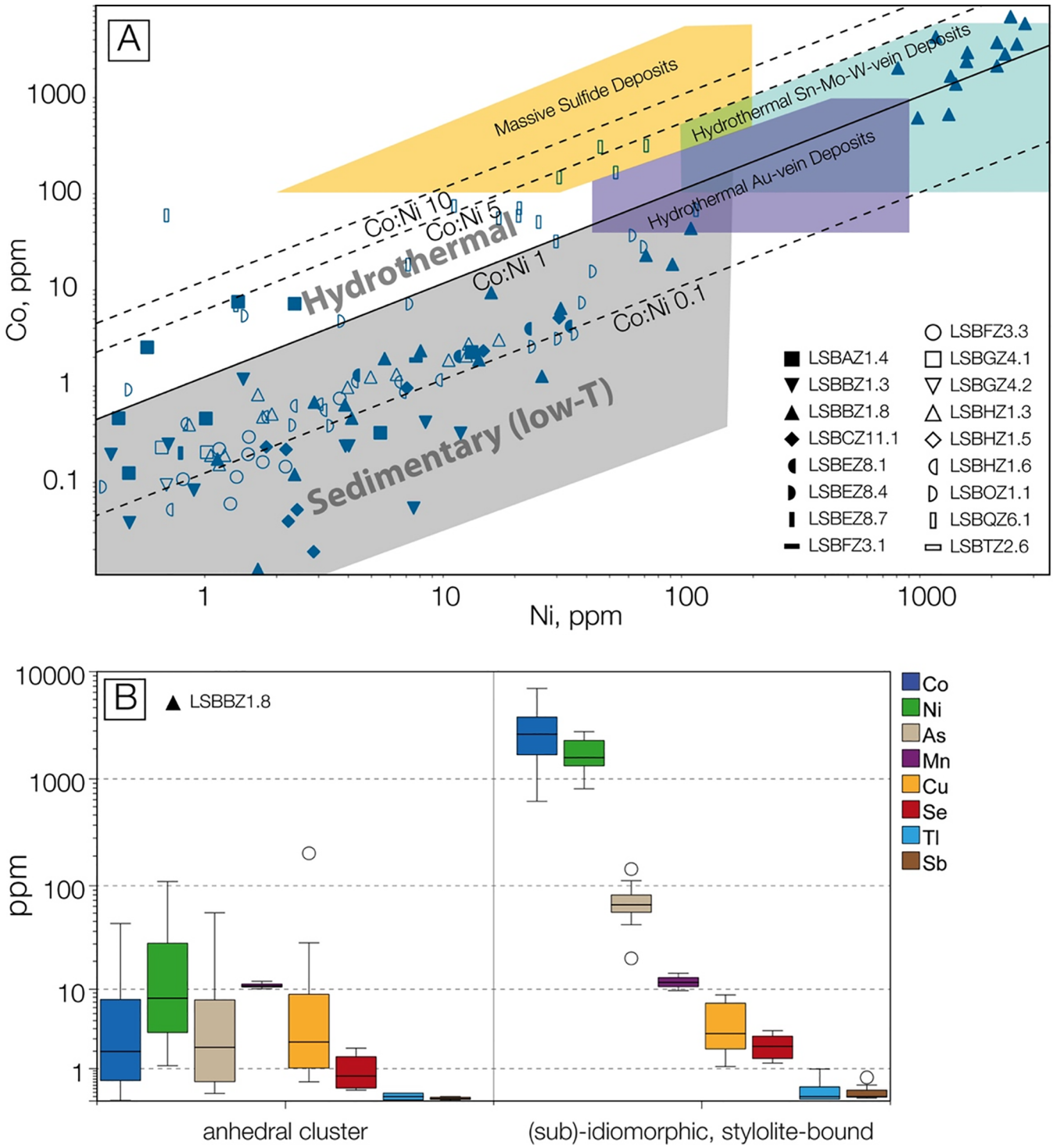

Fig. 9. A: Ni-Co discriminant diagram for pyrite, with Co:Ni ratios and deposit-type fields (after Campbell and Ethier, 1984; Price, 1972). The symbols represent samples from different wells or different depths within one drill core. B: LA-ICP-MS data for selected elements in different types of pyrite from well LSBBZ1.8. The anhedral massive pyrite cluster exhibits comparatively low minor and trace element concentrations while the stylolite-bound euhedral pyrite displays particularly high Co, Ni and As concentrations. The underlying LA-ICP-MS data can be found in the Electronic Appendix (Table EA 2).

hydrothermal fluids (Fig. 13c and Table EA 4).

3.3. Fluid inclusions

Petrographic observations of massive and vein-type sphalerite as well as fluorite mineralization from Zechstein carbonate Ca2 in western and central parts of the LSB revealed an abundance of secondary, pseudo-secondary, and lesser primary fluid inclusions (Fig. 14A–D). Here, we investigated fluid inclusions in Ca1-hosted quartz intergrown with massive dark sphalerite ore, which was mined historically in the Perm mine in the southern part of the LSB (Fig. 5, Fig. 14E, Table EA 6). Homogenization temperatures of these inclusions vary between 143 and 196 °C, whereas salinities range between 24 and 28 wt% NaCl equiv. We additionally studied fluid inclusions hosted in fracture-filling Zn mineralization in Devonian carbonate (Massenkalk) from well LSBQZ1 south of the Osning Thrust Zone (Fig. 14F, see also 3.2.3). Moderately saline (18.2–19.8 wt% NaCl equiv.), sphalerite-hosted fluid inclusions from this setting homogenized at a temperature

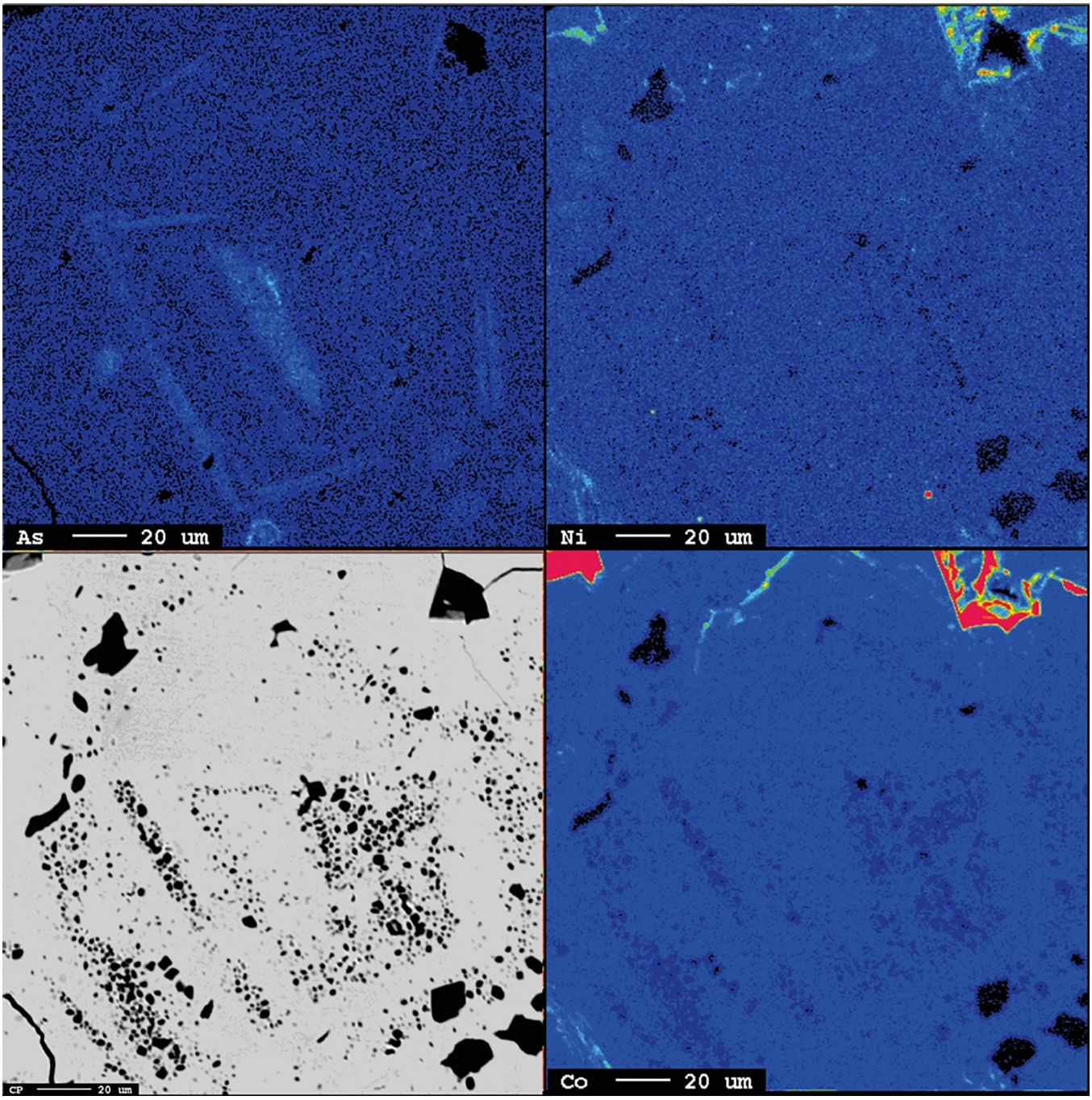

Fig. 10. Multi-element EPMA mapping (blue of pyrite grain exhibiting growth bands which are in part re-traced by inclusions (bottom-left BSE image). Nickel concentrations are below quantifiable limits (< 180 ppm). Cobalt is quite evenly distributed within the grain with median concentrations of 770 ppm. Arsenic is the element that shows the most pronounced variation ranging from below detection (350 ppm) to 640 ppm in the relatively As-rich core. The inclusions do not show any enrichment in Ni, Co or As, which makes it unlikely that they represent Fe-thiosulfates that were identified as intermediate sulfur compounds in pyrite by Kucha and Barnes (1995).

range of 230–245 °C (see also Discussion Fig. 17).

4. Discussion

An increasing number of studies (e.g., Glikson-Simpson and Mastalerz, 2000; Hagemann et al., 2016) highlight the importance of discussing the factors and processes that lead to the formation of mineral deposits in a wider context. The mineral system concept aims to eventually lead to better predictive models for ore deposits and hence more accurate targeting of mineralization at depth. Similar to petroleum systems, where everything revolves around defining a source, migration pathways and a trap, mineralization in sedimentary units is often associated with the presence of a (organic) reductant and fluid pathways that transport metal rich brines to the final depositional site (e.g., McConachie et al., 2000; Taylor, 2000). A conducive tectonic framework, metal, chlorine and sulfur sources, pathways for fluids, driving mechanisms, mixing of fluids, and physico-chemical gradients that lead to the precipitation of ore minerals in a specific setting are crucial aspects that are often ill-defined or entirely unknown, especially in areas with thick overburden. We discuss these aspects in the following sections and present a summary of published data and existing genetic models for the different types of mineralization within the LSB and ABB with their geological, spatial, and temporal context (Table 1). The basin evolution is illustrated in

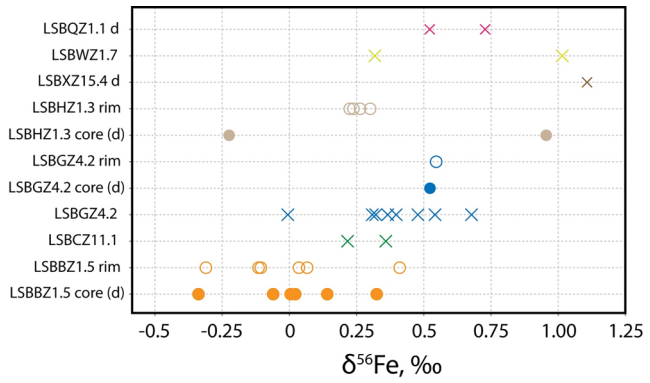

Fig. 11. δ^{56}Fe values for pyrite from the LSB. Core and rim refer to the center and peripheral area of the pyrite grains, d indicates a diagenetic origin, d in brackets assumes a diagenetic origin but a hydrothermal formation of the grain cannot be excluded. For methods see Electronic Appendix 7.6.2.

Fig. 15 and shows maximum temperatures reached during burial in the NEGB and the LSB before basin inversion. Active fluid systems in the NEGB and Harz Mountains (I, II, III, and IV) as well as base metal mineralization of the Polish Kupferschiefer (A, B, C, and D) are included in this context.

4.1. Mineralogy and mineral chemistry

4.1.1. Pyrite

Both diagenetic and hydrothermal pyrite are abundant mineral phases in the Ca2 carbonate in the LSB. The recorded petrographic characteristics of the early diagenetic and subsequent hydrothermal pyrite, match descriptions by Peevler et al. (2003) for pyrite in MVT deposits. Huttel (1989) described two generations of pyrite in the Ca2 dolostone, which are in good agreement our observations from the LSB. However, he did not describe any type of massive pyrite mineralization, i.e. zones where pyrite is the dominant ore mineral and has pervasively replaced the carbonate host rock or filled open spaces.

Chemical signatures of pyrite (Figs. 9 and 11) play an important role in deciphering the complex evolution of mineral deposits and can be employed to fingerprint different styles of mineralization (Abraitis et al., 2004; Bayliss, 1989; Cabral et al., 2011; Deditius et al., 2011; Huston et al., 1995; Roberts, 1982). Several authors have employed Co and Ni ratios to discriminate sedimentary, volcanic, and hydrothermal pyrite from pyrite originating from massive sulfide deposits and hydrothermal veins (Bralia et al., 1979; Campbell and Ethier, 1984; Loftus-Hills and Solomon, 1967; Marques et al., 2006; Price, 1972; Xuexin, 1984). The Co-Ni discriminant diagram shown in Fig. 9A illustrates that most of the measured pyrites from the LSB plot within the sedimentary field, at Co:Ni ratios below 1. The remainder plots in the hydrothermal field (between Co:Ni ratios of 1–5). A cluster of data points (small pyrite grains in dolostone from sample LSBBZ1.8) from the central LSB exhibits the only comparatively elevated Co and Ni concentrations and plots within the hydrothermal Sn-Mo-W-vein deposit field with Co:Ni ratios at around 1. High outliers for Co, Ni, and As concentrations can often be attributed to small (sub)-idiomorphic grains that are directly associated with stylolites (Figs. 6B and 9B). These stylolite-bound grains are interpreted as a late diagenetic/early hydrothermal pyrite generation that formed coeval with the stylolites. Minor and trace element contents in the fluids precipitating the later stage sulfides, including pyrite, therefore must have been comparatively low (Fig. 9B, anhedral cluster). This trend is also reflected in the larger hydrothermal pyrite grains from sample LSBBZ1.8 which exhibit significantly lower Co and Ni concentrations (below 10 and 100 ppm, respectively) than the smaller stylolite-bound grains with Co and Ni contents exceeding 1000 ppm. Stylolite-bound pyrite can also be interpreted as the dissolution (and precipitation) in formerly more porous zones that successively collapsed and underwent pressure dissolution and stylolitization (Rieken, 1988). Cyclical growth bands are common features among the investigated hydrothermal pyrites and can be used to track chemical changes

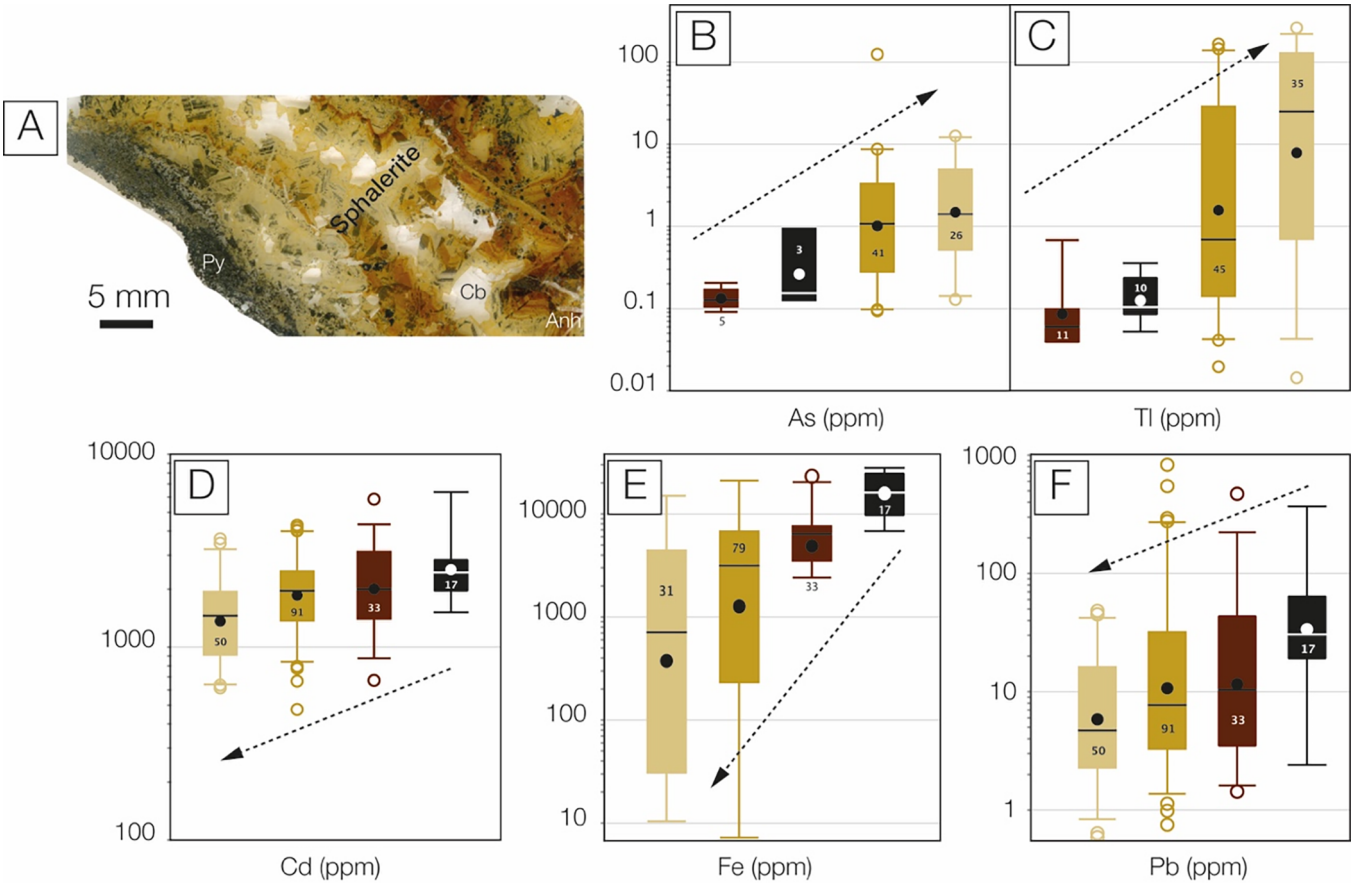

Fig. 12. Arsenic, Tl, Cd, Pb and Fe contents in sphalerite from the LSB grouped by observed color (black, dark-, medium- and light-brown). Earlier generations of sphalerite exhibit significantly higher Fe and slightly higher Cd concentrations whereas later generations can be distinguished by their relatively elevated As and Tl contents. Anh: Anhydrite, Cb: Carbonate, Py: Pyrite. See text for further discussion.

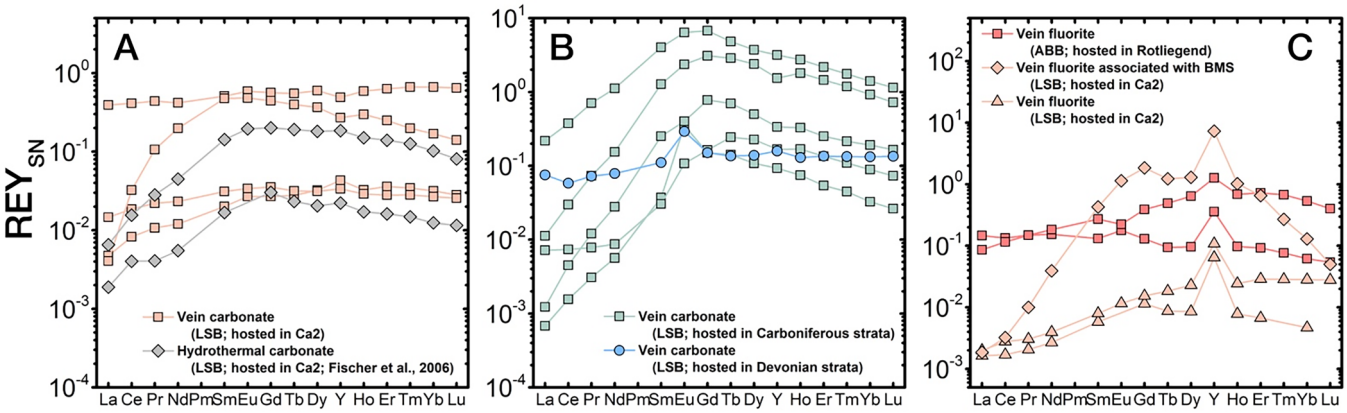

Fig. 13. Shale-normalized REY patterns of hydrothermal vein carbonates found in the LSB hosted in Ca2 (a) and underlying Carboniferous and Devonian strata (b) and of vein fluorites from the LSB and ABB in Ca2, Rotliegend and upper Carboniferous, respectively (c). The rare earth element concentrations shown here can also be found in the Electronic Appendix (Table EA 3). Data are normalized to Post-Archean Australian Shale (PAAS) by Taylor and McLennan (1985).

of mineralizing hydrothermal fluids (e.g., Large et al., 2009) and therefore give evidence of the depositional and post-depositional history of the mineralized areas (e.g. Craig et al., 1998). As illustrated by the multi-element EPMA mapping of a hydrothermal pyrite grain from the Zn-Pb-Fe sulfide mineralization in the LSB in Fig. 10, Co and Ni concentrations are commonly uniformly distributed throughout the grain while As appears to be slightly enriched in the core and certain growth bands. In combination with our preliminary δ^{57}Fe data (Fig. 11), which show no distinguishable trend for diagenetic and hydrothermal pyrite and between core and rim areas within pyrite grains, there is compounding evidence for a single hydrothermal event with a corresponding fluid that was sourced from within the Permian sedimentary rocks and redistributed (dissolved and re-crystallized) the diagenetic pyrite and other pre-existing Fe-sources. An external fluid and iron source, especially of magmatic origin, can be ruled out, as this would be reflected in the δ^{57}Fe data (Horn et al., 2006; Markl et al., 2006) and would contradict published fluid inclusion studies and temperature estimates (e.g., Sośnicka and Lüders, 2018a).

4.1.2. Sphalerite

Sphalerite can incorporate a wide range of foreign cations (e.g., Cook et al., 2009), including concentrations of up to several weight percent of Ga, Ge, and In (Alfantazi and Moskalyk, 2003; Höll et al., 2007; Moskalyk, 2003). Furthermore, it has been shown to exhibit distinct compositional variations across different types of hydrothermal deposits, reflecting formation conditions (Cook et al., 2009; Möller et al., 1983; Palero-Fernández and Martín-Izard, 2005; Ye et al., 2011; Zhu et al., 2016). Strongly zoned minerals such as sphalerites and fluorites are characteristic of post-Variscan mineralization and record changing physical and chemical conditions of the mineralizing fluid(s) (e.g., salinity and temperature, Chapter 3.3) caused by gravitational induced migration, seismic pumping, or pronounced local variability of these governing factors (Behr et al., 1987; Knorsch, 2017; Nadoll et al., 2018).

Sphalerite from the Ca2 carbonate in the LSB exhibits two pronounced compositional trends that correspond with varying sphalerite colors (Fig. 12). Darker (black, dark brown) varieties display significantly higher Fe, Cd, and Pb concentrations whereas the lighter (light brown, beige) varieties have lower Fe, Pb, and Cd but considerably higher As and Tl concentrations. Similar patterns have been observed in sulfides from Polish MVT deposits which were interpreted to represent early (high Fe and Cd, low As and Tl) and late stages (low Cd and Fe, high As and Tl) of mineralization, reflecting fluids that had interacted with different aquifers over time (Sverjensky, 1989; Viets et al., 1996). Fluid-rock interaction and spatial or temporal changes of the fluid are likely to have been governing factors; intrinsic crystallographic controls similar to those described by Nadoll et al. (2018) for fluorite from the LSB may have also contributed to these distinct compositional variations. Knorsch (2017) conducted a detailed investigation of geochemical signatures in sphalerite from the hydrothermal sediment-hosted Zn-Fe-Pb mineralization the LSB. His results show that the overall minor and trace element concentrations in sphalerite, and specifically Ga and In contents are low compared to sphalerite that formed under similar conditions in MVT deposits. He also presents data that strongly suggest that the mineralized zones within the Ca2 dolomite are epigenetic sediment-hosted Fe-Zn-Pb deposits that resemble MVT deposits and were formed at temperatures well below 200 °C, concurring with temperature estimates of ~160 °C by Sośnicka and Lüders (2018a).

4.1.3. Carbonates

Rare earth element and Y abundance, fractionation and anomalies in carbonate minerals such as calcite, magnesite, siderite or dolomite are indicative of 1) the composition of the fluids in which the minerals formed, 2) the chemical composition of the precursor material (i.e., country rock), 3) whether the carbonates are primary or secondary and 4) the physico-chemical environments which the fluid experienced (Bau and Möller, 1992; Debruyne et al., 2016; Möller et al., 1983; 1989). Fischer et al. (2006) investigated the geochemical compositions of carbonates in veins and veinlets in drill cores from the NGB. They found that vein carbonates in the NGB can be subdivided, based on their mode of formation, into three distinct groups: A) Early-stage diagenetic carbonates with seawater-like REY_{SN} patterns, B) late diagenetic carbonates with shale-like (flat) REY_{SN} patterns and C) carbonates with bell-shaped patterns which commonly occur together with Zn-Fe-Pb sulfides and which are interpreted by Fischer et al. (2006) to be hydrothermal in origin. According to them, the latter group formed under elevated temperatures and under reducing conditions. It is noteworthy, that the vein carbonates in the LSB that are associated with Zn-Fe-Pb sulfides were found in drill cores from sites that were significantly enriched in CH_4 compared to other sites east of Osnabrück (Fischer et al., 2006). Some carbonates, such as the fracture-filling carbonate found in LSBHZ2.1, are indeed showing the REY_{SN} patterns of Fischer et al.'s (2006) group C (*Hydrothermal*) in Ca2, which are associated with the occurring sediment-hosted Zn-Fe-Pb sulfides (Fig. 13). The Devonian-hosted vein calcites found in drill core LSBQZ do not show REY_{SN} patterns indicative of hydrothermal mineralization (as defined in Fischer et al., 2006), but exhibit REY_{SN} patterns closely resembling marine carbonates (Tostevin et al., 2016) with positive Eu_{SN} anomalies (Fig. 13). Europium is either di- or trivalent in aqueous solutions and its speciation depends mainly on temperature and to lesser extents on pressure and pH (e.g., Bau, 1991; Lottermoser, 1992; Wood, 1990). Bau (1991) indicated that Eu^{3+} can be reduced to Eu^{2+} in acidic, reducing hydrothermal fluids at temperatures exceeding ca. 250 °C. Europium is therefore decoupled from its strictly trivalent REY neighbors and behaves markedly different, resulting in a fluid enriched in Eu relative to the other REY and a positive Eu_{SN} anomaly, which is also manifested in Ca-bearing minerals (Fig. 13). The positive Eu_{SN} anomalies found in the hydrothermal calcites may therefore indicate that the fluid, at some stage during its evolution and prior to mineral precipitation, was reducing and may have reached temperatures in the range of or higher than 250 °C. The REY_{SN} patterns of the investigated vein carbonates are similar to those found in the marine carbonate host rocks and hence suggest local and very limited mobilization of REY from the marine carbonate host rocks to vein calcites. Hence, it is reasonable to assume that parts of the mineralization found in the LSB are related to significant hydrothermal activity and especially the area around Osnabrück might have been affected by an external heat source such as the postulated Bramsche Massif (Will et al., 2016). This scenario is further supported by positive Eu_{SN} anomalies in hydrothermal vein calcites from the southern LSB as indicated above. Moreover, the REY signatures of carbonate gangue minerals are suitable proxies for the deeply-covered Zn-Fe-Pb sulfide

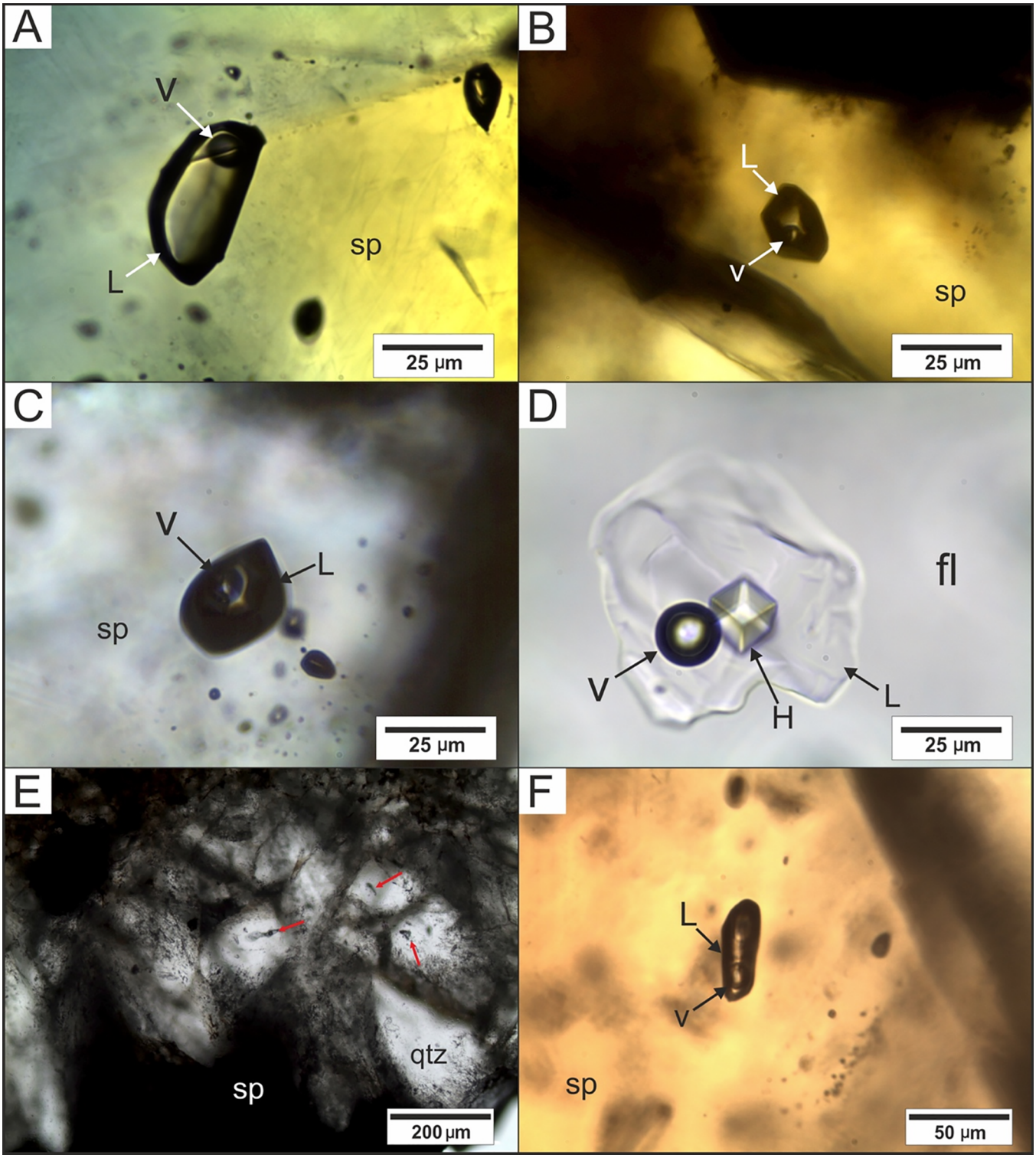

Fig. 14. Microphotographs of fluid inclusions: A, B – two-phase (L + V) aqueous primary isolated fluid inclusions hosted in yellow to orange sphalerites (sp) from the western part of the LSB, C – two-phase (L + V) aqueous fluid inclusion with typical dark appearance hosted in colorless sphalerite (sp) from vein style mineralization in the central part of the LSB, D – three-phase aqueous brine inclusion (L + V + H) hosted in fluorite (fl) vein from the central part of the LSB, E – isolated fluid inclusions (marked by red arrows) in quartz (qtz) crystals intergrown with dark sphalerite (sp) from Perm mine, southern part of the LSB, F – sphalerite (sp)-hosted fluid inclusion from fracture-filling mineralization hosted by Devonian carbonate.

mineralization in the LSB as shown from characteristic bell-shaped REY_{SN} patterns in sulfide-associated carbonate gangue (Fischer et al., 2006). Vein carbonates, therefore, record the REY signature of the fluids and are valuable tools for deciphering and constraining potential metal sources and fluid pathways.

4.1.4. *Fluorite*

Fluorite of diagenetic and hydrothermal origin occurs in all investigated areas but is commonly limited to small disseminated grains or sub-economic veinlets and open space fillings. Möller et al. (1980) showed that diagenetic fluorite formation is linked to the formation of dolomite from calcareous sediments due to

Table 1
Overview table summarizing data on mineralization and associated fluids from different structural units in the South Permian Basin in Northern Germany, namely Flechtingen-Calvörde Block (FCB), Harz Mountains, North-Eastern German Basin (NEGB) and Lower Saxony Basin (LSB). Compiled from Sośnicka and Lüders (2018a), Wüstefeld et al. (2017), Will et al. (2016), Adriasola-Muñoz et al. (2007), Nollet et al. (2005), Schmidt Mumm and Wolfgramm (2004, 2003a, 2002), Lüders (1996), Lüders and Möller (1992), Lüders et al. (2009, 2005, 1993), Reutel et al. (1995), Stedingk et al. (1995).

	Mineralization		Host rocks	Documented fluid types and their origin	Salinity [wt.%NaCl equiv.]	T [°C]	Probable sources of metals and F	Timing of fluid flow
Flechtingen-Calvörde Block	hydrothermal, vein-type	Si-Ca	Lower Permian rhyolitic and andesitic volcanic rocks/Upper Carboniferous	H_2O-NaCl, hydrothermal-magmatic origin (?)	< ~5	>200	-	late stages of Variscan magmatic activity
		Ba-F, F-Ba, Ca, Fe		H_2O-NaCl-(?) H_2O-NaCl	~24-28 ~31 ~1-25	>170 110-178 148-200 148-172 154-167	Fe: Carboniferous and/or Rotliegend volcanics; F-Ca: granite intrusion (?)	Early Triassic to late Cretaceous
Harz Mountains		W, Sb	deformed Paleozoic rocks: Ordovician-Permian	H_2O-NaCl, metamorphic fluids	<5	110-190	unknown	Late Variscan
		F-(Ca)		H_2O-NaCl-$CaCl_2$ brines, granite alteration fluids	~29-36	220-290 270-300		
		Pb-Zn(Ag)		H_2O-NaCl-$CaCl_2$ basement brines of metamorphic origin	22-35	<250 120-150		Late Triassic to Jurassic
		Ba-Fe						Jurassic
		Ba-F, F-Ba		unknown	unknown	unknown	remobilization of F mineralization	Late Cretaceous, basin inversion
North-Eastern German Basin - NEGB	hydrothermal, vein-type	F, F-Ba Ca, Si	Carboniferous sandstones (Si, Ca)/ Upper Rotliegend& Zechstein (F, F-Ba)	H_2O-NaCl±KCl (± Mg, K, Ca, SO_4^{2-}) enriched in Li, Na, K, Cs /±CH_4-CO_2 gas mixtures	9.8 - 16.5 <10	200	leaching of Upper Carboniferous sediments, Rotliegend volcanics	early basin subsidence, early extensional rifting, vanishing stages of Variscan orogeny
				H_2O-NaCl-$CaCl_2$ basinal brines rich in Na, Ca, Mg, Ba, Pb, Zn, Mn /±N_2-CH_4 gas mixtures; late fluids enriched in Fe	<35 25-33 <10	<300 120-180 130-150		basin subsidence and inversion
Lower Saxony Basin - LSB	stratiform, massive and hydrothermal, vein-type	Zn	Devonian carbonates (Massenkalk)	H_2O-NaCl	18.2-19.8	230-245		Variscan (?)
		Si	Carboniferous sandstones/ Upper Jurassic sandstones	H_2O-NaCl /±CH_4-CO_2 gas mixtures	13.8-15.7 3-5	220-260 200-270		Middle to Upper Jurassic, basin subsidence / Lower Cretaceous (?)
				H_2O-NaCl-$CaCl_2$ basinal brines /±CH_4-CO_2-N_2 gas mixtures	17.7-21.6 17-25 20	170-200 164-202 180-240		Late Cretaceous, basin inversion
		Zn-(Pb), Fe, F, Ca	Zechstein carbonate Ca1	H_2O-NaCl-$CaCl_2$ basinal brines	24-28	143-196	unknown	Late Cretaceous, basin uplift
			Zechstein carbonate Ca2	H_2O-NaCl-$CaCl_2$ basinal brines /±CO_2-H_2S-CH_4-N_2 gas mixtures /late CH_4-H_2S-CO_2-N_2 gas mixtures	21-32	158-214 125-208		
		Ca	Middle Buntsandstein	H_2O-$CaCl_2$-NaCl basinal brines	~17.2-24.8	55-122 ~150	dehydration of Zechstein gypsum	Late Jurassic, burial and basin subsidence

Mg^{2+} removal from pore fluids and consequent release of F^- due to breakup of MgF^+ complexes. Seawater and marine pore waters are usually undersaturated in F^- and thus precipitation of fluorite is prevented in oxygenated seawater. Organic material (Correns, 1970; Füchtbauer, 1958), freshwater influx with elevated fluorine concentrations attributed to pegmatitic sources (Kasakov and Sokolova, 1950), or a volcanogenic source (Churakov, 1947; Ivanov, 1967) have been invoked to account for the required saturation to allow the precipitation of diagenetic fluorite. Möller et al. (1976) used Tb/La vs. Tb/Ca atomic ratios of fluorites to distinguish between the different modes of formation (Fig. 16). Diagenetic fluorites have comparably low MREY/LREY ratios whereas hydrothermal and pegmatitic fluorites are significantly enriched in HREY/MREY over LREY. However, adsorption, chemical complexation, changes in temperature and salinity can lead to highly localized variations in fluorite compositions including the REE (Bau, 1991; Bau and Dulski, 1995; Möller et al., 1998; Nadoll et al., 2018; Schwinn and Markl, 2005), making it difficult to attribute different REE signatures to single controls. Usually, adsorption favors the HREE and LREE are more easily held in solution by chemical complexation (Bau et al., 2003) whereas remobilization (Mao et al., 2015) or crystallographic controls (Nadoll et al., 2018) lead to an increasing Tb/La ratio by maintaining the same Tb/Ca ratio. The fluorites found in drill cores of the LSB plot mostly within the sedimentary/diagenetic field (Fig. 16). This is in marked contrast to the Harz and ABB fluorites (Fig. 16, c.f. Nadoll et al., 2018), which plot in the hydrothermal field. The total concentration of REE in fluorites can provide a first-order indication on the potential metal source. For example, the mobilization of REE from marine source rocks will result in much lower fluid concentrations of the REE in comparison to pegmatites, which are highly enriched in REE. The rather low concentrations in LSB fluorites as shown here indicates mobilization from REY-low source rocks. Therefore, Zechstein, Carboniferous or Devonian carbonate rocks could have been potential sources for the REY in the basinal fluids. The fluorites from the ABB and Harz mountains are enriched in total REY relative to LSB fluorites, which points to a markedly different source that is enriched in REY. Potential REY-rich sources in the ABB that were also proposed by Nadoll et al. (2018) are felsic Rotliegend volcanics, which are highly enriched compared to Rotliegend basalts and carbonate rocks. Duschl et al. (2016) described two generations (I and II) of fracture-filling fluorites in Zechstein carbonates at the northern border of the NGB. Fluorite I is enriched in LREYCN and relatively depleted in HREYCN, whereas later fluorite II generation exhibits rather flat REYCN patterns with an enrichment toward the HREY. The authors attributed fluorite I to be a precipitate of a primary basinal fluid, whereas fluorite II shows REY features indicative of remobilized REY from earlier fluorites due to chemical complexation of LREY during remobilization (Duschl et al., 2016). However, Nadoll et al. (2018) argued that the observed compositional variation could also be interpreted as the result of a complex growth, controlled by physico-chemical variability and intrinsic crystallographic factors. Hence, fluorite precipitated by a single hydrothermal event but with distinctly varied compositions recorded in growth bands and sectoral zoning (Nadoll et al., 2018).

4.2. Hydrothermal fluids – sources, pathways and ore forming processes

4.2.1. LSB and ABB – Genetic models

Figs. 15–20 and Table 1 combine our data and a comprehensive compilation of relevant literature values and references to illustrate the current understanding of the genesis, evolution, and structural context of the mineralized zones in Paleozoic units of the NGB. Zones of sediment-hosted hydrothermal sulfide

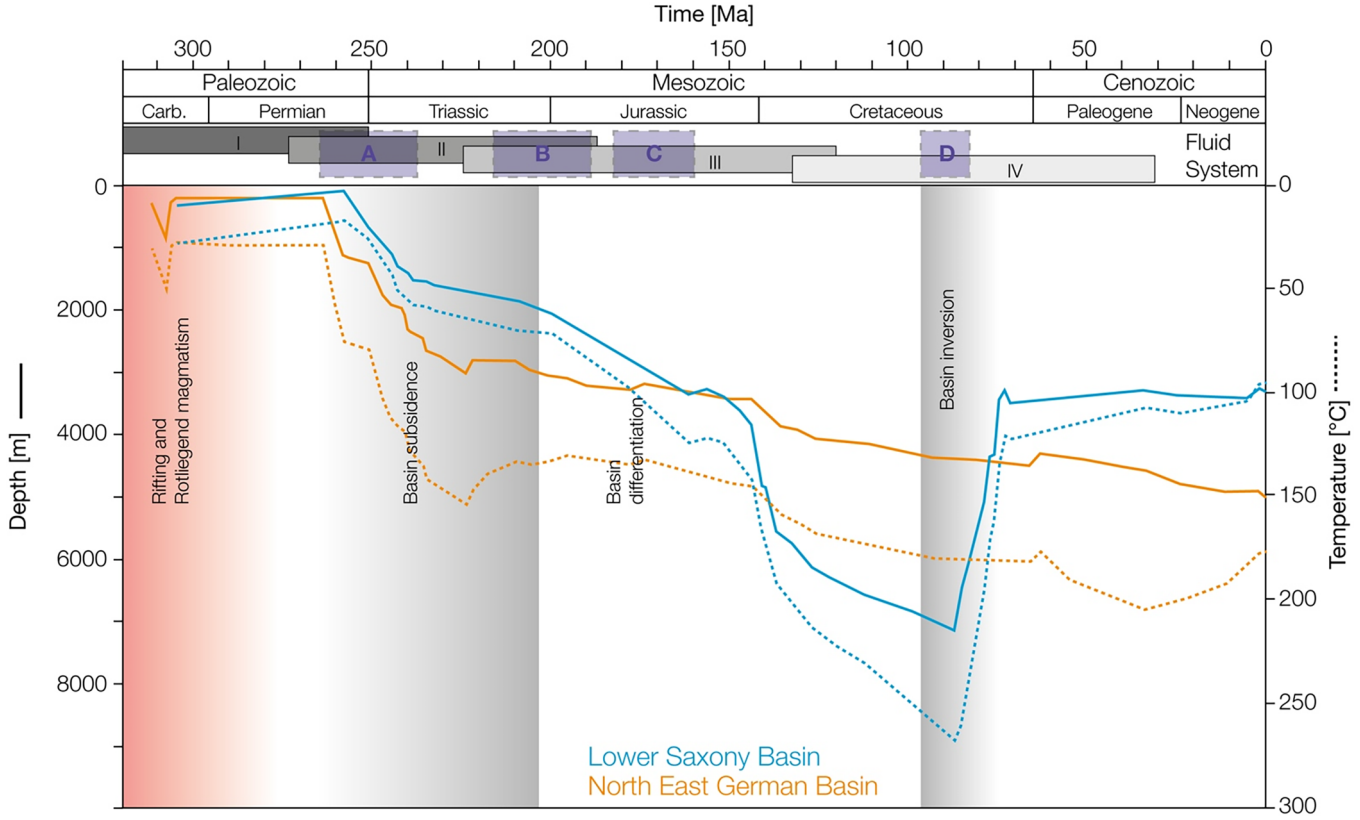

Fig. 15. Basin evolution including burial history (solid lines) and corresponding modelled temperatures (dashed lines) for the LSB (Petmecky et al., 1999) and the NEGB (i.e., ABB) as well as active fluid systems in the NEGB and Harz Mountains (I, II, III, and IV) (after Schmidt Mumm and Wolfgramm, 2004) as well as mineralization events (A, B, C, and D) in the Polish Kupferschiefer (after Alderton et al., 2016, Pletsch et al., 2010). Plotted is the burial history for the Permian base layers. Maximum burial and peak temperatures were reached in the Upper Cretaceous, before basin inversion. (Edited after Littke et al., 2008b, Petmecky et al., 1999; Schmidt Mumm and Wolfgramm, 2004).

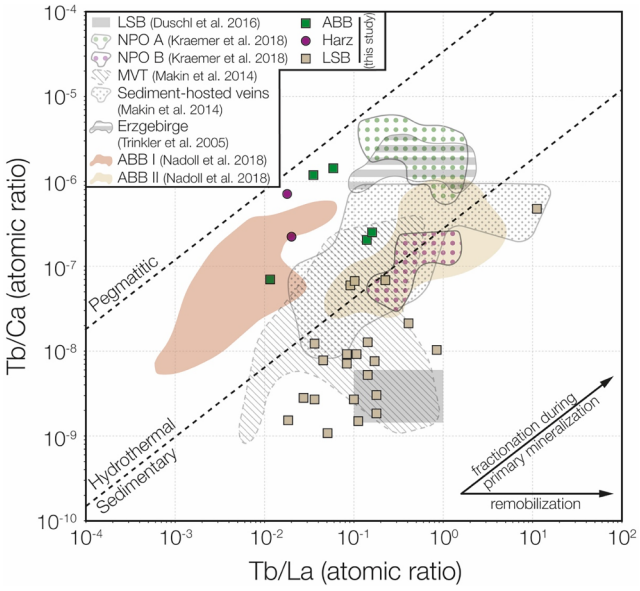

Fig. 16. Tb/La vs Tb/Ca atomic ratio plot (after Möller et al., 1980) of fluorites from the LSB, ABB and Harz (see Electronic Appendix Table EA 4). Note that all ABB fluorites plot in the hydrothermal field, whereas all LSB fluorites exhibit very low Tb/Ca ratios and are presumably sedimentary in origin. The following references are plotted as reference samples for basin-hosted fluorite mineralization: MVT and sediment-hosted veins (Makin et al., 2014), Erzgebirge (Trinkler et al., 2005), ABB I and II (Nadoll et al., 2018) and Pennine Orefield fluorites (Kraemer et al., 2018).

mineralization, specifically sphalerite and galena, have previously been documented in the LSB Zechstein Stassfurt Carbonate (Ca2) by Hubald (1988), Mempel (1962), and Mempel et al. (1965). Hubald (1988) emphasized that a magmatic-hydrothermal origin is the most likely source of the mineralization and noted that a classification as a MVT mineralization can be ruled out due to the relatively elevated temperatures (> 200 °C). Furthermore, he argued that the overall metal contents in Zechstein sediments are too low to warrant the formation of Zn-Fe-Pb sulfide ores as MVT mineralization. Dorn (1957) and Fabian et al. (1957) put the formation of base metal sulfide mineralization in direct context with a Tertiary magmatic episode, whereas Schneider (1952) interprets them as a late Variscan mineralization related to magmatic events at the end of the Variscan orogeny. Both models assume ascending magmatic fluids as the primary source for the Zn-Fe-Pb sulfide mineralization. Other authors prefer a model that links precipitation of ore minerals to descending fluids from the overlying sulfate-rich Zechstein evaporites (Lietz, 1951; Seeliger, 1950; Seidl, 1959) or metal-rich hydrocarbons (Herrmann, 1961). Hydrocarbons have also been invoked as a contributing factor for the alteration and bleaching of red bed sandstones of the lower Permian (Pudlo et al., 2011). However, it has been questioned if brines generated from the Zechstein evaporites and/or hydrocarbons have the potential to form extensive mineralization (Glikson-Simpson and Mastalerz, 2000; Mempel, 1962). Most recently, a model that favors a TSR-control and the precipitation of sediment-hosted Zn-Fe-Pb mineralization due to mixing of basinal brines with contrasting salinities and compositions at depths of up to four kilometers and temperatures up to around 200 °C has been evoked by Sośnicka and Lüders (2018a) and Knorsch (2017). Sośnicka and Lüders (2018a) presented fluid inclusion data from vein-type and massive sphalerite mineralization from Ca2 carbonates that indicate high temperatures (125–208 °C, modal T_h values:~155–165 °C) and high salinities (21–32 wt% NaCl equiv.) of sulfide-ore forming H_2O-NaCl-$CaCl_2$ fluids (Fig. 17, Table 1). Our data from Ca1-hosted quartz intergrown with sphalerite ore plot within very similar temperature-salinity range as data from the Ca2-hosted sphalerites (Fig. 17). These results indicate that Zn-Pb ore-forming fluids in the western, central and southern parts of the LSB could have been of similar nature

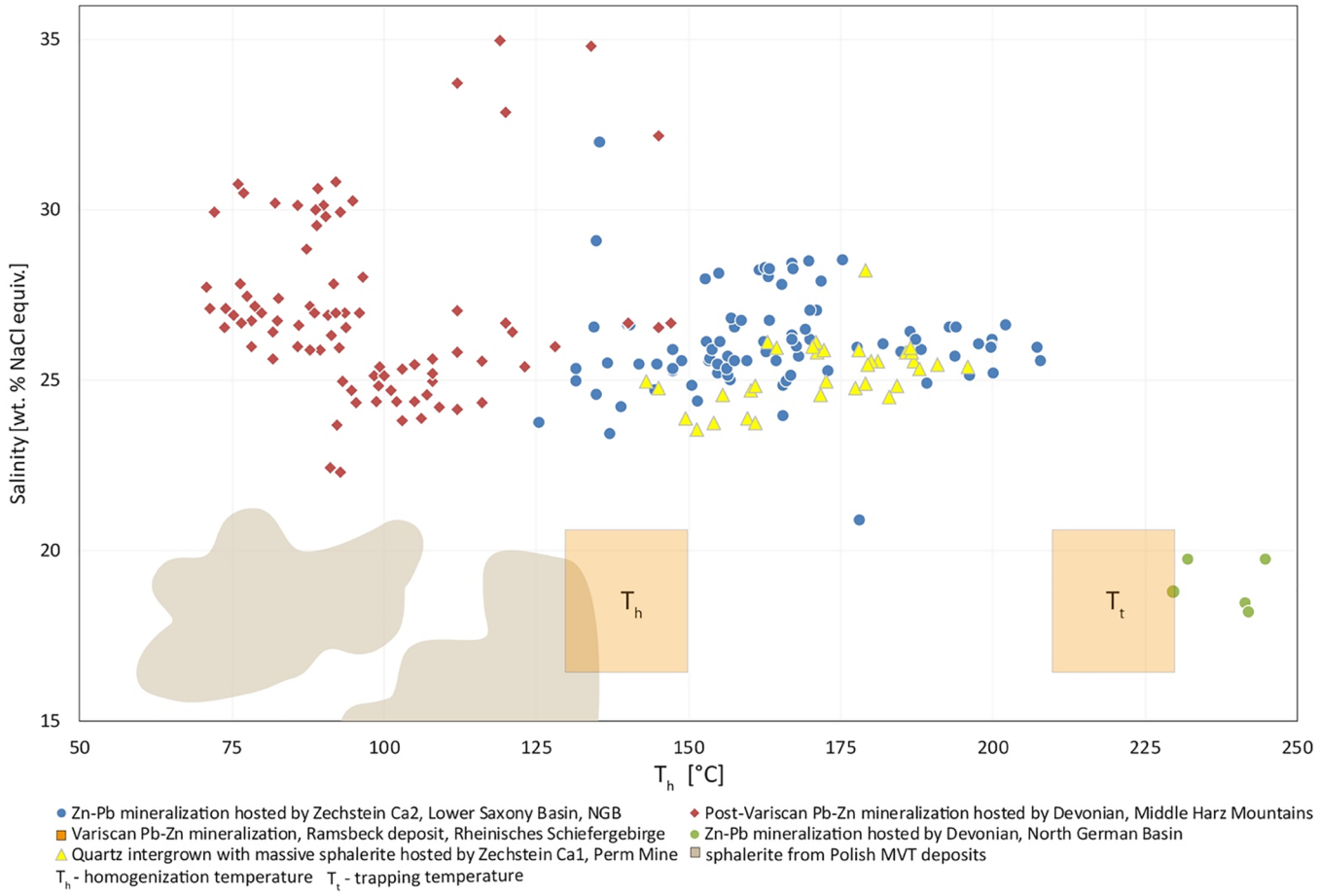

Fig. 17. Bivariate plot illustrating salinity and temperature ranges derived from fluid inclusions hosted in quartz intergrown with sphalerite ore from Perm Mine (southern part of the LSB) and sphalerite-hosted fluid inclusions from fracture-filling mineralization hosted by Devonian carbonate compared to sphalerite-hosted fluid inclusions from: Zn-(Pb) mineralization from central and western part of the LSB (Sośnicka and Lüders, 2018a), Post-Variscan Pb-Zn mineralization of the Middle Harz Mountains (Reutel, 1984), Variscan Pb-Zn mineralization of the Ramsbeck deposit in the Rheinisches Schiefergebirge (Behr et al., 1987) and Triassic-hosted sphalerite ore from Polish MVT deposits of the Silesia-Cracow Zn-Pb district after Leach et al. (1996).

regardless of the host rock. Data plot shown in Fig. 17 indicate that salinities of fluid inclusions hosted in sphalerites and studied Zn ore-related quartz from the LSB are similar to data from Post-Variscan sphalerites from the Middle Harz Mountains, however fluid inclusions from the LSB show distinctly higher temperatures. Our results also show that sphalerites from fracture-fillings in Massenkalk (Devonian) precipitated from fluids of lower salinities and higher temperatures compared to the Ca2-hosted Zn ore-forming fluids from the LSB (Fig. 17). Temperatures and salinities of the Zn-rich fluids migrating in Devonian,

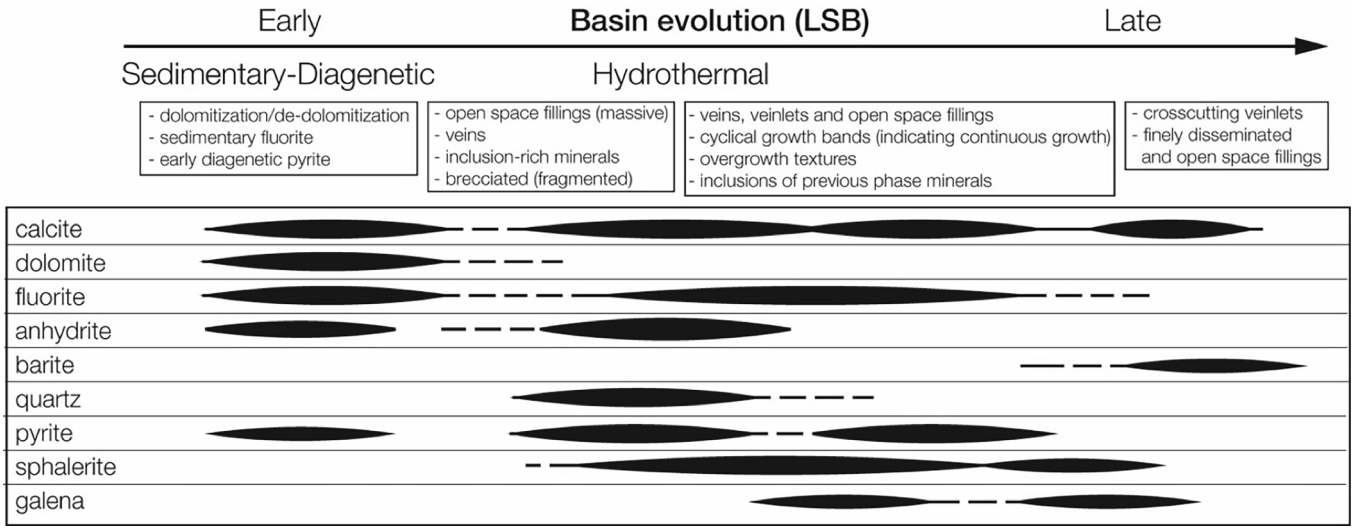

Fig. 18. Schematic paragenetic sequence for the LSB. Note that the length of the individual hydrothermal events may have been short and linked to specific tectonic events rather than a prolonged continuous system that extended temporally over the entire basin evolution (ca. 245 ma).

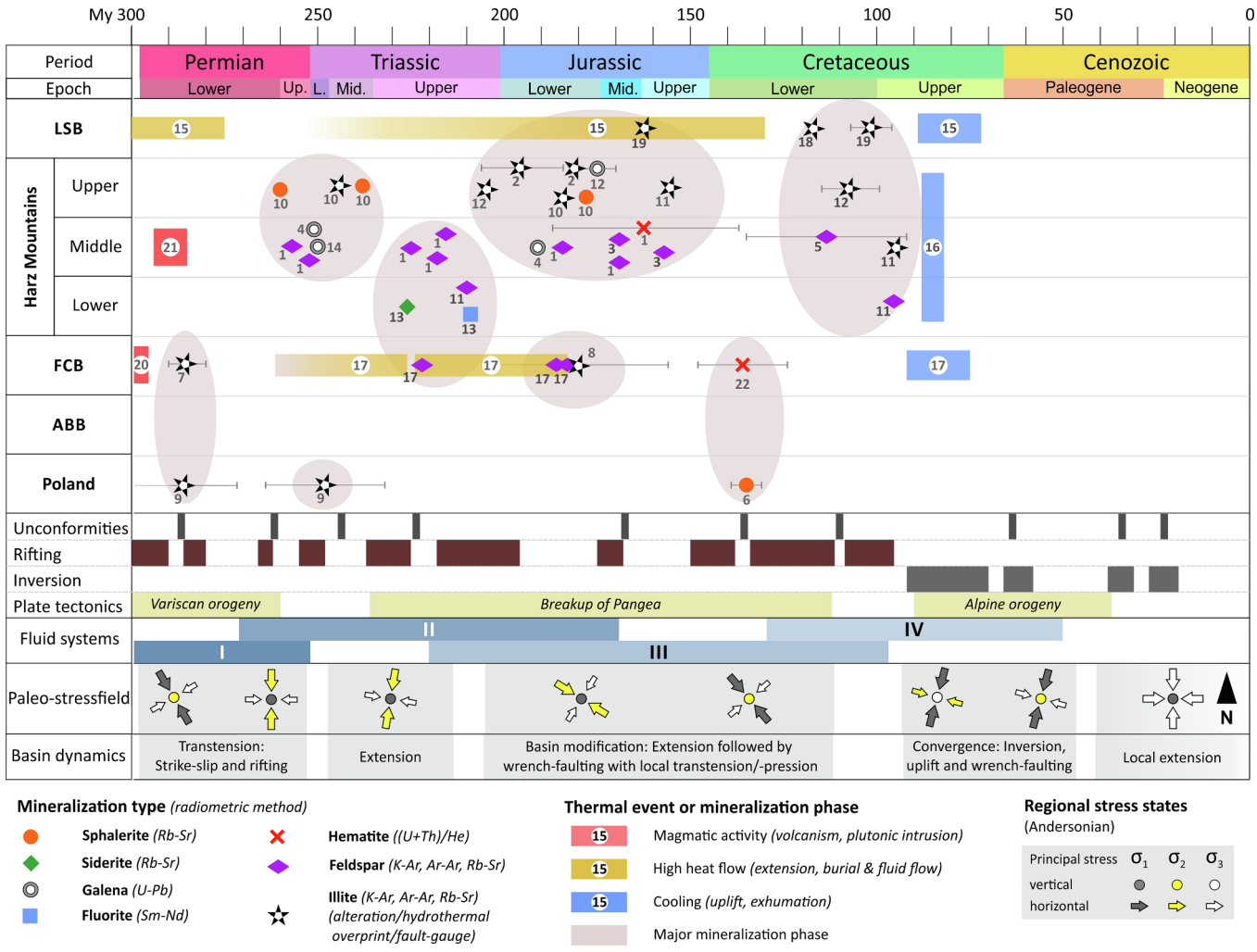

Fig. 19. Compilation of calculated and modelled ages of post-Variscan hydrothermal mineralization in the NGB and adjacent areas. The illustration also provides generalized information on basin dynamics, fluid systems (according to Schmidt Mumm and Wolfgramm, 2004), unconformities, and major paleo-stressfields (Kley et al., 2008; Pharaoh et al., 2010) in the NGB. Please note that paleo-stress directions are simplified for the NGB and may differ locally depending on fault architecture. References used in figure: (1) Hagedorn (1992), (2) Haack and Lauterjung (1993), (3) Mertz et al. (1989), (4) Tischendorf and Franzke (1993), (5) Boness et al. (1990), (6) Heijlen et al. (2003), (7) Schmidt Mumm and Wolfgramm (2003a), (8) Brecht and Wolfgramm (1998), (9) Bechtel et al. (1999), (10) Boness (1987), (11) Hagedorn and Lippolt (1993), (12) Franzke et al. (2007), (13) Schneider et al. (2003), (14) Bielicki and Tischendorf (1991), (15) Adrisola-Muñoz (2007), (16) Eynatten et al. (2008), (17) Fischer et al. (2012), (18) Will et al. (2016), (19) Wüstefeld et al. (2017), (20) Breitkreuz and Kennedy (1999), (21) Obst et al. (2001) (22) Duschl et al. (2018).

are similar to these typical of the early Variscan fluids responsible for the formation of the Pb-Zn Ramsbeck deposit in the Rhenish Massif (Fig. 17). These observations point towards a post-Variscan origin of the investigated fluids in the LSB.

The sulfide mineralization in the LSB shares many characteristics of MVT deposits. For example, MVT type deposits commonly form within platform carbonate sequences in a stable foreland basin with no spatial or temporal relation to igneous rocks (Bradley and Leach, 2003; Leach et al., 2010b). The existence and migration of hydrocarbons has also been proposed as a possible contributing factor for the formation of MVT deposits (e.g., Anderson, 2015; Anderson and Macqueen, 1988; Sverjensky, 1986), however, the crucial temporal relationship between the two remains poorly constrained (Ostendorf et al., 2015). Most Phanerozoic MVT deposits formed during contractional events with extensional faults and wrench tectonics (e.g., Condie, 2000; Leach et al., 2001). Similarly, the LSB mineralization is found in porous carbonate host rocks that were deposited in a shallow marine platform environment associated with thick evaporite successions that provided sulfur (Sośnicka and Lüders, 2017). Several studies have shown that the processes responsible for the formation of many MVT deposits were only active for relatively short time periods, i.e., 1ks to several 10ks years (Leach et al., 2010b; Repetski and Narkiewicz, 1996; Rowan and Goldhaber, 1995). Based on our petrographic and geochemical data we see evidence for short ore formation pulses related to tectonic events (i.e., wrench faulting and basin inversion in the LSB) and fluid flow along faults and folds and rapid mixing of basinal brines as well as continuous, cyclical ore formation. In the LSB, the occurring sulfide mineralization display ore textures that reflect cyclical growth and undisturbed crystallization, even though colloform textures have not been observed. Rapid processes, i.e., fracturing and brecciation of previous ore stages, can also commonly be found in mineralized samples from the LSB (Fig. 18).

Fluid inclusions showing analogous high salinities to our data were reported by Roedder (1984, and references therein), in sphalerites within vugs hosted by Paleozoic carbonates from Ohio, New York, Iowa, Missouri and Tennessee (USA). The authors suggested a common link between these occurrences and MVT Zn-Pb deposits. European MVT deposits of the Silesia-Cracow Zn-Pb district (Poland) indicate that ore-forming fluids in this ore district have never reached salinities and temperatures as high as those typical of ore-forming fluids responsible for the formation of Zechstein-hosted deposits in the NGB (Fig. 17). This difference stems most probably from the distinct origin and nature of the fluids involved in mixing processes in these settings.

The earliest fluids within the ABB are represented by H_2O-NaCl ± KCl fluid inclusions trapped in quartz-chlorite veins crosscutting Carboniferous sandstones (Lüders et al., 2005). These inclusions are enriched in Li, Na, K, and Cs and show medium to high salinities up to 16.5 wt% NaCl equiv. (Table 1) (Lüders et al., 2005). Schmidt Mumm & Wolfgramm (2004, 2002) reported traces of similar medium salinity fluid in early diagenetic quartz, dolomite, calcite, and locally

halite and barite, within Carboniferous and upper Rotliegend strata. These low to medium salinity (< 10 wt% NaCl equiv.) inclusions are compositionally NaCl-dominated, with addition of lesser Ca, Mg, K and sometimes dissolved sulfate (Table 1). Schmidt Mumm and Wolfgramm (2002) suggested that the earliest fluid was associated with early extensional rifting and diminishing stages of the Variscan orogeny and that it was also involved in the early replacement of sulfates and/or their partial re-crystallization as well as compaction and cementation processes. Early aqueous fluids were migrating along with CH_4-CO_2 gases at temperatures of about 200 °C (Table 1) and pressures of ~750 bars during the early stages of basin subsidence (Lüders et al., 2005).

Later, high salinity, H_2O-NaCl-$CaCl_2$ brines were observed as fluid inclusions in younger generation of quartz fracture-fillings hosted by Carboniferous sandstones (Lüders et al., 2005). High-salinity fluid inclusions of similar composition are also contained in quartz, calcite, fluorite, anhydrite and halite in cements and/or fracture-fill mineralization hosted by Rotliegend sediments and Zechstein evaporitic units (Schmidt Mumm and Wolfgramm, 2004, 2002). These fluids show much more elevated concentrations of Na, Ca, Mg, Ba, Pb, Zn, Mn and lower K content compared to the early fluids (Table 1) (Lüders et al., 2005). High-salinity fluids (< 35 wt% NaCl equiv.) that precipitated anhydrite-calcite-siderite hydrothermal veins within the basal units of the ABB reach minimum temperatures of up to 300 °C (Schmidt Mumm and Wolfgramm, 2002). Lüders et al. (2005) suggested that the high-salinity fluids gained their compositions by fluid interaction with sedimentary rocks during burial to great depths.

Aqueous, high-salinity fluid inclusions were contemporaneously trapped with the low density N_2-CH_4 gas mixtures in fracture-filling minerals hosted by Permian strata at minimum temperatures of 120–180 °C and low pressures of 200–400 bars (Lüders et al., 2005). These P-T conditions indicate entrapment during the Upper Cretaceous inversion of the basin (Lüders et al., 2005). Similar fluid inclusions of high-salinity and minimum temperatures of 130–150 °C associated with N_2-CH_4 gas inclusions are also hosted in vein fluorite within Rotliegend sandstones (Table 1) (Lüders et al., 2009). According to Lüders et al. (2009) Rotliegend, high-salinity, formation waters in the ABB were mobilized into the NW-trending, deep-seated faults during uplift in the Upper Cretaceous and were most likely responsible for the formation of hydrothermal F-Ba veins and/or they may represent archives for long-term (> > 10–100 Ma) water-rock interaction. The origin of saline brines in sedimentary basins is however still very much debated (Kloppmann et al., 2001; Möller et al., 2017; Regenspurg et al., 2016). The study of deep formation waters in the ABB provides evidence that formation waters intensely interacted with K-rich minerals in Rotliegend sandstone and/or volcanic rocks and that their composition was not influenced by the influx of any younger meteoric fluids (Lüders et al., 2010, 2009). Our study indicates that formation waters from Rotliegend sandstones from ABB are significantly enriched in Pb with 83–170 mg/l and Zn with concentrations reaching up to 330 mg/l (Table EA7). The Pb and Zn concentrations in the formation waters are comparable to those in fluid inclusions from fracture-filling minerals in Rotliegend sandstones (Lüders et al., 2005), where 150–678 mg/l Pb and 554–1811 mg/l Zn were found. Hence, the compositional similarity between formation waters and the fluid inclusions from the ABB indicate that (i) the formation waters are modern analogues to the fossil fluid systems that lead to the mineralization found in the ABB or (ii) the formation waters have interacted with deeply buried hydrothermal mineralization.

4.2.2. Heat, sulfur and metal sources

The hydrothermal system in the LSB could have been triggered by a short-lasting heat flow within the thermal aureole generated by an igneous intrusion, i.e., the Bramsche Massif (Will et al., 2016). The maximum age of the inferred hydrothermal system related to this hypothetical intrusion is Lower Cretaceous (117 ± 2 Ma) (Will et al., 2016) (Fig. 19, Table 1). Other authors suggested that it was active during the Upper Cretaceous basin inversion (Buntebarth and Teichmüller, 1979; Mundry, 1971; Rose and Gödecke, 1984). Furthermore, a study of hydrothermal fluorites suggest that it could have been active prior to basin inversion in the northern part of the LSB (Duschl et al., 2016). Widespread contact-metamorphic alteration—sericitic alteration, intense silicification and the occurrence of pyrophyllite confine the temperature range to 200–270 °C (Will et al., 2016). The alteration and high thermal maturity, evident in high vitrinite reflectance values (Teichmüller and Teichmüller, 1985), have been attributed to be the thermal footprint of the Bramsche Massif (Scherp and Stadler, 1968; Stadler and Teichmüller, 1971). No such evidence for potential igneous activity has been reported for the ABB. The existence of the Bramsche Massif in the LSB, however, is still contentious and high thermal maturity and hydrothermal mineralization can also be explained by deep burial followed by basin inversion and the introduction of a hydrothermal system that developed along faults during basin rifting (Adriasola-Muñoz et al., 2007; Brink, 2013, 2002; Bruns et al., 2013; Petmecky et al., 1999; Reutel and Lüders, 1998; Stadler and Teichmüller, 1971; Wüstefeld et al., 2017).

Sulfur isotopic data from the ABB indicate prevailing sedimentary sources of sulfur in sulfides (pyrite and chalcopyrite) and, in contrast, magmatic (e.g. Rotliegend volcanics) and Zechstein evaporites for sulfur in sulfates (barite and anhydrite) (Schmidt Mumm and Wolfgramm, 2002). Based on sulfur isotope data the reduced sulfur source for sulfide mineralization across the LSB was ascribed to the Zechstein reservoir carbonate where hydrogen sulfide has been produced by TSR (Sośnicka and Lüders, 2018a). Sulfur isotope data collected by Knorsch (2017) agree with these findings. However, as an early stage sulfate-reducing process BSR is likely to have played a role as well, especially at lower temperatures where TSR is not efficient. Carbon isotope signatures of fluid inclusion gases from hydrothermal minerals indicate that methane has been participating in the TSR (Sośnicka and Lüders, 2018a, 2018b). This implies that composition of gases accompanying fluid migration might have acted as an important control for the sulfide formation in the LSB. Following this concept, the absence of sulfide mineralization in the ABB could be explained by the predominance of nitrogen-rich gases as evidenced from fluid inclusions or lack of mixing with sulfur-rich Zechstein fluids.

High-salinity fluids in the Rotliegend units in the ABB are characterized by elevated Zn and Pb contents (Lüders et al., 2005). Our investigation also found elevated metal contents in Rotliegend formation waters. This further substantiates a first principle assumption that Permian volcanic rocks and/or Carboniferous sandstones/shales (Fig. 5) may be potential sources of ore-forming metals within other mineralized sub-regions of the NGB. Carboniferous tight gas sandstones and Zechstein carbonates in the LSB are of great importance for gas and petroleum exploration as they constitute the reservoir rocks for CH_4-rich gas and oil, which were expelled from Westphalian coals and Posidonia and/or Wealden organic-rich shales. These units may also have acted as a metal source that was leached by deeply penetrating basinal brines of upper Permian origin. Similarly, Schmidt Mumm and Wolfgramm (2003a) suggested upper Carboniferous and Rotliegend volcanic rocks as metal sources.

4.2.3. Structurally-controlled fluid pathways

Fluid systems and their evolution and close link with structurally controlled pathways play a key role in understanding the mineralization processes within the NGB (Table 1). Elevated heat flow and faulting during tectonically active periods such as extensional tectonics and basin inversion are likely to have induced increased fluid migration along (re)-activated fault structures. Fluid migration, fluid mixing, and subsequent ore mineralization in sedimentary basins strongly depend on the existence of these pathways, i.e., mostly (sub)-vertical planar structural elements such as fractures, fault zones, stylolites, etc. that may serve as inter- or intraformational fluid conduits. These structural features are controlled by regional tectonics such as rifting, wrench faulting or reverse faulting and therefore relate to intra-plate crustal dynamics (Littke et al., 2008a). Fig. 19 shows a compilation of modelled and calculated radiometric mineral ages, as well as thermochronological evidence for crustal heating and cooling from the NGB and, to a minor extent, the adjacent Polish Trough that reflect superior trends in terms of crustal deformation, fluid flow and ore mineralization with regard to basin dynamics. In addition, previously established fluid systems for the study area (Schmidt Mumm and Wolfgramm, 2004), as well as regional paleo-stress regimes and major unconformities (Kley et al., 2008; Pharaoh et al., 2010) are presented in Fig. 19 as well. Some of the shown ages are modelled ages and may therefore not reflect true formation ages. However, correlations between basin dynamics, mineralization stages, and fluid systems throughout the NGB can still be established.

Early Permian crustal modification in the NGB is characterized by transtension tectonics beginning with a phase of dextral strike-slip faulting and the formation of WNW-ESE striking steep faults during early Rotliegend. It was subsequently replaced by a first rifting stage that resulted in N-S to NNE-SSW striking graben and halfgraben systems (Gast and Gundlach, 2006). In terms of heat flow and hydrothermal activity, this structural development is accompanied by hydrothermal fluid flow and illite formation due to host rock alteration in the FCB and Poland (Schmidt Mumm and Wolfgramm, 2003b), as well as magmatic activity in the FCB (Breitkreuz and Kennedy, 1999). In the LSB, this period is recorded in the reset of fission-tracks due to increased heat flow, as reported by Adrisola-Muñoz (2007). During the late Rotliegend and Zechstein graben formation was continued due to extensional tectonics that affected the whole NGB and resulted in regional subsidence. This second Permian rifting phase was preceded by crustal relaxation resulting from thermal subsidence and coincides with dating results for fracture-hosted hydrothermal deposits in the Upper and Middle Harz

(Boness, 1987; Gast and Gundlach, 2006; Hagedorn, 1992).

As illustrated in Fig. 19 and Table 1 a variety of mineralization ages and hydrothermal overprint data cluster around the late Permian and early to mid-Triassic. Fault gauge-related illite ages from the Upper Harz and Poland provide strong evidence for hydrothermal alteration (Bechtel et al., 1999; Boness, 1987). Similarily, galena, adularia, and sphalerite ages confirm intense fluid flow and ore mineralization in the Upper and Middle Harz during this time period (Bielicki and Tischendorf, 1991; Boness, 1987; Hagedorn, 1992; Tischendorf and Franzke, 1993). Burial of the LSB was initiated at the same time, as increasing temperatures suggest (Adrisola-Muñoz, 2007). Simultaneously, the FCB experienced an intense thermal event with temperatures between 200 and 250 °C due to rapid burial during the Triassic as partial reset of zircon fission tracks in upper Rotliegend sandstone confirm (Fischer et al., 2012). The same study could verify intense fluid flow in the FCB during Triassic and early Jurassic using K-feldspar ages. The late Permian – early to mid-Triassic mineralization continued during late Triassic as another cluster of mineralization ages from the Middle and Upper Harz shows (Hagedorn, 1992; Schneider et al., 2003). The Triassic mineralization stage was likely controlled by regional WNW-ESE directional extension, which locally resulted in the formation of NNE-SSW striking graben systems throughout the NGB (Fig. 1, Gifhorn Trough) and caused regional subsidence of the whole area in general (Kley et al., 2008).

Triassic extension was followed by a period of increased burial and basin differentiation forced by transtension tectonics that prevailed from early to late Jurassic and affected the whole NGB. The tectonic framework can be generalized as a time of NE-SW directional basin extension due to episodes of wrench faulting, strike-slip faulting and normal faulting along NW-SE to WNW-ESE striking faults that often reflect predominant trends of older (i.e., Variscan) fault systems in the SPB (Pharaoh et al., 2010). This phase of severe structural basin modification and burial correlates with a dominant cluster of mineralization ages from the LSB, Harz, and FCB that prove intense crustal deformation and fluid flow throughout most of the NGB. In the Harz and the FCB fluid-rock interaction is expressed by illite formation (Boness, 1987; Brecht and Wolfgramm, 1998; Franzke et al., 2007; Haack and Lauterjung, 1993; Hagedorn and Lippolt, 1993) while fracture-hosted mineralization is indicated by different stages of adularia, galena, sphalerite, and hematite formation (Boness, 1987; Hagedorn, 1992; Mertz et al., 1989; Tischendorf and Franzke, 1993). In the LSB, thermochronological analysis along with illite dating revealed a constant high heat flow and hydrothermal activity (Adrisola-Muñoz, 2007; Wüstefeld et al., 2017). This trend of increased fluid circulation and heat flow during Jurassic times is also supported by observations from other locations in the SPB as diagenetic illite (chlorite-illite assemblage) ages from Permian sandstones from the North Sea area indicate (Ziegler, 2006). This period can be summarized as the main post-Variscan mineralization phase in the NGB, its formation was possibly controlled by the development of locally deep-reaching structurally-controlled fluid pathways under extensional and transtensional tectonic regimes that favoured basin-wide fluid circulation and mixing of basinal and basement brines (Franzke and Zerjadtke, 1993).

In the early Cretaceous maximum burial and therefore peak temperatures in the LSB were almost reached (Littke et al., 2008a) when basin extension slowly ceased. This phase of basin evolution is also expressed by hematite and Pb-Zn mineralization in the FCB and Poland, respectively (Duschl et al., 2018; Heijlen et al., 2003). Hematite mineralization in the FCB furthermore coincides with a time of strike-slip tectonics in the SPB when Mesozoic subbasins such as the LSB and the Subhercynian Cretaceous Basin, among others, formed pull-apart basins that experienced transtension during late Jurassic-early Cretaceous, while adjacent highs such as the FCB where simultaneously uplifted due to transpression (Scheck-Wenderoth et al., 2008). However, the lack of data on mineralization ages from the Harz and the LSB may suggest a reduced hydrothermal activity in the NGB until mid-Cretaceous times, as formation ages of illite and adularia imply a new phase of tectonic activity in the LSB and the Harz (Boness et al., 1990; Franzke et al., 2007; Hagedorn and Lippolt, 1993; Will et al., 2016; Wüstefeld et al., 2017). This mid- to late Cretaceous mineralization phase coincides with maximum burial and the subsequent onset of basin inversion, which was initiated by a significant change in the tectonic regime. In the late Cretaceous the previously NE-SW extensional stress regime was reversed and a N-S to NE-SW directional contractional regime was established in the NGB, which partly reactivated former normal or strike-slip fault systems as reverse faults and thereby favoured new mineral implacement in previously existing mineralized fractures (Franzke et al., 2007; Franzke and Zerjadtke, 1993). Basin inversion, i.e. the uplift of the Mesozoic basin infill due to compression, did not start before Turonian times (~93.9 Ma), as a comparison of inversion structures from several Mesozoic subbasins in the SPB proves (Pharaoh et al., 2010). This mineralization stage is characterized in terms of fluid pathway development by deep-reaching reverse faults (i.e., the Harz Northern Boundary Fault and the FCB Haldensleben and Gardelegen Faults) (Figs. 1, 3 and 4B), as well as along the southern margin of the LSB (Osning Trust Zone, Figs. 2 and 4A). In late Cretaceous basin inversion peaked, accompanied by basin uplift and partial exhumation of the (pre)-Mesozoic basin infill as evidenced by fission-track data and provenance analysis (Adrisola-Muñoz, 2007; Eynatten et al., 2008; Fischer et al., 2012). Apart from the Ca2-hosted barite mineralization in Bad Sooden-Allendorf (Stoppel and Gundlach, 1978), no Cenozoic mineralization has been reported to date in the NGB.

4.2.4. Fluid migration and mixing

Salinity and temperature gradients and fluid mixing can be inferred to have played a vital role for the basinal brines that eventually precipitated the Zn-Fe-Pb sulfide and fluorite-barite mineralization in the Paleozoic units of the NGB (Behr et al., 1987; Heijlen et al., 2003; Lüders et al., 2010; Muchez and Heijlen, 2003; Richardson and Holland, 1979; Sośnicka and Lüders, 2018a; Spangenberg et al., 1996). Two major basin-wide compositionally distinctive aqueous fluid systems are evident from fluid inclusion studies (Table 1): (a) early, low salinity H_2O-NaCl ± KCl, and (b) high salinity H_2O-NaCl-$CaCl_2$. The low salinity fluids (a) are observed within the older stratigraphic units across the NGB e.g., in the Permo-Carboniferous volcanics as well as sedimentary rocks and Jurassic sandstones. Circulation of this fluid type is associated with different events across the NGB, e.g., development of the Rhenohercynian thrust-and-fold belt (Lüders et al., 1993), vanishing stages of Late Variscan magmatic activity (Schmidt Mumm and Wolfgramm, 2004, 2002), major stages of basin subsidence and uplift (Lüders et al., 2005; Wüstefeld et al., 2017) or an inferred igneous intrusion in the early Cretaceous (Buntebarth and Teichmüller, 1979; Mundry, 1971; Rose and Gödecke, 1984; Stadler and Teichmüller, 1971; Will et al., 2016). The high-salinity fluids (b) are widespread as they are observed in all sub-regions of the NGB within Carboniferous, Rotliegend, Zechstein, and Triassic strata. The high salinity of these fluids resulted from both seawater evaporation and/or halite dissolution (Schöner et al., 2008) whereas the elevated calcium content in the more evolved, NaCl-$CaCl_2$-dominated basinal brines is related to their interactions with sedimentary rocks during deep burial (Gaupp et al., 2008; Schöner et al., 2008). Multiple high-salinity fluid flow episodes are associated with e.g., migration of CH_4-CO_2 ± N_2 ± H_2S or N_2-CH_4 gases during stages of uplift (Duschl et al., 2016; Krooss et al., 2008; Lüders et al., 2009, 2005; Sośnicka and Lüders, 2018a; Wüstefeld et al., 2017), hydrothermal remobilization of the sedimentary-derived fluids (Duschl et al., 2016), or dehydration of gypsum from Zechstein evaporitic sequence during progressive burial (Nollet et al., 2005). Basinal brines with high salinities (up to 320,000 mg/l total dissolved solids) have been observed to yield very high metal contents (i.e., 70 mg/l Pb, 245 mg/l Zn) that are predominantly bound in chloride complexes (Kharaka et al., 1987). The high-salinity fluid type is strictly related to Zn-(Pb), Ba, and Sr mineralization of the LSB, the hematite mineralization in the FCB and Post-Variscan sulfide and fluorite mineralization of the Harz Mountains.

Fault-related hydrothermal activity within the upper Carboniferous tight gas sandstones, exposed in the Piesberg quarry, has been recently investigated by Wüstefeld et al. (2017). There, episodes of tectonically driven fluid migration are recorded by two generations of fracture-filling quartz. Fluid inclusion studies revealed that early quartz-chlorite veins precipitated from moderate salinity (13.8–15.7 wt% NaCl equiv.) fluids at temperatures well above 200 °C (T_t = 220–260 °C) (Table 1) at nearly lithostatic conditions of about ~1000 bars, which corresponds to a depth of about 4.5 km during quartz precipitation (Wüstefeld et al., 2017). Potassium-Argon dating of authigenic illites undertaken by Wüstefeld et al. (2017) yields Middle to Upper Jurassic ages for the high-temperature fluid event (Fig. 19). In contrast, fluid migration probably related to mid-Cretaceous wrench-faulting and the subsequent onset of basin inversion (~96.5–106.7 Ma) is characterized by fluid inclusions of higher salinities (17.7–21.6 wt% NaCl equiv.) and lower temperatures (T_t = 170–200 °C) (Table 1) trapped in younger vein quartz, which precipitated at much lower pressures of 350–400 bars (Fig. 19) (Wüstefeld et al., 2017). Similar temperatures (164–202 °C) and salinities (17–25 wt% NaCl equiv.) of fluids migrating within upper Carboniferous sandstones (Table 1) from Piesberg area were also reported by Adriasola-Muñoz et al. (2007) and within horst structures in the central part of the LSB by Reutel et al. (1995). According to Wüstefeld et al. (2017) the migration of aqueous fluids within Carboniferous sediments occurred along with the migration of hydrocarbons during two major stages of tectonic movements in the LSB basin. The migration of CH_4-CO_2 gases coincided with the emplacement of early quartz veins in the extension-related fractures along the NNW–SSE striking fault zone during burial, whereas the release of the low density CH_4-CO_2-N_2 gas mixtures coincided with precipitation of younger quartz veins during inversion and uplift of the LSB (Wüstefeld et al., 2017). The latter are proximal to the fault

zone and contain sphalerite and marcasite, which is evidence for episodic circulation of Zn- and Fe-bearing fluids during the inversion and uplift stages in the southern LSB. According to Baldschuhn and Kockel (1998) this fault zone relates to the Egge-Graben system which was likely formed in Jurassic times and was partly reactivated during the late Cretaceous basin inversion. Based on fluid inclusion data, chlorite thermometry, and vitrinite reflectance data Reutel et al. (1995) concluded that enhanced heat flow and circulation of hydrothermal fluids within the NW–NNW/SE–SEE trending lineament in the central part of the LSB was related to the formation of horst structures during uplift. Migration of the hydrothermal brines, as supported by structural reconstructions, fluid inclusion, and formation waters data can lead to widespread fluid-wall rock interaction, alteration of sedimentary rocks and eventually the formation of Zn-Pb-Fe sulfide and fluorite barite mineralization (this study, Lüders et al., 2012).

Fluid mixing is regarded as one of the most important processes facilitating mineral precipitation (e.g., Robb, 2011) and is a pivotal factor for the formation of sediment-hosted deposits and for the understanding of MVT ore formation (Leach et al., 2010b, 2010a). Commonly, a significant portion of the history of a basinal brine system is characterized by the precipitation of barren gangue assemblages. Metalliferous fluids can often be linked to specific stratigraphic packages and distinct stages of the basin evolution (Stoffell et al., 2008). The interplay of fluid chemistry and dynamics with the surrounding rocks in the context of the paleogeographic setting (i.e., a carbonate-dominated (LSB) vs. a clastic-dominated (ABB) aquifer system) and the overall structural setup are crucial factors for the formation of sediment-hosted base metal sulfide mineralization (Knorsch, 2017; Sverjensky, 1989). Bons et al. (2014) proposed a fluid migration and mixing model for basinal brines in the Schwarzwald region that evolve through various stages of maturity (i.e., salinity, metal content, depth, T) and form mineral deposits when mixed during rapid ascend—much like what geochemical data, petrographic observations and published records suggest for the NGB. Fluid-rock interaction can evolve a single basinal brine that yields specific base metal and sulfur contents so that brines with a wide spectrum of geochemical characteristics are produced and arrive as a function of time, temperature and host rock composition at the site of metal or barren gangue deposition (Bons et al., 2014; Glikson-Simpson and Mastalerz, 2000; Leach et al., 2010b; Paradis et al., 2007; Sverjensky, 1984). Mixing of fluids was proposed to have occurred basin-wide, i.e. in the ABB (Schmidt Mumm and Wolfgramm, 2003a, 2003b), Upper and Middle Harz Mountains and in the LSB (Knorsch, 2017; Sośnicka and Lüders, 2018a). Our collected oxygen and carbon isotope data also support a model based on two mixing basinal brines in the LSB, which could have been similar to those that led to the Post-Variscan sulfide or barite mineralization in the Harz Mountains (Fig. 20, also see 3.2.3.1). The LSB host rock carbonates display the highest $\delta^{13}C$ and $\delta^{18}O$ values and plot in an area that has been attributed to the Zechstein fluids (i.e., the non-metalliferous pore waters and diagenetic waters of the host rock). The two measurements for hydrothermal carbonates from the Harz Mountains agree in their isotopic ratios with values that have been published by Bechtel and Püttmann (1991), Bechtel et al. (2000), and Zheng and Hoefs (1993) for the Lower Harz mineralization. $\delta^{13}C$ and $\delta^{18}O$ values for Rotliegend-hosted fracture-filling hydrothermal carbonates from the ABB show signatures (median of 16.7% and −8%, respectively) that are similar to isotope ratios typical for metalliferous fluids from the Harz Mountains, supporting the argument that there may be a genetic link between the vein type mineralization in the Harz Mountains and the ABB. Hydrothermal carbonates from the LSB show intermediate $\delta^{13}C$ and $\delta^{18}O$ values at around −5 to +5% and 20%, respectively (Fig. 20).

High-salinity brines are conceived as potential metalliferous fluids in the ABB as they show elevated metal contents, although sulfide mineralization is absent in this part of the NGB. This implies that reduced sulfur-carrying fluid either was not generated within the Zechstein unit in the ABB or it had not mixed with the metal-rich brine to precipitate sulfides, similar to the LSB Zn-Fe-Pb mineralization. This is supported by our data showing low sulfur concentrations (6–14 µg/g) in the Zn-Pb-enriched Rotliegend formation waters. Metal and fluorine contents of potential ore-forming fluids from the LSB, FCB and Harz Mountains are not yet known.

4.3. Kupferschiefer

The close stratigraphic association of the Ca2-hosted Zn-Fe-Pb mineralization with the partly Ca1 (Zechstein limestone)-hosted (Fig. 5) Kupferschiefer warrants a contextual discussion. In economic geology, the term Kupferschiefer includes units in the hanging and footwall (i.e., sandstone, conglomerate, black shale, carbonate rocks and anhydrite) that are host to the multistage sediment-hosted stratabound copper deposit of the same name (Alderton et al., 2016; Borg et al., 2012; Speczik, 1995; Walther and Dill, 1992). A connection with other mineralized districts such as the Spessart (SW Germany) has been proposed by Wagner et al. (2010). They argued that ore forming processes are comparable and may involve Kupferschiefer fluids and structurally controlled migration pathways, for many post-Variscan base metal deposits in Central Europe, especially in close vicinity to Variscan basement blocks such as the Rhenish Massif, the Spessart or the Harz Mountains. Other authors (e.g., Borg et al., 2012; Speczik, 1995; Vaughan et al., 1989) pointed out that both sedimentary-diagenetic and hydrothermal processes play a pivotal role in the Kupferschiefer formation and may be a blueprint for similar sediment-hosted deposits in the NGB. However, a direct link, petrographically or geochemically, between the Kupferschiefer and the Ca2-hosted Zn-Fe-Pb mineralization in the LSB has not been observed in our investigation.

4.4. Concluding remarks

Our investigation confirms early findings by Mempel (1962) that sediment-hosted Zn-Fe-Pb sulfide mineralization is restricted to the LSB, representing a paleogeographic shallow shelf or margin position in the NGB, as opposed to the basin center represented by the ABB. In the LSB, the evaporites and carbonate shelf sediments—the latter hosting bitumen and hydrocarbons—yielded the necessary fluid, salinity, and sulfur sources to warrant the mineralization of Zn-Pb-Fe sulfides at temperatures of around 143–196 °C from high salinity metalliferous fluids, as confirmed by stable isotope and fluid inclusion data, in the Ca2 carbonate. Furthermore, stable isotope data from hydrothermal carbonates support a fluid mixing model for sulfide deposition in the LSB. The observed mineralization and structural features point toward a fluid system driven by hydrothermal (brine) convection along structurally-controlled pathways in the LSB as well as the ABB. Carboniferous shales, Permo-Carboniferous volcanics of varying composition, and Zechstein carbonates can be inferred as metal or REE sources, respectively. A primary magmatic fluid component can be ruled out in both areas. The trace element composition and especially the REY makeup of the different types of hydrothermal mineralization in the ABB and LSB point towards different fluid compositions in the two areas that reflect the significant differences in the fluid evolution between the ABB and the LSB, e.g., vein fluorites found in the ABB have considerably higher REY concentrations than those found in the LSB. Compositional similarities between lower Permian formation waters and fluid inclusions from mineralization hosted in lower Permian strata in the ABB indicate that these highly saline brines might be modern analogues to the fossil fluid

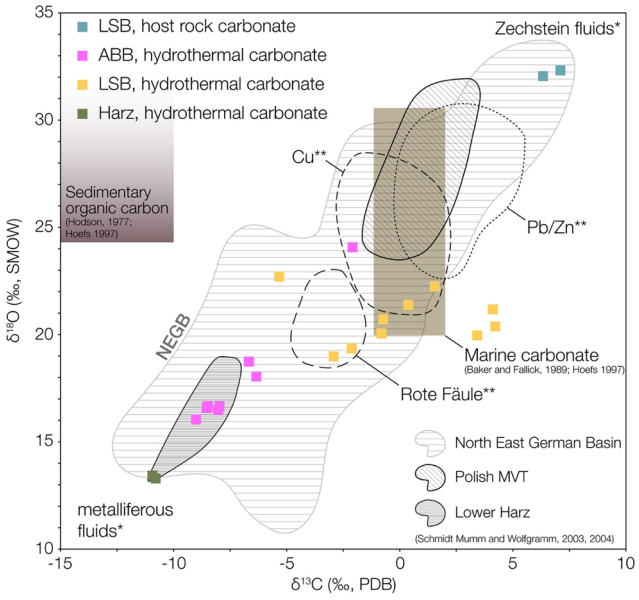

Fig. 20. Isotopic ratios of $\delta^{13}C$ and $\delta^{18}O$ of carbonates (calcite and dolomite) from the LSB, the NEGB and the Harz mountains. Hatched area represents the range of isotopic ratios based on data by Schmidt Mumm and Wolfgramm (2004, 2003a) and references therein, i.e., Bechtel and Püttmann (1991), Bechtel et al. (2000), Zheng and Hoefs (1993), and Wolfgramm (2002). *Zones of metalliferous (Pre-Zechstein) and Zechstein fluids (formation waters) (after Schmidt Mumm and Wolfgramm, 2004). **Isotopic ratios for various types of Kupferschiefer mineralization in Germany (Schmidt Mumm and Wolfgramm, 2004 and references therein). See Electronic Appendix Table EA 5 for underlying data.

systems which lead to the mineralization in the ABB, or that the formation waters have interacted with deep-seated hydrothermal mineralization.

The Ca2-hosted sulfide mineralization in the LSB bears many trademarks of an MVT deposit and can be linked to the Upper Cretaceous basin inversion which created or reactivated faults that acted as pathways for metal rich basinal brines (c.f., Knorsch, 2017; Sośnicka and Lüders, 2018a). Steeply dipping fluorite and hematite veins hosted in sedimentary and volcanic rocks in the ABB and the FCB are expressions of a reactivation of fault structures and fluid systems during the early Cretaceous. Our analytical results and petrographic observations support a strong correlation between the structural evolution of the NGB and related fracture-hosted hydrothermal mineralization in terms of fracture formation due to faulting and associated fracture porosity, fluid migration, intra-basinal P/T conditions, and ore emplacement. Our results are in good agreement with findings from other inter- to intracontinental ore deposits within extensional tectonic regimes worldwide (e.g., Robb, 2011). Moreover, our investigation of the observed Zn-Fe-Pb and fluorite-barite mineralization illustrates the applicability of the mineral system scale approach, known from petroleum exploration, to mineral deposits hosted in sedimentary basins (c.f. McCuaig et al., 2018). The combination of structural, mineralogical, and geochemical investigations presented here provide a first comprehensive inventory and characterization of the mineralized zones in the NGB and offer valuable insights into the conditions and governing factors that controlled the formation of the post-Variscan deep-seated hydrothermal mineralization in Paleozoic units of the LSB and ABB. It is striking that radiometric mineralization ages from the LSB and the ABB are scarce or completely missing, which stresses the importance of future research on fracture-hosted ore mineralization in both study areas with special emphasis on age dating, structural control, and metal budgets in the corresponding fluids.

Acknowledgements

Firstly, we would like to thank Volker Lüders, Michael Bau, Reiner Klemd, and Jonas Kley for initiating the project and supervising our combined research efforts. We thank ExxonMobil Production Deutschland GmbH, Wintershall Holding GmbH, and Neptune Energy GmbH (formerly Engie) for granting us access to their drill cores and providing us with relevant data. We are also grateful for the timely and professional help by our technical staff—Helene Brätz (FAU Erlangen-Nuremberg), Peter Späthe and Uli Schüßler (Universität Würzburg), Erika Kurahashi and Annika Moje (Jacobs University Bremen) and thank Michael Joachimski (FAU Erlangen-Nuremberg) for the oxygen and carbon isotope analyses. Ingo Horn (Leibniz University Hannover) and Felix Makoviak are thanked for collection of the Fe-isotope data. Furthermore, we thank Matthias Franz for proofreading, Reimar Seltmann for handling the manuscript and Harald Dill, Harry Kucha and two anonymous reviewers for providing feedback that helped to strengthen the manuscript. This research has been funded by the German Ministry of Education and Research (BMBF)—Grant number 033R165.

Appendix A. Supplementary data

Supplementary data to this article can be found online at https://doi.org/10.1016/j.oregeorev.2019.01.022.

References

Abraitis, P.K., Pattrick, R.A.D., Vaughan, D.J., 2004. Variations in the compositional, textural and electrical properties of natural pyrite: a review. Int. J. Miner. Process. 74, 41–59. https://doi.org/10.1016/j.minpro.2003.09.002.

Adriasola-Muñoz, Y., Littke, R., Brix, M.R., 2007. Fluid systems and basin evolution of the western Lower Saxony Basin, Germany. Geofluids 7, 335–355. https://doi.org/10.1111/j.1468-8123.2007.00186.x.

Adrisola-Muñoz, Y., 2007. The Thermal History of The Western Lower Saxony Basin. RWTH Aachen, Germany.

Alderton, D.H.M., Selby, D., Kucha, H., Blundell, D.J., 2016. A multistage origin for Kupferschiefer mineralization. Ore Geol. Rev. 79, 535–543. https://doi.org/https://doi.org/10.1016/j.oregeorev.2016.05.007.

Alfantazi, A.M., Moskalyk, R.R., 2003. Processing of indium: a review. Miner. Eng. 16, 687–694. https://doi.org/https://doi.org/10.1016/S0892-6875(03)00168-7.

Anderson, G.M., 2015. Kerogen as a source of sulfur in MVT deposits. Econ. Geol. 110, 837–840. https://doi.org/10.2113/econgeo.110.3.837.

Anderson, G.M., Macqueen, R.W., 1988. Mississippi Valley–type lead-zinc deposits. In: Roberts, R.G., Sheahan, P.A. (Eds.), Ore Deposit Models. Geological Association of Canada Geoscience Canada, pp. 79–90.

Bachmann, G.H., Grosse, S., 1989. Struktur und Entstehung des Norddeutschen Beckens – geologische und geophysikalische Interpretation einer verbesserten Bouguer-Schwerekarte. Das Norddtsch. Becken. Geophys. Untersuchungen des tieferen Untergrundes.

Bachmann, G.H., Hoffmann, N., 1997. Development of the Rotliegend Basin in Northern Germany. Geol. Jahrb. D 103, 9–31.

Bachmann, G.H., Hoffmann, N., 1995. Bildung und Entwicklung des Norddeutschen Rotliegend- Beckens, in: Plein, E. (Ed.), Stratigraphie von Deutschland I. Norddeutsches Rotliegend-Becken. Rotliegend Monographie Teil II. Cour.Forsch.-Inst. Senckenberg, Frankfurt a.M.

Baldschuhn, R., Best, G., Kockel, F., 1991. Inversion tectonics in the north-west German basin. In: Spencer, A.M. (Ed.), Generation, Accumulation, and Production of Europe's Hydrocarbons. Special Publication of the European Association of Petroleum No. 1. Oxford University Press, Oxford, pp. 149–159.

Baldschuhn, R., Binot, F., Fleig, S., Kockel, F., 2001. Geotektonischer Atlas von Nordwest-Deutschland und dem deutschen Nordsee-Sektor.

Baldschuhn, R., Kockel, F., 1999. Das Osning-Lineament am Südrand des Niedersachsen-Beckens. Zeitschrift der Dtsch. Geol. Gesellschaft 150, 673–695.

Baldschuhn, R., Kockel, F., 1998. Der Untergrund von Hannover und seiner Umgebung. Berichte der Naturhistorischen Gesellschaft 140, 5–98.

Bau, M., 1991. Rare-earth element mobility during hydrothermal and metamorphic fluid-rock interaction and the significance of the oxidation state of europium. Chem. Geol. 93, 219–230. https://doi.org/https://doi.org/10.1016/0009-2541(91)90115-8.

Bau, M., Dulski, P., 1995. Comparative study of yttrium and rare-earth element behaviours in fluorine-rich hydrothermal fluids. Contrib. Mineral. Petrol. 119, 213–223. https://doi.org/10.1007/BF00307282.

Bau, M., Möller, P., 1992. Rare earth element fractionation in metamorphogenic hydrothermal calcite, magnesite and siderite. Mineral. Petrol. 45, 231–246. https://doi.org/10.1007/bf01163114.

Bau, M., Romer, R.L., Lüders, V., Dulski, P., 2003. Tracing element sources of hydrothermal mineral deposits: REE and Y distribution and Sr-Nd-Pb isotopes in fluorite from MVT deposits in the Pennine Orefield, England. Miner. Depos. 38, 992–1008. https://doi.org/10.1007/s00126-003-0376-x.

Bayliss, P., 1989. Crystal chemistry and crystallography of some minerals within the pyrite group. Am. Mineral. 74, 1168–1176.

Bechtel, A., Elliott, W.C., Wampler, J.M., Oszczepalski, S., 1999. Clay mineralogy, crystallinity, and K/Ar ages of illites in the Polish Zechstein Basin: implications for the age of the Kupferschiefertype mineralization. Econ. Geol. 94, 261–272.

Bechtel, A., Ghazi, A.M., Elliott, W.C., Oszczepalski, S., 2001. The occurrences of the rare earth elements and the platinum group elements in relation to base metal zoning in the vicinity of Rote Fäule in the Kupferschiefer of Poland. Appl. Geochem. 16, 375–386.

Bechtel, A., Püttmann, W., 1991. The origin of the Kupferschiefer-type mineralization in the Richelsdorf Hills, Germany, as deduced from stable isotope and organic geochemical studies. Chem. Geol. 91, 1–18. https://doi.org/https://doi.org/10.1016/0009-2541(91)90012-G.

Bechtel, A., Shieh, Y.-N., Elliott, W.C., Oszczepalski, S., Hoernes, S., 2000. Mineralogy, crystallinity and stable isotopic composition of illitic clays within the Polish Zechstein basin: implications for the genesis of Kupferschiefer mineralization. Chem. Geol. 163, 189–205.

Behr, H.J., Gerler, J., 1987. Inclusions of sedimentary brines in post-Variscan mineralizations in the Federal Republic of Germany–a study by neutron activation analysis. Chem. Geol. 61, 65–77. https://doi.org/https://doi.org/10.1016/0009-2541(87)90028-3.

Behr, H.J., Horn, E.E., Frentzel-Beyme, K., Reutel, C., 1987. Fluid inclusion characteristics of the Variscan and post-Variscan mineralizing fluids in the Federal Republic of Germany. Chem. Geol. 61, 273–285. https://doi.org/https://doi.org/10.1016/0009-2541(87)90046-5.

Benox, D., Ludwig, A.O., Schulze, W., Schwab, G., Hartmann, H., Knebel, G., Januszewski, I., 1997. Struktur und Entwicklung mesozoischer Störungszonen in der Südwest-Altmark. Hallesches Jahrb. Geowiss. B 19, 83–114.

Betz, D., Führer, F., Greiner, G., Plein, E., 1987. Evolution of the Lower Saxony Basin. Tectonophysics 137, 127–170. https://doi.org/https://doi.org/10.1016/0040-1951(87)90319-2.

Bielicki, K.-H., Tischendorf, G., 1991. Lead isotope and Pb-Pb model age determinations of ores from Central Europe and their metallogenic interpretation. Contrib. Mineral. Petrol. 106, 440–461.

Blundell, D.J., Freeman, R., Mueller, S., 1992a. A Continent Revealed: The European Geotraverse: Structure and Dynamic Evolution. https://doi.org/10.1017/cbo9780511608261.

Blundell, D.J., Mueller, S.T., Mengel, K., 1992b. Geodynamics of Europe. In: Blundell, D.J., Freeman, R., Mueller, S. (Eds.), A Continent Revealed. Cambridge University Press, Cambridge, pp. 215–232. https://doi.org/10.1017/cbo9780511608261.009.

Boigk, H., 1981. Erdöl und Erdölgas in der Bundesrepublik Deutschland. Enke, Stuttgart.

Boigk, H., 1968. Gedanken zur Entwicklung des Niedersächsischen Tektogens. Geol. Jahrb. 85, 861–900.

Boness, M., 1987. Die radiometrische Altersbestimmung der Pb-Zn-Lagerstätte Grund (Harz) mit der Rb-Sr-Methode. Universität Göttingen, Göttingen.

Boness, M., Haack, U., Feldmann, K.S., 1990. Rb/Sr-Datierung der hydrothermalen Pb-Zn-Vererzung von Bad Grund (Harz). BRD. Chemie der Erde 50, 125.

Bons, P.D., Fusswinkel, T., Gomez-Rivas, E., Markl, G., Wagner, T., Walter, B., 2014. Fluid mixing from below in unconformity-related hydrothermal ore deposits. Geology 42, 1035–1038.

Borg, G., Piestrzyński, A., Bachmann, G.H., Püttmann, W., Walther, S., Fiedler, M., 2012. An overview of the European kupferschiefer deposits. Spec. Publ. – Soc. Econ. Geol. 16, 455–486.

Borsdorf, K.H., 1976. Fluoritmineralisationen in Tiefbohrungen am Gardelegener Abbruch/Altmark. Zentrales Geologisches Institut, Berlin.

Bradley, D.C., Leach, D.L., 2003. Tectonic controls of Mississippi Valley-type lead–zinc mineralization in orogenic forelands. Miner. Depos. 38, 652–667.

Bralia, A., Sabatini, G., Troja, F., 1979. A revaluation of the Co/Ni ratio in pyrite as geochemical tool in ore genesis problems. Miner. Depos. 14, 353–374. https://doi.org/10.1007/bf00206365.
Brecht, G.A., Wolfgramm, M., 1998. Mesozoic thermal activity in the NE-German Basin recorded in authigenic phyllosilicates of Permocarboniferous SiO2-rich volcanic rocks. In: Novotny, J. (Ed.), Proceedings of the 15th Conference on Clay Mineralogy and Petrology. Masaryk University, Faculty of Science, Brno, pp. 30–31.
Breitkreuz, C., Kennedy, A., 1999. Magmatic flare-up at the Carboniferous/Permian boundary in the NE German Basin revealed by SHRIMP zircon ages. Tectonophysics 302, 307–326.
Brink, H.-J., 2013. Die Intrusion von Bramsche – ein Irrtum im invertierten Niedersächsischen Becken? Zeitschrift der Dtsch. Gesellschaft für Geowissenschaften 164, 33–48. https://doi.org/10.1127/1860-1804/2013/0011.
Brink, H.-J., 2005. The evolution of the North German Basin and the metamorphism of the lower crust. Int. J. Earth Sci. 94, 1103–1116. https://doi.org/10.1007/s00531-005-0037-7.
Brink, H.-J., 2002. Die Anomalien von Bramsche: wieder eine offene Frage? Erdöl, Erdgas, Kohle 18–22.
Brink, H.J., Dürschner, H., Trappe, H., 1992. Some aspects of the late and post-Variscan development of the Northwestern German Basin. Tectonophysics 207, 65–95. https://doi.org/https://doi.org/10.1016/0040-1951(92)90472-I.
Bruns, B., di Primio, R., Berner, U., Littke, R., 2013. Petroleum system evolution in the inverted Lower Saxony Basin, northwest Germany: a 3D basin modeling study. Geofluids 13, 246–271. https://doi.org/10.1111/gfl.12016.
Buntebarth, G., Teichmüller, R., 1979. Zur Ermittlung der Paläotemperaturen im Dach des Bramscher Intrusivs aufgrund von Inkohlungsdaten. Fortschr Geol Rheinl u Westf 27, 171–182.
Cabral, A.R., Beaudoin, G., Munnik, F., 2011. Lead in diagenetic pyrite: evidence for Pb-tolerant bacteria in a red-bed Cu deposit, Quebec Appalachians, Canada. Mineral. Mag. 75, 295–302.
Campbell, F.A., Ethier, V.G., 1984. Nickel and cobalt in pyrrhotite and pyrite from the Faro and Sullivan orebodies. Can. Mineral. 22, 503–506.
Churakov, A.N., 1947. The Russian plateau and the alkaline rocks boarding it. Izv. Akad. Nauk S.S.S.R., Set. Geol. 1, 83–104.
Condie, K.C., 2000. Episodic continental growth models: afterthoughts and extensions. Tectonophysics 322, 153–162.
Cook, N.J., Ciobanu, C.L., Pring, A., Skinner, W., Shimizu, M., Danyushevsky, L., Saini-Eidukat, B., Melcher, F., 2009. Trace and minor elements in sphalerite: A LA-ICPMS study. Geochim. Cosmochim. Acta 73, 4761–4791. https://doi.org/https://doi.org/10.1016/j.gca.2009.05.045.
Correns, O.W., 1970. Sedimentgesteine. In: Barth, T.F.W., Correns, C.W., Eskola, P. (Eds.), Die Entstehung Der Gesteine. Springer, Berlin, pp. 116–262.
Craig, J.R., Vokes, F.M., Solberg, T.N., 1998. Pyrite: physical and chemical textures. Miner. Depos. 34, 82–101.
Dadlez, R., 2006. The Polish Basin – relationship between the crystalline, consolidated and sedimentary crust. Geol. Q. 50, 43–58.
Dadlez, R., Narkiewicz, M., Stephenson, R.A., Visser, M.T.M., van Wees, J.-D., 1995. Tectonic evolution of the Mid-Polish Trough: modelling implications and significance for central European geology. Tectonophysics 252, 179–195.
Debruyne, D., Hulsbosch, N., Muchez, P., 2016. Unraveling rare earth element signatures in hydrothermal carbonate minerals using a source-sink system. Ore Geol. Rev. 72, 232–252. https://doi.org/10.1016/j.oregeorev.2015.07.022.
Deditius, A.P., Utsunomiya, S., Reich, M., Kesler, S.E., Ewing, R.C., Hough, R., Walshe, J., 2011. Trace metal nanoparticles in pyrite. Ore Geol. Rev. 42, 32–46.
Dill, H.G., 1996. The late Variscan and early Alpine Metallogeny in Central Europe, in: Grecula, P., Nemeth, Z. (Eds.), Variscan Metallogeny in the Alpine Orogenic Belt. pp. 93–108.
Dill, H.G., Sachsenhofer, R.F., Grecula, P., Sasvári, T., Palinkaš, L.A., Borojević-Šoštarić, S., Strmić-Palinkaš, S., Prochaska, W., Garuti, G., Zaccarini, F., Arbouille, D., Schulz, H.-M., 2008a. Fossil fuels, ore and industrial minerals. In: McCann, T. (Ed.), The Geology of Central Europe Volume 2: Mesozoic and Cenozoic. Geological Society of London.
Dill, H.G., Sachsenhofer, R.F., Grecula, P., Sasvári, T., Palinkaš, L.A., Borojević-Šoštarić, S., Strmić-Palinkaš, S., Prochaska, W., Garuti, G., Zaccarini, F., Arbouille, D., Schulz, H.-M., Schmidt, B., Locmelis, B., 2008b. In: The Geology of Central Europe Volume 2: Mesozoic and Cenozoic. Geological Society of London, pp. 749–1149.
Doornenbal, H., Stevenson, A., 2010. Petroleum Geological Atlas of the Southern Permian Basin Area. EAGE Publications B.V.
Dorn, P., 1957. Der junge Vulkanismus im Braunschweiger Raum. Geol. Jb. 74, 105–116.
Duschl, F., Navabpour, P., Dunkl, I., Kley, J., 2018. Fault kinematics in the Thuringian Basin and the Flechtingen-Calvörde Block, Germany–The role of Jurassic extension tectonics in regional deformation patterns, in: EGU General Assembly Conference Abstracts. EGU.
Duschl, F., van den Kerkhof, A., Sosa, G., Leiss, B., Wiegand, B., Vollbrecht, A., Sauter, M., 2016. Fluid inclusion and microfabric studies on Zechstein carbonates (Ca2) and related fracture mineralizations: New insights on gas migration in the Lower Saxony Basin (Germany). Mar. Pet. Geol. 77C, 300–322. https://doi.org/10.1016/j.marpetgeo.2016.06.020.
Eynatten, H. von, Voigt, T., Meier, A., Franzke, H.-J., Gaupp, R., 2008. Provenance of Cretaceous clastics in the Subhercynian Basin: Constraints to exhumation of the Harz Mountains and timing of inversion tectonics in Central Europe. Int. J. Earth Sci. 97, 1315–1330. https://doi.org/10.1007/s00531-007-0212-0.
Fabian, H.-J., Mueller, G., Roese, K.-L., 1957. Eine sideritisch-sideroplesitische Vererzung in einer Zechstein-Bohrung des Erdgasfeldes Rehden (Krs. Diepholz). Neues Jb. Geol. u. Paäontol. 105, 205–219.
Fischer, C., Dunkl, I., von Eynatten, H., Wijbrans, J.R.A.N., Gaupp, R., 2012. Products and timing of diagenetic processes in Upper Rotliegend sandstones from Bebertal (North German Basin, Parchim Formation, Flechtingen High, Germany). Geol. Mag. 149, 827–840. https://doi.org/10.1017/s0016756811001087.
Fischer, M., Botz, R., Schmidt, M., Rockenbauch, K., Garbe-Schönberg, D., Glodny, J., Gerling, P., Littke, R., 2006. Origins of CO2 in permian carbonate reservoir rocks (Zechstein, Ca2) of the NW-German Basin (Lower Saxony). Chem. Geol. 227, 184–213. https://doi.org/10.1016/j.chemgeo.2005.09.014.
Franke, D., Hoffmann, N., Lindert, W., 1996. The Variscan deformation front in East Germany. Part 2: tectonic interpretation. Z. angew. Geol. 42, 44–56.
Franzke, H.J., Müller, R., Voigt, T., von Eynatten, H., 2007. Paleo-Stress Paths in the Harz Mountains and surrounding areas (Germany) between the Triassic and the Upper Cretaceous. Zeitschrift für Geol. Wissenschaften 35, 141–156.
Franzke, H.J., Voigt, T., von Eynatten, H., Brix, M., Burmester, G., 2004. Geometrie und Kinematik der Harznordrandstörung, erläutert an Profilen aus dem Gebiet von Blankenburg. Geowissenschaftliche Mitteilungen von Thüringen 11, 39–62.
Franzke, H.J., Zerjadtke, W., 1993. Structural Control of Hydrothermal Vein Mineralizations in the Lower Harz Mountains. In: Möller, P., Lüders, V. (Eds.), Formation of Hydrothermal Vein Deposits. A Case Study of the Pb-Zn, Barite and Fluorite Deposits of the Harz Mountains. Monograph Series on Mineral Deposits, pp. 13–33.
Füchtbauer, H., 1958. Die petrographische Unterscheidung der Zechsteindolomite im Emsland durch ihren Säurerückstand. Erdöl Kohle 11, 689–693.
Gabriel, G., Jahr, T., Jentzsch, G., Melzer, J., 1997. Deep structure and evolution of the Harz Mountains: results of three-dimensional gravity and finite-element modeling. Tectonophysics 270, 279–299.
Gast, R., 1988. Rifting im Rotliegend Niedersachsens. Geowissenschaften 6, 115–122.
Gast, R., Gundlach, T., 2006. Permian strike slip and extensional tectonics in Lower Saxony, Germany. Zeitschrift der Dtsch. Gesellschaft für Geowissenschaften 157, 41–56.
Gast, R., Pasternak, M., Piske, J., Rasch, H.-J., 1998. Das Rotliegend im Nordostdeutschen Raum, Stratigraphie, Fazies und Diagenese. Geol. Jb. A149, 59–79.
Gaupp, R., Gast, R., Forster, C., 2000. Late Permian Playa Lake Deposits of the Southern Permian Basin (Central Europe). AAPG Stud. Geol.
Gaupp, R., Möller, P., Lüders, V., di Primio, R., Littke, R., 2008. Fluids in sedimentary basins: an overview. In: Littke, R., Bayer, U., Gajewski, D., Nelskamp, S. (Eds.), Dynamics of Complex Intracontinental Basins: The Central European Basin System. Springer, pp. 345–366.
Gemmer, L., Nielsen, S.B., Bayer, U., 2003. Late Cretaceous-Cenozoic evolution of the North German Basin—results from 3-D geodynamic modelling. Tectonophysics 373, 39–54. https://doi.org/10.1016/s0040-1951(03)00282-8.
Gemmer, L., Nielsen, S.B., Huuse, M., Lykke-Andersen, H., 2002. Post-mid-Cretaceous eastern North Sea evolution inferred from 3D thermo-mechanical modelling. Tectonophysics 350, 315–342.
Gerling, P., Geluk, M.C., Kockel, F., Lokhorst, A., Lott, G.K., Nicholson, R.A., 1999. 'NW European Gas Atlas' – new implications for the Carboniferous gas plays in the western part of the Southern Permian Basin. In: Fleet, A.J., Boldy, S.A.R. (Eds.), Petroleum Geology of Northwest Europe. Geological Society of London, pp. 799–808. https://doi.org/10.1144/0050799.
Glennie, K.W., 1995. Permian and Triassic rifting in northwest Europe. Geol. Soc. London, Spec. Publ. 91, 1–5. https://doi.org/10.1144/gsl.sp.1995.091.01.01.
Glennie, K.W., 1990. Rotliegend sediment distribution: a result of late Carboniferous movements. Geol. Soc. London, Spec. Publ. 55, 127–138. https://doi.org/10.1144/gsl.sp.1990.055.01.06.
Glikson-Simpson, M., Mastalerz, M., 2000. Organic Matter and Mineralisation: Thermal Alteration, Hydrocarbon Generation and Role in Metallogenesis. Kluwer Academic.
Göthel, M., 2012. Aktuelle Informationen zur stratigraphischen Zuordnung eustatisch und tektonisch kontrollierter Ablagerungssequenzen des Zechsteins im Rahmen der plattentektonischen und paläogeographischen Situation zwischen Gondwana und dem geotektonischen Puzzle Europ. Brand. geowiss. Beitr. 19, 29–42.
Haack, U., Lauterjung, J., 1993. Rb/Sr dating of hydrothermal overprint in Bad Grund by mixing lines. In: Möller, P. (Ed.), Formation of Hydrothermal Vein Deposits. Borntraeger, Berlin, pp. 103–112.
Hagedorn, B., 1992. (U_Th)/He-, K/Ar- und Rb/Sr-Chronologie von Hämatit und Adular hydrothermaler Lagerstätten des Harzes. Ruprecht-Karls-Univerität Heidelberg.
Hagedorn, B., Lippolt, H.J., 1993. Isotopic age Constraints for Epigenetic Mineralizations in the Harz Mountains (Germany) from K-Ar and Rb-Sr Data of Authigenic K-Feldspars. Monogr. Ser. Miner. Depos. 30, 87–102.
Hagemann, S.G., Lisitsin, V.A., Huston, D.L., 2016. Mineral system analysis: quo vadis. Ore Geol. Rev. 76, 504–522. https://doi.org/https://doi.org/10.1016/j.oregeorev.2015.12.012.
Hansen, M.B., Scheck-Wenderoth, M., Hübscher, C., Lykke-Andersen, H., Dehghani, A., Hell, B., Gajewski, D., 2007. Basin evolution of the northern part of the Northeast German Basin: insights from a 3D structural model. Tectonophysics 437, 1–16.
Harms, F.-J., 1984. Perm. In: Klassen, H. (Ed.), Geologie Des Osnabrücker Berglandes. Naturwissenschaftliches Museum Osnabrück, Osnabrück, pp. 79–113.
Hecht, C.A., Lempp, C., Scheck, M., 2003. Geomechanical model for the post-Variscan evolution of the Permocarboniferous-Mesozoic basins in Northeast Germany. Tectonophysics 373, 125–139.
Heijlen, W., Muchez, P., Banks, D.A., Schneider, J., Kucha, H., Keppens, E., 2003. Carbonate-hosted Zn-Pb deposits in Upper Silesia, Poland: origin and evolution of mineralizing fluids and constraints on genetic models. Econ. Geol. 98, 911–932. https://doi.org/10.2113/gsecongeo.98.5.911.
Herrmann, A.G., 1961. Über die Einwirkung Cu-, Sn-, Pb- und Mn-haltiger Erdölwässer auf die Staßfurt-Serie des Süd-Harzbezirkes. N. Jb. Miner. 60–67.
Höll, R., Kling, M., Schroll, E., 2007. Metallogenesis of germanium—a review. Ore Geol. Rev. 30, 145–180. https://doi.org/https://doi.org/10.1016/j.oregeorev.2005.07.

034.
Horn, I., von Blanckenburg, F., Schoenberg, R., Steinhoefel, G., Markl, G., 2006. In situ iron isotope ratio determination using UV-femtosecond laser ablation with application to hydrothermal ore formation processes. Geochim. Cosmochim. Acta 70, 3677–3688. https://doi.org/10.1016/j.gca.2006.05.002.
Hubald, U., 1988. Mineralisation und Genese der Blei-Zink-Vererzung im Hauptdolomit der Bohrung Barenburg Z8 (Nordwestdeutsches Becken). Inst. für Mineral. und Lagerstättenlehre RWTH Aachen. RWTH Aachen, Aachen.
Hübscher, C., Hansen, M.B., Triñanes, S.P., Lykke-Andersen, H., Gajewski, D., 2010. Structure and evolution of the Northeastern German Basin and its transition onto the Baltic Shield. Mar. Pet. Geol. 27, 923–938. https://doi.org/https://doi.org/10.1016/j.marpetgeo.2009.10.017.
Huston, D.L., Sie, S.H., Suter, G.F., Cooke, D.R., Both, R.A., 1995. Trace elements in sulfide minerals from eastern Australian volcanic- hosted massive sulfide deposits: part I. Proton microprobe analyses of pyrite, chalcopyrite, and sphalerite, and part II. Selenium levels in pyrite: comparison with δ 34S values and impl. Econ. Geol. 90, 1167–1196. https://doi.org/10.2113/gsecongeo.90.5.1167.
Huttel, P., 1989. Das Stassfurt-Karbonat (Ca2) in Süd-Oldenburg: Fazies und Diagenese eines Sediments am Nordhang der Hunte-Schwelle. Geol. Inst. Georg-August-Univ.
Ivanov, V.V, 1967. Principal geochemical environments and processes of the formation of hydrothermal waters in regions of recent volcanic activity, in: Vinogradov, A.P. (Ed.), Chemistry of the Earth's Crust. Vol. II. Jerusalem, pp. 260–281.
Josten, K.-H., Köwing, K., Rabitz, A., 1984. Oberkarbon. In: Klassen, H. (Ed.), Geologie Des Osnabrücker Berglandes. Naturwissenschaftliches Museum Osnabrück, Osnabrück, pp. 7–77.
Kasakov, A.V., Sokolova, E.I., 1950. Conditions of the formation of fluorite in sedimentary rocks (The fluorite system). (English translation by V.L. Skitzky, Special Libraries Association Translation Pool, New York, N.Y.). Tr. Inst. Geol. Nauk. Akad. Nauk S.S.S.R. Geol. Ser. 40, 22–64.
Kharaka, Y.K., Maest, A.S., Carothers, W.W., Law, L.M., Lamothe, P.J., Fries, T.L., 1987. Geochemistry of metal-rich brines from central Mississippi Salt Dome basin, U.S.A. Appl. Geochemistry 2, 543–561. https://doi.org/10.1016/0883-2927(87)90008-4.
Kley, J., Franzke, H.-J., Jähne, F., Krawczyk, C.M., Lohr, T., Reicherter, K., Scheck-Wenderoth, M., Sippel, J., Tanner, D., van Gent, H., Group, S.P.P.S.G., 2008. Stress and Strain. In: Littke, R., Bayer, U., Gajewski, D., Nelskamp, S. (Eds.), Dynamics of Complex Intracontinental Basins. Springer, Berlin, Heidelberg, pp. 97–124.
Kley, J., Voigt, T., 2008. Late Cretaceous intraplate thrusting in central Europe: effect of Africa-Iberia-Europe convergence, not Alpine collision. Geology 36, 839. https://doi.org/10.1130/g24930a.1.
Kloppmann, W., Négrel, P., Casanova, J., Klinge, H., Schelkes, K., Guerrot, C., 2001. Halite dissolution derived brines in the vicinity of a Permian salt dome (N German Basin). Evidence from boron, strontium, oxygen and hydrogen isotopes. Geochim. Cosmochim. Acta 65, 4087–4101.
Knorsch, M., 2017. Geochemical fingerprinting and origin of hydrothermal sulfides in the Zechstein Ca2 carbonate in the North German Basin. Unpubl. MSc thesis. Friedrich-Alexander-Universität Erlangen-Nürnberg, Erlangen.
Kockel, F., 2003. Inversion structures in Central Europe - expressions and reasons, an open discussion. Netherlands J. Geosci. 82, 367–382.
Kockel, F., 2002. Rifting processes in NW-Germany and the German North Sea Sector. Netherlands J. Geosci. 81, 149–158. https://doi.org/10.1017/s0016774600022381.
Kockel, F., 1994. Geotektonischer Atlas von NW-Deutschland 1: 300.000: Hannover: Bundesanstalt für. Geowissenschafen und Rohstoffe.
Kraemer, D., Viehmann, S., Banks, D., Sumonduur, A.D., Koeberl, C., Bau, M., 2018. Regional variations in fluid formation and metal sources in MVT mineralization in the Pennine Orefield, UK: Implications from rare earth element and yttrium distribution, Sr-Nd isotopes and fluid inclusion compositions of hydrothermal vein fluorites. Unpublished manuscript.
Krawczyk, C.M., Stiller, M., 1999. Reflection seismic constraints on Paleozoic crustal structure and Moho beneath the NE German Basin, DEKORP-BASIN Research Group. Tectonophysics 314, 241–253.
Krooss, B.M., Plessen, B., Machel, H.G., Lüders, V., Littke, R., 2008. Origin and distribution of non-hydrocarbon gases. In: Littke, R., Bayer, U., Gajewski, D., Nelskamp, S. (Eds.), Dynamics of Complex Intracontinental Basins. The Central European Basin System. Springer, pp. 433–458.
Kucha, H., Barnes, H.L., 1995. Compounds with mixed and intermediate sulfur valences in pyrite from the Amelia Mine, Southwest Wisconsin. Miner. Depos. https://doi.org/10.1007/BF00208880.
Kucha, H., Przybylowicz, W., Lankosz, M., van Langevelde, F., Traxel, K., 1993. EPMA, micro-PIXE, synchrotron microprobe and TEM study of visible and invisible accumulations of Au and PGE in black shale and organic matrix, Kupferschiefer, Poland. Mineral. Mag. 57, 103–112.
Lamarche, J., Scheck-Wenderoth, M., 2005. 3D structural model of the Polish Basin. Tectonophysics 397, 73–91. https://doi.org/10.1016/j.tecto.2004.10.013.
Large, R.R., Danyushevsky, L., Hollit, C., Maslennikov, V., Meffre, S., Gilbert, S., Bull, S., Scott, R., Emsbo, P., Thomas, H., Singh, B., Foster, J., 2009. Gold and trace element zonation in pyrite using a laser imaging technique: Implications for the timing of gold in orogenic and carlin-style sediment-hosted deposits. Econ. Geol. 104, 635–668.
Leach, D.L., Bradley, D., Lewchuk, M.T., Symons, D.T., de Marsily, G., Brannon, J., 2001. Mississippi Valley-type lead–zinc deposits through geological time: implications from recent age-dating research. Miner. Depos. 36, 711–740. https://doi.org/10.1007/s001260100208.
Leach, D.L., Bradley, D.C., Huston, D., Pisarevsky, S.A., Taylor, R.D., Gardoll, S.J., 2010. Sediment-hosted lead-zinc deposits in earth history. Econ. Geol. 105, 593–625. https://doi.org/10.2113/gsecongeo.105.3.593.
Leach, D.L., Taylor, R.D., Fey, D.L., Diehl, S.F., Saltus, R.W., 2010b. A Deposit Model for Mississippi Valley-Type Lead-Zinc Ores, in: Mineral Deposit Models for Resource Assessment. Scienti c Investigations Report 2010–5070–A. U.S. Department of the Interior, U.S. Geological Survey.
Leach, D.L., Viets, J.G., Kozlowski, A., Kibitlewski, S., 1996. Geology, geochemistry, and genesis of the Silesia-Cracow zinc-lead district, Southern Poland, in: Sangster, D.F. (Ed.), Carbonate-Hosted Lead-Zinc Deposits. Society of Economic Geologists, pp. 144–170.
Legler, B., Gebhardt, U., Schneider, J.W., 2005. Late Permian non-marine–marine transitional profiles in the central Southern Permian Basin, northern Germany. Int. J. Earth Sci. 94, 851–862. https://doi.org/10.1007/s00531-005-0002-5.
Lietz, J., 1951. Sulfidische Klufterze im Deckgebirge des Salzstockes Reitbrook. Mitt. Staatsinst. Hambg. 20, 110–118.
Littke, R., Bayer, U., Gajewski, D., Nelskamp, S., 2008a. Dynamics of Complex Intracontinental Basins. Springer.
Littke, R., Scheck-Wenderoth, M., Brix, M.R., Nelskamp, S., 2008b. Subsidence, inversion and evolution of the thermal field. In: Littke, R., Bayer, U., Gajewski, D., Nelskamp, S. (Eds.), Dynamics of Complex Intracontinental Basins. Springer, pp. 125–153.
Loftus-Hills, G., Solomon, M., 1967. Cobalt, nickel and selenium in sulphides as indicators of ore genesis. Miner. Depos. 2, 228–242. https://doi.org/10.1007/bf00201918.
Lokhorst, A., Adlam, K., Brugge, J.V.M., David, P., Diapari, L., Fermont, W.J.J., Geluk, M., Gerling, P., Heckers, J., Kockel, F., Kotarba, M., Laier, T., Lott, G.K., Milaczewski, E., Milaczewski, L., Nicholson, R.A., von Platen, F., Pokorski, J., 1998. NW European Gas Atlas – composition and isotope ratios of natural gases. NITG, Haarlem.
Lottermoser, B.G., 1992. Rare earth elements and hydrothermal ore formation processes. Ore Geol. Rev. 7, 25–41. https://doi.org/10.1016/0169-1368(92)90017-F.
Lüders, V., 1996. Contribution of infrared microscopy to fluid inclusion studies in some opaque minerals (wolframite, stibnite, bournonite): metallogenic implications. Econ. Geol. 91, 1462–1468.
Lüders, V., Gerler, J., Hein, U.F., Reutel, C., 1993. Chemical and thermal development of ore-forming solutions in the Harz Mountains: a summary of fluid inclusion studies, in: Möller, P., Lüders, V. (Eds.), Formation of Hydrothermal Vein Deposits. A Case Study of the Pb-Zn, Barite and Fluorite Deposits of the Harz Mountains. pp. 117–132.
Lüders, V., Möller, P., 1992. Fluid evolution and ore deposition in the Harz Mountains (Germany). Eur. J. Mineral. 4, 1053–1068. https://doi.org/10.1127/ejm/4/5/1053.
Lüders, V., Plessen, B., di Primio, R., 2012. Stable carbon isotopic ratios of CH4–CO2-bearing fluid inclusions in fracture-fill mineralization from the Lower Saxony Basin (Germany)–a tool for tracing gas sources and maturity. Mar. Pet. Geol. 30, 174–183. https://doi.org/https://doi.org/10.1016/j.marpetgeo.2011.10.006.
Lüders, V., Plessen, B., Romer, R.L., Weise, S.M., Banks, D.A., Hoth, P., Dulski, P., Schettler, G., 2010. Chemistry and isotopic composition of Rotliegend and Upper Carboniferous formation waters from the North German Basin. Chem. Geol. 276, 198–208. https://doi.org/10.1016/j.chemgeo.2010.06.006.
Lüders, V., Plessen, B., Vonhof, H.B., Weise, S.M., Banks, D.A., Romer, R.L., Schneider, J., 2009. Ancient and present-day fluids in the Altmark, central North German Basin. 20th Eur. Curr. Res. Fluid Inclusions – ECROFI Meet. (Granada, Spain 2009).
Lüders, V., Reutel, C., Hoth, P., Banks, D.A., Mingram, B., Pettke, T., 2005. Fluid and gas migration in the North German Basin: fluid inclusion and stable isotope constraints. Int. J. Earth Sci. 94, 990–1009. https://doi.org/10.1007/s00531-005-0013-2.
Lützner, H., Kowalczyk, G., 2013. Stratigraphie von Deutschland X: Rotliegend Teil I: Innervariscische Becken. Schweizerbart Science Publishers, Stuttgart.
Makin, S.A., Simandl, G.J., Marshall, D., 2014. Fluorite and its potential as an indicator mineral for carbonatite-related rare earth element deposits. Br. Columbia Geol. Surv. Pap. 2014–1, 207–212.
Mao, M., Simandl, G.J., Spence, J., Marshall, D., 2015. Fluorite trace-element chemistry and its potential as an indicator mineral: Evaluation of LA-ICP-MS method. Br. Columbia Geol. Surv. Pap. 2015, 14.
Markl, G., von Blanckenburg, F., Wagner, T., 2006. Iron isotope fractionation during hydrothermal ore deposition and alteration. Geochim. Cosmochim. Acta 70, 3011–3030. https://doi.org/https://doi.org/10.1016/j.gca.2006.02.028.
Marques, A.F.A., Barriga, F., Chavagnac, V., Fouquet, Y., 2006. Mineralogy, geochemistry, and Nd isotope composition of the Rainbow hydrothermal field, Mid-Atlantic Ridge. Miner. Depos. 41, 52–67. https://doi.org/10.1007/s00126-005-0040-8.
Marx, J., Huebscher, H.-D., Hoth, K., Korich, D., Kramer, W., 1995. Vulkanostratigraphie und Geochemie der Eruptivkomplexe, in: Plein, E. (Ed.), Stratigraphie von Deutschland I. Norddeutsches Rotliegend-Becken. Rotliegend Monographie Teil II. Cour.Forsch.-Inst. Senckenberg, Frankfurt a.M.
Maystrenko, Y., Bayer, U., Brink, H.J., Littke, R., 2008. The Central European Basin System – an Overview. In: Littke, R., Bayer, U., Gajewski, D., Nelskamp, S. (Eds.), Dynamics of Complex Intracontinental Basins. Springer, Berlin, Heidelberg, pp. 15–34.
McConachie, B.A., Lindsay, J.F., Glikson, M., 2000. Influence of basin fill architecture on fluid flow and ore genesis in the Mount Isa Basin, Northern Australia. In: Glikson-Simpson, M., Mastalerz, M. (Eds.), Organic Matter and Mineralisation: Thermal Alteration, Hydrocarbon Generation and Role in Metallogenesis. Kluwer Academic, pp. 120–148.
McCuaig, T.C., Scarselli, S., O'Connor, T., Busuttil, S., McCormack, N., 2018. The Power of a Systems Approach to Mineral and Petroleum Exploration in Sedimentary Basins, in: Arribas R., A.M., Mauk, J.L. (Eds.), Metals, Minerals, And Society, SEG Special Publication 21. Society of Economic Geologists, pp. 39–62.
Mempel, G., 1962. Verbreitung und Genese der Buntmetallerz-Spuren in den paläozoischen und mesozoischen Sedimenten Nordwestdeutschlands. Zeitschrift für Erzbergabu und Met. 15, 62–72.
Mempel, G., Fesser, H., Gundlach, H., 1965. Untersuchungen an Zinkblende und Bleiglanz aus Geoden Nordwestdeutschlands. Erzmetall 285–292.
Mertz, D.F., Lippolt, H.-J., Schnorrer-Köhler, G., 1989. Early Cretaceous mineralizing activity in the St. Andreasberg ore district (Southwest Harz, Germany). Miner. Depos. 24, 9–13.

Möller, P., Bau, M., Dulski, P., Lüders, V., 1998. REE and yttrium fractionation in fluorite and their bearing on fluorite formation. In: Hagni, R.D. (Ed.), Proceedings of the Ninth Quadren- Nial IAGOD Symposium. Schweizerbart, Stuttgart, Germany, pp. 575–592.
Möller, P., Cerny, P., Saupe, F., 1989. Lanthanides, Tantalum and Niobium: Mineralogy, Geochemistry, Characteristics of Primary Ore Deposits, Prospecting, Processing and Applications Proceedings of a workshop in Berlin, November 1986. Springer Berlin Heidelberg.
Möller, P., Dulski, P., Schneider, H.-J., 1983. Interpretation of Ga and Ge Content in Sphalerite from the Triassic Pb-Zn Deposits of the Alps. In: Schneider, H.-J. (Ed.), Mineral Deposits of the Alps and of the Alpine Epoch in Europe : Proceedings of the IV. ISMIDA Berchtesgaden, October 4–10, 1981. Springer Berlin Heidelberg, Berlin, Heidelberg, pp. 213–222. https://doi.org/10.1007/978-3-642-68988-8_23.
Möller, P., Lüders, V., 1993. Formation of hydrothermal vein deposits: a case study of the Pb-Zn, barite and fluorite deposits of the Harz Mountains. Monogr. Ser. Miner. Depos.
Möller, P., Lüders, V., De Lucia, M., 2017. Formation of Rotliegend Ca-Cl brines in the North German Basin compared to analogues in the geological record. Chem. Geol. 459, 32–42. https://doi.org/https://doi.org/10.1016/j.chemgeo.2017.04.001.
Möller, P., Parekh, P.P., Schneider, H.-J., 1976. The application of Tb/Ca-Tb/La abundance ratios to problems of fluorspar genesis. Miner. Depos. 11, 111–116. https://doi.org/10.1007/bf00203098.
Möller, P., Schulz, S., Jacob, K.H., 1980. Formation of fluorite in sedimentary basins. Chem. Geol. 31, 97–117. https://doi.org/https://doi.org/10.1016/0009-2541(80)90070-4.
Moskalyk, R.R., 2003. Gallium: the backbone of the electronics industry. Miner. Eng. 16, 921–929. https://doi.org/https://doi.org/10.1016/j.mineng.2003.08.003.
Muchez, P., Heijlen, W., 2003. Origin and migration of fluids during the evolution of sedimentary basins and the origin of Zn-Pb deposits in Western and Central Europe. J. Geochemical Explor. 78, 553–557. https://doi.org/https://doi.org/10.1016/S0375-6742(03)00017-7.
Müller, C., Jähne-Klingberg, F., von Goerne, G., Binot, F., Röhling, H.-G., 2016. Vom Geotektonischen Atlas ("Kockel-Atlas") zu einem 3D-Gesamtmodell des Norddeutschen Beckens: Basisinformationen zum tieferen Untergrund von Norddeutschland. Zeitschrift der Dtsch. Gesellschaft für Geowissenschaften 167, 65–106. https://doi.org/10.1127/zdgg/2016/0072.
Mundry, E., 1971. Der Temperaturverlauf im Dach des Bramscher Massivs nach der Wärmeleitungstheorie. Fortschr Geol Rheinl u Westf 18, 539–546.
Nadoll, P., Rehm, M., Duschl, F., Klemd, R., Kraemer, D., Sośnicka, M., 2018. REY and Trace Element Chemistry of Fluorite from Post-Variscan Hydrothermal Veins in Paleozoic Units of the North German Basin. Geosciences 8, 283. https://doi.org/10.3390/geosciences8080283.
Nollet, S., Hilgers, C., Urai, J., 2005. Sealing of fluid pathways in overpressure cells: a case study from the Buntsandstein in the Lower Saxony Basin (NW Germany). Int. J. Earth Sci. (Geol. Rundsch.) 94, 1039–1055. https://doi.org/10.1007/s00531-005-0492-1.
Obst, K., Katzung, G., Haupt, U., 2001. Dyke magmatism in the central Harz mountains and its implication for Late Variscan extensional tectonics. Neues Jahrb. fur Geol. und Palaontologie-Abhandlungen.
Ostendorf, J., Henjes-Kunst, F., Mondillo, N., Boni, M., Schneider, J., Gutzmer, J., 2015. Formation of Mississippi Valley–type deposits linked to hydrocarbon generation in extensional tectonic settings: Evidence from the Jabali Zn-Pb-(Ag) deposit (Yemen). Geology 43, 1055–1058. https://doi.org/10.1130/G37112.1.
Palero-Fernández, F.J., Martín-Izard, A., 2005. Trace element contents in galena and sphalerite from ore deposits of the Alcudia Valley mineral field (Eastern Sierra Morena, Spain). J. Geochemical Explor. 86, 1–25. https://doi.org/https://doi.org/10.1016/j.gexplo.2005.03.001.
Paradis, S., Hannigan, P., Dewing, K., 2007. Mississippi Valley-type lead-zinc deposits. In: Goodfellow, W.D. (Ed.), Mineral Deposits of Canada: A Synthesis of Major Deposit-Types, District Metallogeny, the Evolution of Geological Provinces, and Exploration Methods: Geological Association of Canada, Mineral Deposits Division, Special Publication No. 5, pp. 185–203.
Peevler, J., Fayek, M., Misra, K.C., Riciputi, L.R., 2003. Sulfur isotope microanalysis of sphalerite by SIMS: constraints on the genesis of Mississippi valley-type mineralization, from the Mascot-Jefferson City district. East Tennessee. J. Geochemical Explor. 80, 277–296.
Petmecky, S., Meier, L., Reiser, H., Littke, R., 1999. High thermal maturity in the Lower Saxony Basin-intrusion or deep burial. Tectonophysics 304, 317–344.
Pharaoh, T.C., Dusar, M., Geluk, M.C., Kockel, F., Krawczyk, C.M., Krzywiec, P., Scheck-Wenderoth, M., Thybo, H., 2010. Tectonic evolution. In: Doornenbal, H., Stevenson, A. (Eds.), Petroleum Geological Atlas of the Southern Permian Basin Area. EAGE Publ, Houten, pp. 25–57.
Piestrzyński, A., 1990. Uranium and thorium in the Kupferschiefer formation, Lower Zechstein, Poland. Miner. Depos. 25, 146–151.
Piestrzyński, A., Wodzicki, A., 2000. Origin of the gold deposit in the Polkowice-West Mine, Lubin-Sieroszowice Mining District, Poland. Miner. Depos. 35, 37–47. https://doi.org/10.1007/s001260050004.
Plein, E., 1995. Norddeutsches Rotliegend-Becken. Rotliegend Monographie Teil II. Stratigr. von Deutschl. I.
Plein, E., 1993. Bemerkungen zum Ablauf der paläogeographischen Entwicklung im Stefan und Rotliegend des Norddeutschen Beckens. In: Müller, P.E., Porth, H. (Eds.), Zur Geologie Und Kohlenwasserstoff-Führung Des Perm Im Ostteil Der Norddeutschen Senke. Schweizerbart, Hannover, pp. 99–116.
Pletsch, T., Appel, J., Clayton, C.J., Duin, E.J.T., Faber, E., Gorecki, W., Kombrink, H., Kosakowski, P., Kuper, G., Kus, J., Lutz, R., Mathiesen, A., Ostertag-Henning, C., Papiernek, B., Van Bergen, F., 2010. Petroleum generation and migration. In: Doornenbal, H., Stevenson, A. (Eds.), Petroleum Geological Atlas of the Southern Permian Basin Area. EAGE publications, Houten, pp. 225–253.
Price, B.J., 1972. Minor elements in pyrites from the Smithers map area, B.C. and exploration applications of minor element studies. University of British Columbia.
Pudlo, D., Albrecht, D., Ganzer, L., Gaupp, R., Kohlhepp, B., Meyer, R., Reitenbach, V., Wienand, J., 2011. Petrophysical, facies and mineralogical-geochemical investigations of Rotliegend sandstones from the Altmark natural gas field in Central Germany. Energy Procedia 4, 4648–4655. https://doi.org/https://doi.org/10.1016/j.egypro.2011.02.425.
Regenspurg, S., Feldbusch, E., Norden, B., Tichomirowa, M., 2016. Fluid-rock interactions in a geothermal Rotliegend/Permo-Carboniferous reservoir (North German Basin). Appl. Geochem. 69 (69), 12–27. https://doi.org/10.1016/j.apgeochem.2016.03.010.
Repetski, J.E., Narkiewicz, M., 1996. Conodont color and surface textural alteration in the Muschelkalk (Triassic) of the Silesian-Cracow Zn-Pb district, Poland. In: Gorecka, E., Leach, D.L. (Eds.), Carbonate-Hosted Zinc-Lead Deposits in the Silesian-Cracow Area, Poland. Wydawnictwa Geologiczne, Warsaw, Poland, pp. 113–122.
Reutel, C., 1984. Mikrothermometrische Untersuchungen an Flüssigkeitseinschlüssen der Mineralisationen des St. Andreasberger Erzreviers und des Rosenhöfer Gangzuges (Harz). Universität Göttingen.
Reutel, C., Lüders, V., 1998. Fluid-Evolution und Gasmigration im südlichen Rand- bereich des Nordostdeutschen Beckens — Untersuchungen an Flüssigkeitseinschlüssen in Kluftmineralisationen und Werra-Anhydrit. Geol. Jahrb. A 149, 169–183.
Reutel, C., Lüders, V., Hoth, P., 1995. Gas migration and accumulation along lineament structures – Lower Saxony Basin (NW Germany). Bol. la Soc. Mineral. 18, 205–207.
Richardson, C.K., Holland, H.D., 1979. Fluorite deposition in hydrothermal systems. Geochim. Cosmochim. Acta 43, 1327–1335. https://doi.org/https://doi.org/10.1016/0016-7037(79)90122-4.
Rieken, R., 1988. Lösungszusammensetzung und Migrationsprozesse von Paläofluidsystemen im NDB. Göttinger Arb. zur Geol. und Paläontologie 37, 116.
Robb, L.J., 2011. Introduction to Ore-forming Processes. Blackwell Publishing.
Roberts, F.I., 1982. Trace element chemistry of pyrite: A useful guide to the occurrence of sulfide base metal mineralization. J. Geochem. Explor. 17, 49–62.
Roedder, E., 1984. Fluid Inclusions. Reviews in mineralogy, reviews in mineralogy. Mineral. Soc. Amer.
Rose, K.H., Gödecke, C.P., 1984. Mineral-Neubildungen des Onsabrücker Berglandes im Vergleich mit dem übrigen Nordwestdeutschland. In: Klassen, H. (Ed.), Geologie Des Osnabrücker Berglandes. Naturwissenschaftliches Museum Osnabrück, Osnabrück, pp. 567–643.
Rowan, E.L., Goldhaber, M.B., 1995. Duration of mineralization and fluid-flow history of the Upper Mississippi Valley zinc-lead district. Geology 23, 609–612.
Scheck-Wenderoth, M., Krzywiec, P., Zühlke, R., Maystrenko, Y., Froitzheim, N., 2008. Permian to Cretaceous tectonics. In: McCann, T. (Ed.), The Geology of Central Europeeology of Central Europe. The Geological Society of London, London, pp. 990–1030.
Scheck-Wenderoth, M., Lamarche, J., 2005. Crustal memory and basin evolution in the Central European Basin System—new insights from a 3D structural model. Tectonophysics 397, 143–165. https://doi.org/10.1016/j.tecto.2004.10.007.
Scheck, M., Bayer, U., 1999. Evolution of the Northeast German Basin – inferences from a 3D structural model and subsidence analysis. Tectonophysics 313, 145–169.
Scheck, M., Bayer, U., Otto, V., Lamarche, J., Banka, D., Pharaoh, T., 2002. The Elbe Fault System in North Central Europe – a basement controlled zone of crustal weakness. Tectonophysics 360, 281–299.
Scherp, A., Stadler, G., 1968. Die pyrophyllitführenden Tonschiefer des Ordoviziums im Elbesattel und Ihre Genese. N. Jb. Miner. 108, 142–165.
Schmidt Mumm, A., Wolfgramm, M., 2004. Fluid systems and mineralization in the north German and Polish Basin. Geofluids 4, 315–328.
Schmidt Mumm, A., Wolfgramm, M., 2003a. Stable isotope relationships of mineralisation in the North Eastern German Basin. J. Geochemical Explor. 78–79, 261–265. https://doi.org/10.1016/S0375-6742(03)00143-2.
Schmidt Mumm, A., Wolfgramm, M., 2003b. Thermal evolution of the eastern north german basin: a fluid inclusion study. Göttinger Arb. zur Geol. und Paläontologie 565, 86–94.
Schmidt Mumm, A., Wolfgramm, M., 2002. Diagenesis and fluid mobilisation during the evolution of the North German Basin – evidence from fluid inclusion and Sulphur isotope analysis. Mar. Pet. Geol. 19, 229–246.
Schneider, H., 1952. Über einige Beziehungen der Erzvorkommen im Osnabrücker Raum zum varistischen Magmatismus. Zeitschrift der Dtsch. Geol. Gesellschaft 104, 516–533.
Schneider, J., Haack, U., Stedingk, K., 2003. Rb-Sr dating of epithermal vein mineralization stages in the eastern Harz Mountains (Germany) by paleomixing lines. Geochim. Cosmochim. Acta 67, 1803–1819. https://doi.org/10.1016/s0016-7037(02)01223-1.
Scholle, P.A., Peryt, T.M., Ulmer-Scholle, D.S., 1995. The Permian of Northern Pangea – Volume 1: Paleogeography, Paleoclimates, Stratigraphy, 1st ed. Springer.
Schöner, R., Lüders, V., Ondrak, R., Gaupp, R., Möller, P., 2008. Fluid-rock interactions. In: Littke, R., Bayer, U., Gajewski, D., Nelskamp, S. (Eds.), Dynamics of Complex Sedimentary Basins. The Example of the Central European Basin System. Springer, Berlin, Heidelberg, pp. 389–410.
Schröder, L., Plein, E., Bachmann, G.H., 1995. Stratigraphische Neugliederung des Rotliegend im Norddeutschen Becken. Geol. Jahrb. R. A A 148, 21.
Schumacher, K.-H., May, F., 1993. Varianz lagerstättengenetischer Parameter im Rotliegenden der westlichen Altmark. Geol. Rundschau A 131, 261–270.
Schwinn, G., Markl, G., 2005. REE systematics in hydrothermal fluorite. Chem. Geol. 216, 225–248. https://doi.org/https://doi.org/10.1016/j.chemgeo.2004.11.012.
Seeliger, E., 1950. Pseudohydrothermale Pb-Zn-Erzgänge im Ruhrgebiet und im Gebiet von Velbert-Lintorf: eine Untersuchung über die Einflüsse heißer Zechsteinsalzlösungen auf Pb-Zn-Erze am Beispiel der Erzgänge von Christian Levin

in Essen und von Stein V in Hüls bei Reckling. Akademie-Verlag.
Seidl, K., 1959. Über die Bildung von Bitumen bei der Dolomitisierung von Kalkgesteinen unter der Einwirkung von Salzsolen. N. Jb. Miner. 4, 85–92.
Senglaub, Y., Littke, R., Brix, M.R., 2006. Numerical modelling of burial and temperature history as an approach for an alternative interpretation of the Bramsche anomaly, Lower Saxony Basin. Int. J. Earth Sci. 95, 204–224. https://doi.org/10.1007/s00531-005-0033-y.
Sośnicka, M., Lüders, V., 2018a. Super-deep, TSR-controlled Phanerozoic MVT type Zn-Pb deposits hosted by Zechsetin reservoir carbonate, Lower Saxony Basin. Germany. Chem. Geol.
Sośnicka, M., Lüders, V., 2018b. Fluid inclusion evidence for methane-dominated thermochemical sulfate reduction in the North German Basin, in: PACROFI 14 Abstract Volume, in Press. Pan-American Current Research on Fluid Inclusions, Houston, Texas.
Sośnicka, M., Lüders, V., 2017. TSR-controlled Zn-Pb mineralization in Zechstein carbonate (Ca2) in the Lower Saxony Basin, Germany, in: ECROFI 2017 Biennial Meeting. Nancy, France.
Spangenberg, J., Fontboté, L., Sharp, Z.D., Hunziker, J., 1996. Carbon and oxygen isotope study of hydrothermal carbonates in the zinc-lead deposits of the San Vicente district, central Peru: a quantitative modeling on mixing processes and CO2 degassing. Chem. Geol. 133, 289–315. https://doi.org/https://doi.org/10.1016/S0009-2541(96)00106-4.
Speczik, S., 1995. The Kupferschiefer mineralization of central Europe: new aspects and major areas of future research. Ore Geol. Rev. 9, 411–426.
Stackebrandt, W., 1986. Beiträge zur tektonischen Analyse ausgewählter Bruchzonen der Subherzynen Senke und angrenzender Gebiete (Aufrichtungszone, Flechtinger Scholle). Veröffentlichungen des Zentralinstituts für Physik der Erde 79.
Stadler, G., Teichmüller, R., 1971. Zusammenfassender Überblick über die Entwicklung des Bramscher Massiv und des Niedersächsischen Tektogens. Fortschr. Geol. Rheinld. u. Westf. 18, 547–564.
Stedingk, K., Ehling, B.-C., Knoth, W., Germann, K., Schwab, M., 1995. Epigenetic mineralizing processes in the Northeastern Rhenohercynian Belt (Harz Mountains, Flechtingen-Rosslau Block), in: Mineral Deposits: From Their Origin to Their Environmental Impacts. Proceedings of the Third Biennial SGA Meeting, Prague, Czech Republic.
Stoffell, B., Appold, M.S., Wilkinson, J.J., McClean, N.A., Jeffries, T.E., 2008. Geochemistry and Evolution of Mississippi Valley-Type Mineralizing Brines from the Tri-State and Northern Arkansas Districts Determined by LA-ICP-MS Microanalysis of Fluid Inclusions. Econ. Geol. 103, 1411–1435. https://doi.org/10.2113/gsecongeo.103.7.1411.
Stollhofen, H., Bachmann, G.H., Barnasch, J., Bayer, U., Beutler, G., Franz, M., Kästner, M., Legler, B., Mutterlose, J., Radies, D., 2008. Upper Rotliegend to Early Cretaceous basin development. In: Littke, R., Bayer, U., Gajewski, D., Nelskamp, S. (Eds.), Dynamics of Complex Intracontinental Basins: The Example of the Central European Basin System. Springer, pp. 181–210.
Stoppel, D., Gundlach, H., 1978. Zur Geologie und Bergbaugeschichte der Schwerspat- und Kobalterzvorkommen im Unterwerra-Grauwackengebirge und Rickelsdorfer Gebirge. Aufschluß 28, 261–285.
Stottmeister, L., Poblozki, B., 1999. Die geologische Entwicklung der Altmark–eine Übersicht. Mitt. Geol. Sachsen-Anhalt 5, 45–72.
Sverjensky, D.A., 1989. Chemical evolution of basinal brines that formed sediment-hosted Cu- Pb-Zn deposits. Geol. Assoc. Canada Spec. Pap. 36, 127–134.
Sverjensky, D.A., 1986. Genesis of mississippi valley-type lead-zinc deposits. Annu. Rev. Earth Planet. Sci. 14, 177.
Sverjensky, D.A., 1984. Oil field brines as ore-forming solutions. Econ. Geol. 79, 23–37. https://doi.org/10.2113/gsecongeo.79.1.23.
Tanner, D.C., Krawczyk, C.M., 2017. Restoration of the Cretaceous uplift of the Harz Mountains, North Germany: evidence for the geometry of a thick-skinned thrust. Int. J. Earth Sci. 145, 101. https://doi.org/10.1007/s00531-017-1475-8.
Taylor, D., 2000. Introduction—A "soft-rock" petroleum-type approach to exploration for "hard-rock" minerals in sedimentary basins. In: Glikson-Simpson, M., Mastalerz, M. (Eds.), Organic Matter and Mineralisation: Thermal Alteration, Hydrocarbon Generation and Role in Metallogenesis. Kluwer Academic, pp. 1–12.
Taylor, S.R., McLennan, S.M., 1985. The Continental Crust: Its Composition and Evolution. Blackwell Scientific Publication, Carlton.
Teichmüller, M., Teichmüller, R., 1985. Inkohlungsgradienten in der Anthrazitfolge des Ibbenbürener Karbons. Fortschr. Geol. Rheinl. Westfal. 33, 231–253.
Tischendorf, G., Franzke, H.J., 1993. On the genesis of Permian and Post-Permian hydrothermal mineralisations in the Harz Mts according to new Pb-isotope measurements. In: Möller, P. (Ed.), Formation of Hydrothermal Vein Deposits. Borntraeger, Berlin, pp. 65–76.
Tostevin, R., Shields, G.A., Tarbuck, G.M., He, T., Clarkson, M.O., Wood, R.A., 2016. Effective use of cerium anomalies as a redox proxy in carbonate-dominated marine settings. Chem. Geol. 438, 146–162. https://doi.org/10.1016/j.chemgeo.2016.06.027.
Trinkler, M., Monecke, T., Thomas, R., 2005. Constraints on the genesis of yellow fluorite in hydrothermal barite–fluorite veins of the erzgebirge, eastern germany: evidence from optical absorption spectroscopy, rare-earth-element data, and fluid-inclusion investigations. Can. Mineral. 43, 883–898.
van Wees, J.D., Stephenson, R.A., Ziegler, P.A., Bayer, U., McCann, T., Dadlez, R., Gaupp, R., Narkiewicz, M., Bitzer, F., Scheck, M., 2000. On the origin of the Southern Permian Basin, Central Europe. Mar. Pet. Geol. 17, 43–59. https://doi.org/https://doi.org/10.1016/S0264-8172(99)00052-5.
Vaughan, D., Sweeny, M., Friedrich, G., Diedel, R., Hanczyk, C., 1989. The Kupferschiefer: an overview with an appraisal of the different types of mineralization. Econ. Geol. 84, 1003–1027.
Viets, J.G., Hofstra, A.H., Emsbo, P., Kozlowski, A., 1996. The composition of fluid inclusions in ore and gangue minerals from the Silesian-Cracow Mississippi Valley-type Zn-Pb deposits Poland: Genetic and environmental implications. Pr. – Panstw. Inst. Geol. 154, 85–103.
Wagner, T., Okrusch, M., Weyer, S., Lorenz, J., Lahaye, Y., Taubald, H., Schmitt, R.T., 2010. The role of the Kupferschiefer in the formation of hydrothermal base metal mineralization in the Spessart ore district, Germany: insight from detailed sulfur isotope studies. Miner. Depos. 45, 217–239. https://doi.org/10.1007/s00126-009-0270-2.
Walther, H.W., Dill, H.G., 1992. Die Bodenschätze Mitteleuropas-Ein Überblick, in: Walter, R. (Ed.), Geologie von Mitteleuropa. pp. 410–466.
Will, P., Lüders, V., Wemmer, K., Gilg, H.A., 2016. Pyrophyllite formation in the thermal aureole of a hydrothermal system in the Lower Saxony Basin, Germany. Geofluids 16, 349–363. https://doi.org/10.1111/gfl.12154.
Wilson, M., Neumann, E.R., Davies, G.R., Timmerman, M.J., Heeremans, M., Larsen, B.T., 2003. In: Permo-Carboniferous Magmatism and Rifting in Europe, https://doi.org/10.1144/gsl.sp.2004.223.
Wolfgramm, M., 2002. Fluidentwicklung und Diagenese im Nordostdeutschen Becken – Petrographie, Mikrothermometrie und Geochemie stabiler Isotope. Math. Fak. Martin-Luther-Universität Halle-Wittenberg.
Wood, S.A., 1990. The aqueous geochemistry of the rare-earth elements and yttrium. Chem. Geol. 82, 159–186. https://doi.org/https://doi.org/10.1016/0009-2541(90)90080-Q.
Wrede, V., 2005. Stratigraphie von Deutschland V – Das Oberkarbon (Pennsylvanium) in Deutschland. Courier Forschungsinstitut Senckenberg, pp. 254.
Wüstefeld, P., Hilse, U., Lüders, V., Wemmer, K., Koehrer, B., Hilgers, C., 2017. Kilometer-scale fault-related thermal anomalies in tight gas sandstones. Mar. Pet. Geol. 86, 288–303. https://doi.org/10.1016/j.marpetgeo.2017.05.015.
Xuexin, S., 1984. Minor elements and ore genesis of the Fankou lead-zinc deposit. China. Miner. Depos. 19, 95–104. https://doi.org/10.1007/bf00204667.
Ye, L., Cook, N.J., Ciobanu, C.L., Yuping, L., Qian, Z., Tiegeng, L., Wei, G., Yulong, Y., Danyushevskiy, L., 2011. Trace and minor elements in sphalerite from base metal deposits in South China: A LA-ICPMS study. Ore Geol. Rev. 39, 188–217. https://doi.org/https://doi.org/10.1016/j.oregeorev.2011.03.001.
Zheng, Y.-F., Hoefs, J., 1993. Stable isotope geochemistry of hydrothermal mineralizations in the Harz Mountains: I. Carbon and oxygen isotopes of carbonates and implications for the origin of hydrothermal fluids. In: Möller, P., Lüders, V. (Eds.), Formation of Hydrothermal Vein Deposits. A Case Study of the Pb-Zn, Barite and Fluorite Deposits of the Harz Mountains. Monograph Series on Mineral Deposits, pp. 169–187.
Zhu, Z.-Y., Cook, N., Yang, T., Ciobanu, C., Zhao, K.-D., Jiang, S.-Y., 2016. Mapping of Sulfur Isotopes and Trace Elements in Sulfides by LA-(MC)-ICP-MS: Potential Analytical Problems, Improvements and Implications. Minerals 6, 110.
Ziegler, K., 2006. Clay minerals of the Permian Rotliegend Group in the North Sea and adjacent areas. Clay Miner. 41, 355–393.
Ziegler, P.A., 1990. Geological Atlas of Western and Central Europe. Shell Int. Pet. Maatsch. B.V.
Ziegler, P.A., 1987. Late Cretaceous and Cenozoic intra-plate compressional deformations in the Alpine foreland—a geodynamic model. Tectonophysics 137, 389–420. https://doi.org/https://doi.org/10.1016/0040-1951(87)90330-1.
Ziegler, P.A., 1977. Geology and hydrocarbon provinces of the North Sea. GeoJournal 1, 7–32. https://doi.org/10.1007/bf00189601.